**The Dissertation Committee for Uarporn Nopmongcol Certifies that this is the approved version of the following dissertation:**

# Heterogeneous Reactions on Atmospheric Carbonaceous Particles

**Committee:**

David T. Allen, Supervisor

Charles B. Mullins

Elena C. McDonald-Buller

Gary T. Rochelle

Richard L. Corsi

# Heterogeneous Reactions on Atmospheric Carbonaceous Particles

**by**

**Uarporn Nopmongcol, B.Eng.**

**Dissertation**

Presented to the Faculty of the Graduate School of

The University of Texas at Austin

in Partial Fulfillment

of the Requirements

for the Degree of

**Doctor of Philosophy**

**The University of Texas at Austin**

**December 2005**

## Dedication

To my parents, Dr. Pradit Nopmongcol and Tipsuda Nopmongcol.

## Acknowledgement

I would like to express my deep gratitude to Dr. David Allen, my supervisor, for his guidance and support throughout the course of my graduate studies. I also would like to extend my gratitude to Dr. Yosuke Kimura, who assisted me on computer programming and offered helpful suggestions countless times. I acknowledge my parents, Dr. Pradit Nopmongcol and Tipsuda Nopmongcol for their unlimited love and care. I am also thankful to Jason Kenney who has always stuck by my side and made every moment in Austin delightful. Finally, I acknowledge my friends for their love and friendship that make what I do possible.

# Heterogeneous Reactions on Atmospheric Carbonaceous Particles

Publication No._____

Uarporn Nopmongcol, Ph.D.

The University of Texas at Austin, 2005

Supervisor: David T. Allen

Elevated particle concentrations in the atmosphere have received significant attention due to their multiple effects from urban to global scales. The sources and formation mechanisms of these air pollutants, however, are poorly understood, especially atmospheric reactions involving oxidation and condensation of gas phase hydrocarbons, catalyzed by atmospheric particles. This work examines these particle catalyzed, gas to particle transformation processes, through detailed photochemical modeling of air quality episodes in Texas. Two heterogeneous reaction pathways were incorporated into a widely used photochemical model. The pathways that were examined were (1) Heterogeneous formation of sulfuric acid on carbonaceous particles and (2) Acid catalyzed condensation reactions of low molecular weight aldehydes. The impact of these pathways on air quality in Texas was examined for a period during which wildfires generated significant amounts of carbonaceous atmospheric aerosol. This episode was chosen for analysis because the rates of the heterogeneous

reactions were expected to be significant during this period, leading to observable signals in ambient data.

Simulations, together with ambient data, indicated that wood smoke mediated sulfate formation reactions, not accounted for in most current photochemical models, may have led to 5-10 $\mu g/m^3$ of sulfate formation. In photochemical simulations, wood-smoke mediated sulfate formation was modeled by calculating the rate of impingement of $SO_2$ molecules on the wood smoke particles, and then assuming that a fraction of the impingements resulted in reaction. For reaction probabilities on the order of 0.01, the model predicted magnitudes, spatial distributions and temporal distributions of sulfate concentrations consistent with observations.

Simulations, together with ambient data, indicated that acid aerosol mediated organic aerosol formation reactions, not accounted for in most current photochemical models, may have led to 1-5 $\mu g/m^3$ of organic aerosol. In photochemical simulations, acid mediated organic aerosol formation was modeled by calculating the rate of impingement of aldehyde molecules on acidic particles, and then assuming that a fraction of the impingements resulted in reaction. For reaction probabilities on the order of 0.0005, the model predicted magnitudes, spatial distributions and temporal distributions of organic aerosol consistent with observations.

Ambient data and model results in this work demonstrated that the heterogeneous reactions on carbonaceous particles are significant. The methodology developed in this work, most importantly, can be applied to other heterogeneous reactions to be incorporated into a photochemical model.

# Table of Contents

# List of Tables

# List of Figures

# Table of Acronyms

| | |
|---|---|
| BRAVO | The Big Bend Regional Aerosol and Visibility Observational Study |
| CAMx (CAMx4.11x) | Comprehensive Air Quality Model with Extensions (version 4.11x) |
| CB-IV (CBIV)(CB4) | Carbon Bond IV chemical mechanism |
| EPA | Environmental Protection Agency |
| FRM | Federal Reference Method (for monitoring $PM_{2.5}$) |
| GC-ARCH | Gulf Coast Aerosol Research and Characterization Program |
| HGBPA | Houston-Galveston & Beaumont-Port Arthur |
| NAAQS | National Ambient Air Quality Standard |
| OC | Organic Carbon (in $PM_{2.5}$) |
| PBL | Planetary Boundary Layer |
| PM | Particulate Matter |
| $PM_{2.5}$ | Particulate Matter with aerodynamic diameters less than 2.5 microns |
| SOA | Secondary organic aerosol |
| SVOC | Semi-Volatile Organic Compound |
| TCEQ | Texas Commission on Environmental Quality |
| TEOM | Tapered Element Oscillating Microbalance |
| TXAQS (TEXAQS2000) | Texas Air Quality Study (in the year 2000) |
| VOC | Volatile Organic Compound |
| wt% | Percentage by weight |
| Tot C | Total carbon |
| Tot PM | Total Fine PM |

# Chapter 1 Introduction

### *1.1 PARTICULATE MATTER OVERVIEW*

Particulate matter, or PM, is the general term used for solid or liquid phase materials, including dust, dirt, soot, smoke, and aqueous droplets in the atmosphere. The condensed phase in the atmosphere is also referred to as particulates, particles, and aerosols. Particulate matter is not a single pollutant, but rather a heterogeneous mixture containing individual particles of different sizes and chemical compositions. The composition varies with place, season and weather conditions, generally containing inorganic salts and acids, organic compounds and liquid water. The size of the most important particles with respect to atmospheric chemistry and physics are in the range from a few nanometers (nm) to tens of micrometers (μm) in diameter. Depending upon their slow rates of sedimentation, particles of less than 10 μm normally remain suspended in air for days, or longer, while larger particulates settle out of the air under the influence of gravity in a short period of time.

Particulate matter in the atmosphere can either absorb or scatter light, and therefore directly influence the Earth's radiation balance (Andreae and Crutzen 1997; Pilinis et al. 1995), contributing to global climate change and visibility degradation. PM can also have effects on vegetation and ecosystems, such as causing damage and soiling to plants and materials (Grantz et al. 2003). Further, epidemiological studies have shown that particles in urban are associated with adverse health impacts, such as asthma, early death due to effects on the cardiopulmonary system and lung cancer (EPA 1996; Laden et al. 2000; Pope et al. 2002). For all of these impacts, the extent of the impact depends on particle composition and size.

Because the various impacts of elevated particle concentrations depend on the size of the particles, particulate matter is characterized according to its aerodynamic diameter. In 1987, the US Environmental Protection Agency (EPA) introduced National Ambient Air Quality Standards (NAAQSs) for particles smaller than 10 μm in diameter, commonly called $PM_{10}$. $PM_{10}$ is able to penetrate the upper respiratory tract. In 1997, the

standard was modified to include particles smaller than 2.5 μm in diameter, commonly called $PM_{2.5}$. $PM_{2.5}$, also known as fine particulate matter, penetrates deeper into the respiratory system than larger particles, posing greater threats to human health.

### *1.2 SECONDARY AEROSOL*

The sources (both local and regional) of atmospheric particles can be classified as primary (directly emitted from the sources into the environment) or secondary. Primary particulate matter sources include fires, industrial point sources, mobile (vehicular) sources, cooking, and other minor sources. Secondary particulate matter is formed in the atmosphere by reactions of gaseous species. Secondary sources are generally characterized into inorganic and organic categories. In urban areas of the United States, primary emissions account for approximately 40-50 % of fine PM mass, while secondary emissions account for 50-60% of fine PM mass, and potentially larger fractions at rural sites (Allen D.T. 2002).

Because secondary particulate matter is a significant fraction of the total particle mass, secondary particulate matter has received significant attention over the past decade. Most of this attention has been focused on processes that either occur in the gas phase or in the condensed phase. An example of a widely studied gas phase process is the oxidation of $SO_2$ by the hydroxyl radical, producing sulfuric acid, which condenses into the particle phase. An example of a widely studied condensed phase process is the dissolution of $SO_2$ into aqueous particles, with subsequent oxidation by hydrogen peroxide to form sulfuric acid. In contrast to these widely studied gas and condensed phase processes, are processes that occur at interfaces between gas, liquid and solid phases in the atmosphere. An example of a surface/heterogeneous process is the catalytic conversion of $SO_2$ to sulfuric acid on soot-like particles in the atmosphere (Novakov T. 1974). There is an increasing body of evidence indicating that these surface processes are important in particle formation and growth. This thesis will examine surface (heterogeneous) processes involving atmospheric particles, particularly focusing on reactions important in urban atmospheres.

Examples of these processes include chemical reactions of nitrogen oxides on the surface of oxide, carbonate, soot and mineral dust particles (Grassian 2002). In addition, the acid-catalyzed reactions of gas phase carbonyls were reported to be a major class of heterogeneous reactions in urban areas where concentrations of particulate matter are high (Jang and Kamens 2001a; Jang et al. 2002).

### *1.3 RESEARCH OBJECTIVES*

Evidence for these heterogeneous/surface reaction pathways has largely been based on laboratory experiments; ambient observational evidence of these surface/heterogeneous pathways has been limited. **The first objective of this research is to examine observational data for events where these reactions are likely to be important**. The pathways to be examined are:

1) Heterogeneous formation of sulfuric acid on carbonaceous particles, and
2) Acid catalyzed condensation reactions of low molecular weight aldehydes.

For both of these pathways, key observational data are available for southeast Texas during the summer of 2000.

Understanding the impact of surface or heterogeneous reaction processes in the atmosphere at regional scales will require that the rates of these processes be included in comprehensive photochemical models. **The second objective of this research is to incorporate these two major heterogeneous/surface pathways into a widely used photochemical model known as the Comprehensive Air Quality Model, with extensions, CAMx.**

The rates of heterogeneous reactions are dependent on many variables and the sensitivity of those rates, spatially and temporally, remain relatively unknown. **The final objective of this research is to use to the modified photochemical grid model to investigate a sensitivity of heterogeneous reactions to many key variables.** This objective can be accomplished by applying the modified photochemical grid model to Southeast Texas during the same period that the field measurements are available.

### *1.4 DISSERTATION STRUCTURE*

Chapter 2 presents observational evidence indicating the importance of sulfate formation on carbonaceous particles and chapter 3 describes a computational approach for incorporating these reactions into photochemical models. Similarly, Chapter 4 reports on field data that indicate the possible significance of acid catalyzed organic condensation reactions and describes the incorporation of these pathways into a regional photochemical model. Finally, Chapter 5 summarizes the major findings of this research and presents recommendations for future work.

# Chapter 2 Heterogeneous formation of sulfate on carbonaceous particles- Part 1: Observational Evidence

Before developing detailed computational models of surface reactions for atmospheric aerosol, it is useful to examine observational data for events where these reactions are likely to be important. Detailed evaluation of observational data can lead to more specific hypotheses regarding the mechanisms of heterogeneous/surface processes. The first section in this chapter qualitatively describes a photochemical episode that exhibits evidence of sulfate formation on carbonaceous particles. The second section describes the evidence quantitatively, and the last section presents a brief summary of this chapter.

### *2.1 WOOD SMOKE EPISODE*

Biomass burning, including prescribed burning and forest wildfires, leads to substantial atmospheric emissions of particulate matter and other pollutants. These emissions may significantly impact air quality over length scales of hundreds to thousands of kilometers during periods of intense fire activity (Crutzen and Andreae 1990).

During August and September 2000, air quality in the Houston area was significantly impacted by forest fires. This period will be referred to as the wood smoke episode. This episode coincided with two coordinated air quality field studies, the Texas Air Quality Study (TexAQS 2000), and the Gulf Coast Aerosol Research and Characterization experiment (GC-ARCH or the Houston PM Supersite). Consequently, for this period, extensive modeling data sets and observational data are available.

The period of most intense fire activity was August 30 to September 8, with the highest fire emissions occurring on September 4 and 6. Junquera et al. (2005) developed a detailed inventory of fire locations and emissions for this period and reported that, on some days, total fine PM emissions from fires exceeded 300,000 kg/day. In contrast to the intense fire activity that occurred from August 30 through September 8, relatively little fire activity occurred from the beginning of August until August 28, in the Houston area. Figure 2.1 shows ambient $PM_{2.5}$ concentrations, recorded at six monitors using

Tapered Element Oscillating Microbalances (TEOM), on days with low and high fire activity.

24-hour averaged $PM_{2.5}$ and sulfate mass concentrations for this period are shown in Table 2.1. The average values for the August 25-28 period represent conditions on days with low fire activity, and September 4-6 are days with intense fire activity. Sulfate concentrations averaged 13.50 and 3.81 $\mu g/m^3$ on September 6 and August 25-28, respectively. These data indicate that during days with intense fire activity, both high particulate matter concentrations and high sulfate concentrations were observed. Additional data, with finer temporal resolution, lead to the same conclusion. Table 2.2 shows hourly average sulfate concentrations at three sites in the Houston area and Figure 2.2 shows sulfate concentrations measured using an Aerodyne Aerosol Mass Spectrometer on days with low and high fire activity. Figure 2.3 shows the locations of the sampling sites identified in Tables 2.1 and 2.2 and Figures 2.1 and 2.2.

**Table 2.1.** Average sulfate concentrations and total $PM_{2.5}$ mass ($\mu g/m^3$, measured using filter samples), for days with extensive fires (September 4-6) and days with few fires (August 25-28) (Russell et al. 2004b)

| | 4-Sep | | 5-Sep | | 6-Sep | | 25-28 Aug | |
|---|---|---|---|---|---|---|---|---|
| Site Description | Sulfate | Total Mass | Sulfate | Total Mass | Sulfate | Total Mass | Sulfate | Total Mass |
| Channelview C15/C115 | 5.39 | 17.30 | 8.39 | 27.40 | 16.00 | 38.40 | 3.89 | 10.18 |
| Conroe C65 | NA | NA | 8.07 | 25.40 | 11.60 | 24.50 | 4.22 | 14.90 |
| Galveston Airport C34/C109/C152 | 4.94 | 12.20 | 7.44 | 24.20 | 13.30 | 43.20 | 3.41 | 7.08 |
| Houston Aldine C8/C108/C150 | 5.61 | 18.70 | 7.62 | 27.00 | 13.30 | 43.60 | 3.99 | 10.55 |
| Houston Bayland Park C53/C146/C181 | 5.12 | 15.40 | 6.91 | 21.60 | 12.60 | 39.50 | 3.43 | 7.53 |
| Houston Deer Park 2 C35/139 | 6.92 | 18.00 | 7.43 | 27.30 | 13.95 | 42.80 | 3.32 | 8.05 |
| HRM-3 Haden Road C603/C114 | 7.90 | 18.10 | 8.26 | 27.00 | 14.20 | 38.70 | 4.52 | 15.15 |
| La Porte Airport during TEXAQS | 5.63 | 16.71 | 7.52 | 27.71 | 13.06 | 42.21 | 3.73 | 8.12 |
| Avg. of all sites ($ug/m^3$) | 5.98 | 16.62 | 7.70 | 25.95 | 13.50 | 39.11 | 3.81 | 10.19 |

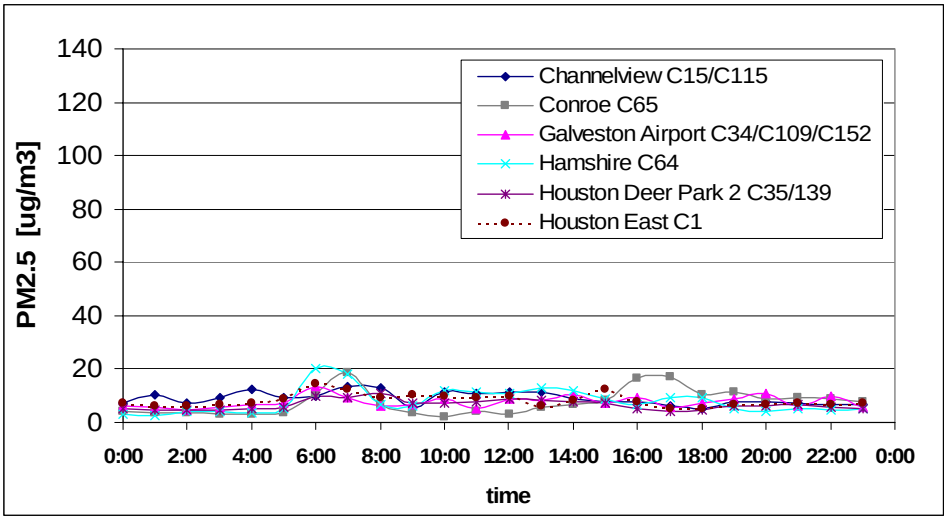


(a)

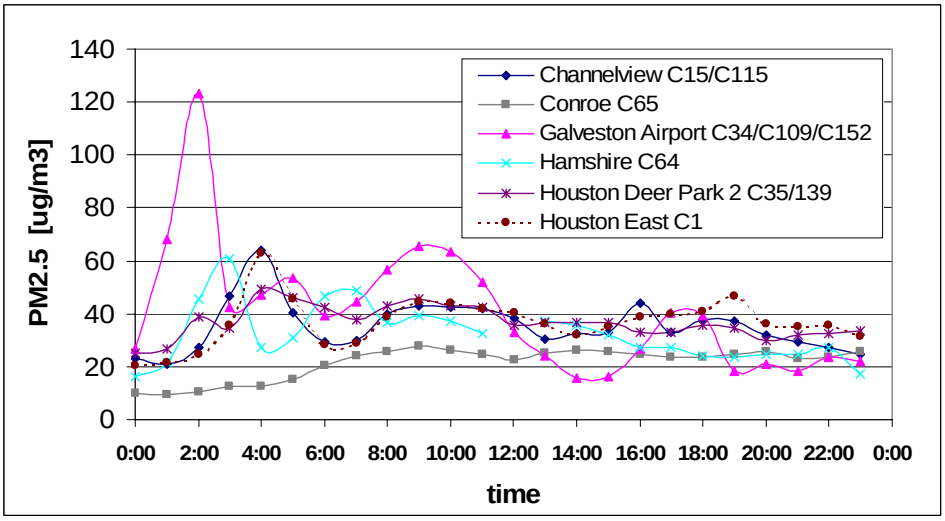


(b)

**Figure 2.1.** $PM_{2.5}$ concentrations, as measured by TEOMs, for (a) a period with few fire events - August 25 - 28, 2000 (b) a day with extensive emissions from fires -September 6 (Russell et al. 2004)

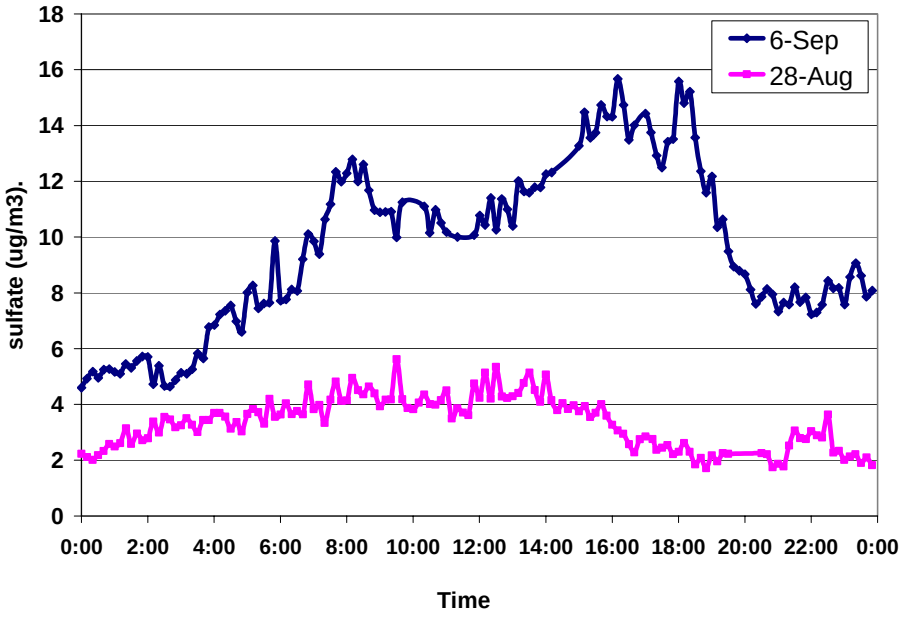


**Figure 2.2.** Sulfate concentrations (μg/m$^3$, 10 minute average, measured at the LaPorte site (LAP), using an Aerodyne Aerosol Mass Spectrometer), for a day with extensive fires (September 6) and a day with few fires (August 28) (Canagaratna et al. 2005)


**Figure 2.3.** Measurement sites for TEOMs (black dots) and near real-time sulfate monitors (red dots)

**Table 2.2.** Sulfate concentrations ($\mu g/m^3$, hourly average, measured at the Aldine(ALD) and LaPorte (LAP) sites in Houston, using an Aerodyne Aerosol Mass Spectrometer and flash volatilization), for days with extensive fires (September 4, 6) and a day with few fires (August 28) (Canagaratna et al. 2005)

| DATE | 28th August | | 4th September | | 6th September | |
|---|---|---|---|---|---|---|
| Time | ALD | LPT | ALD | LPT | ALD | LPT |
| 0:00 | 1.94 | 2.28 | 4.33 | 2.90 | 5.90 | 5.16 |
| 1:00 | 2.28 | 2.80 | 4.30 | 2.86 | 5.64 | 5.47 |
| 2:00 | 2.45 | 3.30 | 4.06 | 2.31 | 5.52 | 4.90 |
| 3:00 | 2.69 | 3.39 | 3.81 | 2.34 | 5.30 | 5.91 |
| 4:00 | 2.28 | 3.41 | 3.61 | 2.41 | 5.92 | 7.29 |
| 5:00 | 2.45 | 3.71 | 3.60 | 2.53 | 6.15 | 8.09 |
| 6:00 | 2.27 | 3.94 | 3.58 | 2.75 | 7.65 | 8.85 |
| 7:00 | 2.84 | 4.10 | 3.30 | 2.47 | 9.09 | 11.30 |
| 8:00 | 3.25 | 4.47 | 3.54 | 2.69 | 11.01 | 11.82 |
| 9:00 | 3.69 | 4.31 | 3.48 | 1.87 | 12.03 | 10.76 |
| 10:00 | 2.80 | 4.18 | 3.97 | 2.56 | 13.32 | 10.58 |
| 11:00 | 7.42 | 3.94 | 5.52 | 4.29 | 13.80 | 10.29 |
| 12:00 | 4.32 | 4.58 | 6.22 | 5.12 | 14.61 | 10.81 |
| 13:00 | 4.58 | 4.67 | 7.54 | 5.80 | 14.96 | 11.85 |
| 14:00 | 3.05 | 3.92 | 7.06 | 5.99 | 15.93 | 14.19 |
| 15:00 | 4.19 | 3.68 | 6.79 | 5.44 | 17.31 | 14.47 |
| 16:00 | 4.11 | 2.75 | 6.92 | 5.44 | 20.96 | 13.62 |
| 17:00 | 3.45 | 2.44 | 6.59 | 7.21 | 21.78 | 13.28 |
| 18:00 | 2.39 | 2.12 | 7.12 | 9.90 | 20.60 | 9.48 |
| 19:00 | 3.17 | 2.15 | 7.72 | 9.09 | 19.29 | 7.83 |
| 20:00 | 2.29 | 2.02 | 6.68 | 7.62 | 19.25 | 7.69 |
| 21:00 | 2.57 | 2.66 | 6.74 | 6.62 | 16.34 | 7.87 |
| 22:00 | 2.48 | 2.66 | 6.86 | 6.22 | 14.90 | 8.32 |
| 23:00 | 2.75 | 2.01 | 6.93 | 5.06 | 14.62 | 8.38 |

### *2.2 OBSERVATIONAL EVIDENCE FOR SULFATE FORMATION ON CARBONACEOUS PARTICLES*

The high concentrations of sulfate on high fire days could be due to direct emission of sulfate from the forest fires, or due to displacement of chloride in the fire emissions by sulfate, or due to secondary aerosol formation through chemical reactions, possibly heterogeneous reactions.

The primary evidence suggesting that direct emissions from fires are not the cause of the high sulfate concentrations observed during the fire events comes from chemical composition studies of wood smoke. Hays et al. (2002) investigated $PM_{2.5}$ emissions from open burning of fine (foliar) fuels, pine species, common to fire-prone Southeast Texas ecosystems. Non-detectable mass of sulfate was reported. A small fraction of

elemental sulfur was observed, but the fraction was far less than the sulfate mass observed in ambient particles during the fire events.

Another line of evidence indicating that direct emissions from biomass burning produce low sulfate concentrations is based on analyses using the compound levoglucosan (1,6-anhydro-$\beta$-D-glucose) as a wood smoke tracer. Pine and oak wood smoke profiles (and especially levoglucosan concentrations) from the work of Schauer et al. (2001) were employed, along with ambient measurements of levoglucosan, to estimate the contributions of fire emissions to particulate matter

Yue and Fraser (2004) measured polar organic species including levoglucosan from fine particle samples collected at three sites (La Porte, Aldine and HRM-3) in the Houston area during TexAQS2000. These data were used to estimate the contribution of wood burning to ambient particulate matter mass (see Table 2.4) and other particle components, such as sulfate (see Table 2.5). To perform these calculations, ambient levoglucosan concentrations (shown in the second column of Table 2.4-2.5) were multiplied by ratios of particulate matter to levoglucosan determined in source profiles experiments performed by Schauer et al (1996) (shown in Table 2.3). Pine and hardwood oaks account for a majority of the biomass in Texas (Wiedinmyer et al. 2001), thus, the source profiles (PM emitted/levoglucosan emitted) for both pine burning and oak burning were multiplied by the observed levoglucosan concentrations. This yielded estimates of the amount of PM in the observed aerosol that were due to fires, assuming that pine was the fuel and assuming oak was the fuel. As shown in Table 2.4, the differences in the estimated contributions of fires do not depend on the assumption of fuel type. For both fuel assumptions, wood smoke contributed between 10% and 30% of PM mass at the Aldine site on September 6 and 8, respectively. However, the same calculation procedure for sulfate (multiplying observed levoglucosan by the ratio of sulfate to levoglucosan in source tests) leads to the conclusion that the direct emission of sulfate contributed by wood burning was less than 1% of observed ambient sulfate concentrations.

**Table 2.3.** Reported Wood Smoke Emission and Calculated ratios of each compound to levoglucosan. Source[a]: Schauer et al (2001)

| | Fireplace wood Combustion | |
|---|---|---|
| | **Pine** | **Oak** |
| **Emission[a] (mg/Kg of wood burned)** | | |
| Levoglucosan (mg/kg) | 1375 | 706 |
| Fine PM (g/Kg of wood burned) | 9.5 ± 1 | 5.1 ± 0.5 |
| Sulfate (mg/Kg) | 11.4 | 20.91 |
| **Weight Ratio of compound to levoglucosan** | | |
| Sulfate/Levoglucosan | 0.008 | 0.030 |
| Fine PM/Levoglucosan | 6.9 | 7.2 |

**Table 2.4.** Ambient Levoglucosan concentrations (ng/m$^3$) and PM2.5 concentrations (ug/m$^3$) at monitoring sites in Houston area and estimated PM2.5 concentrations and percentage of PM2.5 mass due to fires (assuming pine and oak as fuels).

| | Ambient | | Estimated PM2.5 from fires | | | |
|---|---|---|---|---|---|---|
| | Levoglucosan[a] | PM2.5[b] | Assuming Pine as fuel | | Assuming Oak as fuel | |
| Date | ng/m$^3$ | ug/m$^3$ | ug/m$^3$ | % PM2.5 from fires | ug/m$^3$ | % PM2.5 from fires |
| | | | Aldine | | | |
| 27-Aug | 150.75 | 9.6 | 1.04 | 10.85 | 1.09 | 11.34 |
| 2-Sep | 205.34 | 16.6 | 1.42 | 8.55 | 1.48 | 8.94 |
| 6-Sep | 593.68 | 43.6 | 4.1 | 9.41 | 4.29 | 9.84 |
| 8-Sep | 565.39 | 13.3 | 3.91 | 29.37 | 4.08 | 30.71 |
| | | | HRM-3 | | | |
| 27-Aug | 20.83 | 14.5 | 0.14 | 0.99 | 0.15 | 1.04 |
| 2-Sep | 63.24 | 17.4 | 0.44 | 2.51 | 0.46 | 2.63 |
| 6-Sep | 184.87 | 38.7 | 1.28 | 3.3 | 1.34 | 3.45 |
| 8-Sep | 460.88 | 11.8 | 3.18 | 26.99 | 3.33 | 28.21 |
| | | | La Porte | | | |
| 27-Aug | 133.93 | 8.7 | 0.93 | 10.63 | 0.97 | 11.11 |
| 2-Sep | 101.86 | 15.3 | 0.7 | 4.59 | 0.74 | 4.8 |
| 6-Sep | 393.39 | 42.2 | 2.72 | 6.44 | 2.84 | 6.73 |
| 8-Sep | 287.6 | 11.5 | 1.99 | 17.22 | 2.08 | 18 |

Source: [a] Yue and Fraser (2004), [b] Russell et al. (2004b)

**Table 2.5.** Ambient Levoglucosan concentrations ($ng/m^3$) and sulfate concentrations ($ug/m^3$) at monitoring sites in Houston area and estimated sulfate concentrations ($ng/m^3$) and percentage of sulfate mass that biomass (pine and wood) burning contributed to.

| | Ambient | | Estimated sulfate | | | |
|---|---|---|---|---|---|---|
| | Levoglucosan[a] | Sulfate[b] | Assuming Pine as fuel | | Assuming Oak as fuel | |
| Date | $ng/m^3$ | $ug/m^3$ | $SO_4$ | % $SO_4$ from fires | $SO_4$ | % $SO_4$ from fires |
| | | | Aldine | | | |
| 27-Aug | 150.75 | 4.23 | 1.25 | 0.03 | 4.46 | 0.11 |
| 2-Sep | 205.34 | 6.41 | 1.7 | 0.03 | 6.08 | 0.09 |
| 6-Sep | 593.68 | 13.3 | 4.92 | 0.04 | 17.58 | 0.13 |
| 8-Sep | 565.39 | 4.34 | 4.69 | 0.11 | 16.75 | 0.39 |
| | | | HRM-3 | | | |
| 27-Aug | 20.83 | 4.87 | 0.17 | 0 | 0.62 | 0.01 |
| 2-Sep | 63.24 | 6.75 | 0.52 | 0.01 | 1.87 | 0.03 |
| 6-Sep | 184.87 | 14.2 | 1.53 | 0.01 | 5.48 | 0.04 |
| 8-Sep | 460.88 | 4.79 | 3.82 | 0.08 | 13.65 | 0.28 |
| | | | La Porte | | | |
| 27-Aug | 133.93 | 4.72 | 1.11 | 0.02 | 3.97 | 0.08 |
| 2-Sep | 101.86 | 7.94 | 0.84 | 0.01 | 3.02 | 0.04 |
| 6-Sep | 393.39 | 13.06 | 3.26 | 0.02 | 11.65 | 0.09 |
| 8-Sep | 287.6 | 4.43 | 2.38 | 0.05 | 8.52 | 0.19 |

Source: [a] Yue and Fraser (2004), [b] Russell et al. (2004b)

Buzcu et al. (2005) employed the same pine and oak wood smoke profiles in a source apportionment model, and concluded that secondary sulfate represents almost all sulfate measured at three sites in Houston. Moreover, secondary sulfate increased 40-43% at each site during the wood smoke episode. This analysis provides additional evidence indicating that direct primary emissions from wildfire smoke did not play a role in creating high sulfate concentrations in ambient particulate matter.

The data summarized to this point suggest that direct emissions of sulfate from fires are not the cause of the high sulfate concentrations observed during the fire period. Another possible cause of the high concentrations of sulfate on high fire days could be displacement of chloride in the fire emissions by sulfate.

Particulate matter from fires is emitted at high temperature. At these temperatures, many inorganic materials, such as KCl, volatize and then condense onto particle surfaces. Chloride displacement occurs when $SO_2$ and atmospheric $O_2$ react with KCl forming

particulate phase $K_2SO_4$. If sulfate substituted all chlorides, 1 mol $SO_4^{2-}$ will displace 2 mol of $Cl^-$. With this assumption, the maximum possible $SO_4^{2-}$ mass generated through this sulfur displacement reaction can be estimated by using known values of Cl mass per total carbon or per total particle mass in fire emissions. By converting Cl mass to a molar basis and applying a factor of 2 and sulfate molecular weight, the estimated mass of $SO_4^{2-}$ formation via chloride displacement can be obtained. Table 2.6 shows estimated $SO_4^{2-}$ formation using Cl mass from various literature sources. The estimation suggests that chloride displacement involving particles released during the burning of pine and oak, which account for a majority of the biomass in Texas, contribute less than 5 percent of the sulfate mass observed in fine particles during the wood smoke episode. It should be noted, however, that chloride concentrations vary significantly, depending on type of biomass, stage of fire and its intensity. Hays et al. (2002) showed that mass ratio of Cl/total carbon was about 0.045 for Western Hemlock (pinus) fires. Cachier et al. (1996) reported that the average mass ratio of chloride/total carbon during an African fire was about 0.105. Other data on Cl content in fire emissions are shown in Table 2.6. But even with this uncertainty, overall mass balances indicate that chloride displacement is not the dominant cause of high sulfate concentrations during the wood smoke episode.

Additional evidence supporting the conclusion that chloride displacement is a relatively minor contributor to the high sulfate concentrations observed during the wood smoke episode is provided by potassium concentrations. If chloride displacement were significant, relatively high potassium concentrations should be observed. Concentrations of potassium measured in various monitoring sites in the Houston-Galveston area are shown in Figure 2.4. These concentrations are two orders of magnitude lower than sulfate concentrations. Moreover, there is no relationship between these two concentration profiles. This analysis provides additional evidence indicating that Cl-displacement is not a major contributor to high sulfate concentrations observed in Houston area. However, its effect should not be overlooked.

**Table 2.6.** PM2.5 and Chlorine concentrations from biomass burning and estimated sulfate formed through chloride displacement (Tot C = total carbon, Tot PM = total fine particles)

| Ref | Fuel Type | Species /Locations | Tot C/PM2.5 | Cl/Tot C | $\%SO_4^{2-}$/Tot C if all Cl replaced by sulfate | $\%SO_4^{2-}$ in PM mass if all Cl replaced by sulfate |
|---|---|---|---|---|---|---|
| (Hays et al. 2002) | Various Pinus Foliar fuels | West Hemlock | 0.75 | 0.045 | 12.223 | 4.333 |
| | | Loblolly | | ND | | |
| (Schauer et al. 2001) | Fireplace Wood fuels | Pine wood | 0.574 | 0.008 | 1.087 | 0.624 |
| | | Oak wood | 0.623 | 0.005 | 0.700 | 0.436 |
| (Cachier H. 1996) | Prescribed Fire Savanna biomass | Lamto | 70 | 0.054 | 7.268 | 5.087 |
| | | KNP | 46 | 0.105 | 14.130 | 6.500 |
| | | | | **Cl/Tot PM** | | **$\%SO_4^{2-}$ in PM mass if all Cl replaced by sulfate** |
| (Robinson et al. 2004) | Prescribed Fire Flaming stage Ponderosa pine | Crowley | | 0.002 | | 0.29 |
| | | A1 Mt | | 0.001 | | 0.15 |
| | | Woody Mt | | 0.001 | | 0.13 |
| | | Belmont | | 0.0004 | | 0.06 |
| | | Botanica-Park (grassland fire) | | 0.015 | | 2.08 |

*All ratio values are based on mass

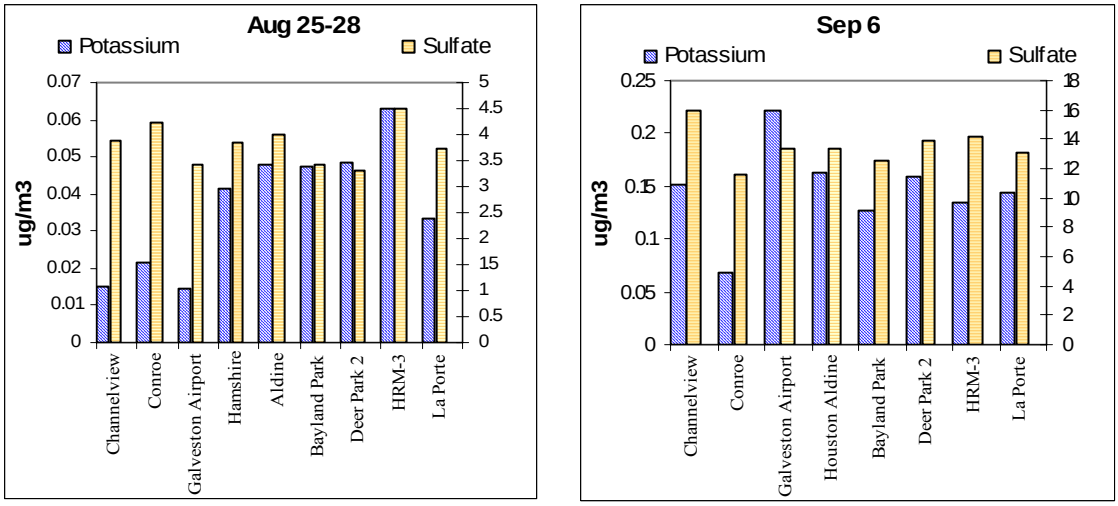


**(a)** **(b)**

**Figure 2.4.** Potassium and Sulfate concentrations measured at various monitors in HGBPA Subdomain; (a) on August 25th-28th, 2000 (average over the period), (b) on September 6th, 2000. (Left axis applies to Potassium and right applies to sulfate)

If direct emissions of sulfate and chloride displacement do not explain the observed sulfate, then it is likely that other chemical reactions transforming $SO_2$ to sulfate are the dominant source. Chemical pathways for $SO_2$ oxidation to sulfate include (1) the homogeneous oxidation of $SO_2$ by OH• in the gas phase, (2) the condensed-phase reactions of $SO_2$ with active oxidants such as peroxides and ozone, and (3) the heterogeneous reactions of $SO_2$ on non-aqueous carbonaceous particles (more detail on oxidation pathways is available in Appendix A)

(1) In the gas phase, $SO_2$ reacts with OH radical to form $H_2SO_4$ and $H_2SO_4$ condenses on available particles. This homogeneous reaction can produce very high sulfate concentrations if the atmosphere has significant $SO_2$ and OH• mixing ratios. Figure 2.5 shows that $SO_2$ concentrations on days with and without intense fire activity were comparable, at the La Porte site. In addition, as shown in Figure 2.6, OH• measurements imply persistent diurnal distributions throughout the measurement period, with no evidence of elevated concentrations during the wood smoke episode. These data suggest that $SO_2$ and OH• concentrations were not particularly elevated during days of

intense fire activity, so observational data indicate that gas phase reactions do not explain the enhanced sulfate formation during the wood smoke episode; regional photochemical modeling calculations reported later in this thesis also confirm this.

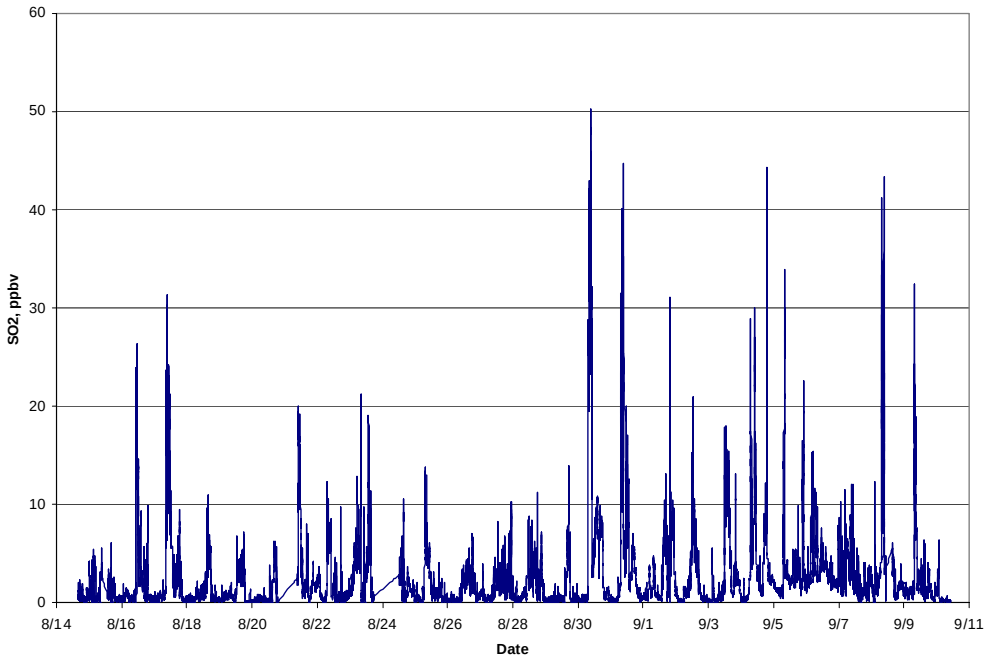


**Figure 2.5.** Sulfur dioxide concentrations at La Porte site during the Texas Air Quality Study, in ppbv. Source: ftp.al.noaa.gov (accessed on 7/3/2003)

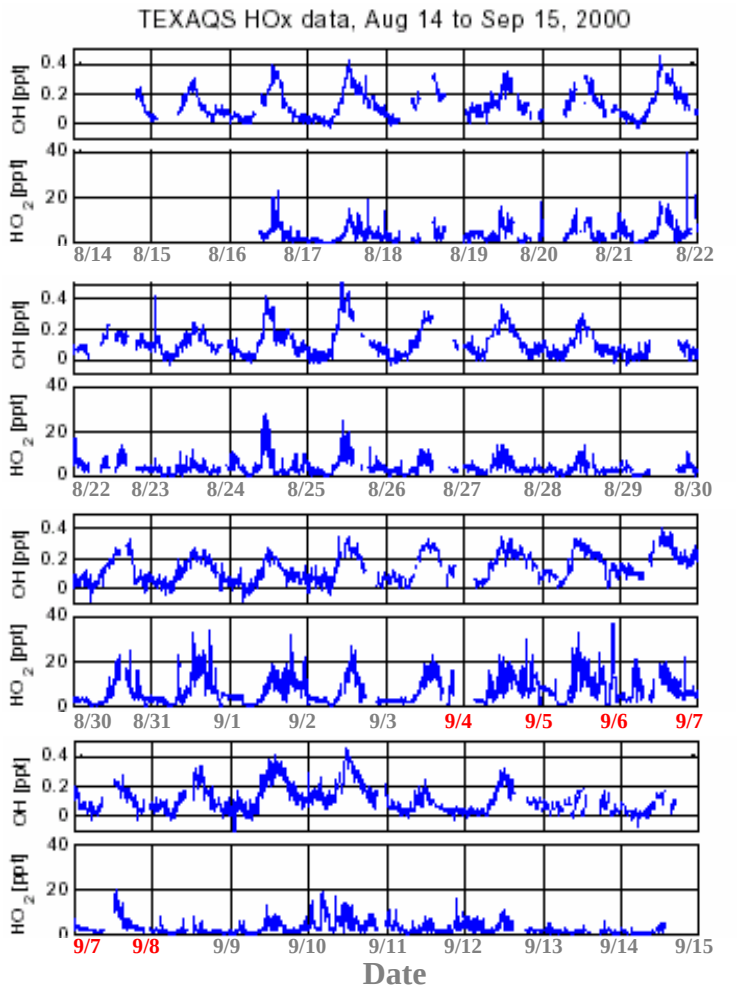


**Figure 2.6.** Free radical concentrations measured at the La Porte site during the Texas Air Quality Study; a number of days exhibit high $HO_2$ concentrations at night. Days with intense fires are highlighted in red Source: (Martinez et al. 2001)

(2) Hydration of wood smoke particles leads to increased aqueous phase volumes and aqueous phase reactions. Wood smoke particles are initially emitted as dry and relatively hydrophobic materials; these hydrophobic particles can then undergo atmospheric reactions, making them hydrophilic and able to take up water. The volume of water taken up by the particles will depend not only on the particle mass available, but also on the size distribution of the particles. High-flow differential mobility analyzers (DMAs) were used to collect aerosol size distributions at downwind sites, and typical data are presented in Figure 2.7 (Gasparini et al. 2004). Although TDMA measurements

were not made during this time period, a growth factor of about 1.4 was observed at a Houston site during summer conditions for a dry diameter of 0.16 microns. This growth factor falls between values reported in literature studies for biomass burning (Hameri et al. 2001; Zhou 2001).

A preliminary estimate of the volume of aqueous phase available for sulfate formation can be made by applying the growth factor of 1.4 to the size distributions of particles collected at Laporte on 6$^{th}$ Sep, 2000, shown in Figure 2.7. The size distribution can be broken down to number counts for each size bin. For each size bin, an initial volume and a final volume after growth can be calculated. The difference between these two volumes is the volume of water added onto particles.

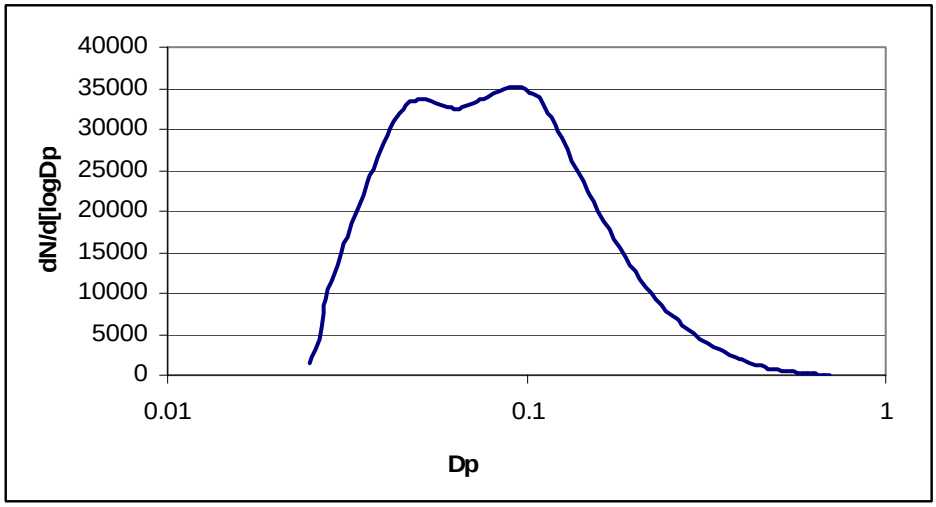


**Figure 2.7.** Aerosol size distributions and number concentrations (cm$^{-3}$) collected at Laporte, Houston on 6$^{th}$ Sep, 2000. Source: http://eosweb.larc.nasa.gov/project/narsto/table_narsto.html#houston

An upper bound estimate of the volume of aqueous phase condensed onto wood smoke particles (roughly 50 μg/m$^3$), together with upper bound estimates of the aqueous concentration of $SO_2$ (based on the maximum observed gas phase $SO_2$ concentration of 66 ppbv) and the aqueous oxidation rate [500% h$^{-1}$, (Seinfeld and Pandis 1998)] lead to a sulfate formation rate of only 2x10$^{-13}$ g m$^{-3}$ h$^{-1}$. This upper bound suggests that the

increase in the volume of aqueous phase in the atmosphere due to wood smoke, with no new chemistry due to the wood smoke, is not likely to explain the high sulfate concentrations during the wood smoke episode.

(3) Thus, only gas-particle-phase surface reactions are left as a possible explanation for the sulfate formation observed in the wood smoke episode. Conversion of $SO_2$ gas into sulfate aerosol has been observed on the surface of carbonaceous particles (Brodzinsky et al. 1980; Mamane and Gottlieb 1989; Novakov T. 1974). In addition to directly forming sulfate, these reactions of $SO_2$ with carbonaceous particles can convert hydrophobic particle surfaces into hydrophilic surfaces. A variety of mechanisms for $SO_2$ oxidation reactions on carbonaceous surfaces have been proposed, involving a variety of oxidizing species (Baldwin 1982; Britton and Clarke 1980; Liberti et al. 1978; Novakov T. 1974; Tartarelli et al. 1978).

In this work, our focus will not be on evaluating mechanisms, but rather demonstrating that rates of heterogeneous reactions can be sufficiently high to explain the observed sulfate enhancements during the wood smoke episode. In the next chapter, photochemical air quality modeling is used to characterize the magnitude of sulfate formation due to various reaction mechanisms. The modeling results will demonstrate that homogeneous and condensed phase reactions are sufficient to accurately predict sulfate concentrations on days with no fires, but not on days with fires.

# Chapter 3: Sulfate Formation
# Part 2: Computational approach

As described in chapter 2, observational data collected during a wood smoke episode in southeast Texas led to the conclusion that the formation of secondary sulfate was significantly enhanced by the presence of the wood smoke. A variety of possible explanations of the enhanced sulfate formation were examined, and eliminated until only gas-particle-phase surface reactions are left to explain the enhanced sulfate formation. In order to evaluate heterogeneous/surface oxidation mechanisms, it will be necessary to employ air quality models. Photochemical air quality modeling will be used in this work to characterize the magnitude of both homogeneous and heterogeneous reaction mechanisms. If the model performs acceptably during periods when heterogeneous processes are not expected to be important (periods other than the wood smoke episode), then these same emission and meteorological inputs can be used under conditions when heterogeneous processes are expected to be significant.

The first section in this chapter presents an overview of photochemical grid model used in this work. The second section describes an impingement calculation approach for modeling gas-particle-phase surface reactions, followed by model performance evaluation and modeling results. Finally, a brief summary concludes the chapter and highlights the important findings from the modeling.

### *3.1 PHOTOCHEMICAL MODELING*

Regional photochemical models were used to investigate processes that could lead to enhanced formation of secondary sulfate. Regional photochemical models simulate emission, chemical transformation, horizontal advection and diffusion, vertical transport and diffusion, dry deposition, and wet deposition of species in the atmosphere. Although any comparable photochemical grid model could be used, the comprehensive air quality model with extensions (CAMx) (ENVIRON 2005) was selected for this study because it is currently being used by the State of Texas for attainment demonstrations in areas that have violated the National Ambient Air Quality Standards for ozone. Several model

performance evaluations have been performed on the photochemical model formulations used in this work (ENVIRON 2003; AER 2003)

The modeling domain was a nested regional/urban scale 36-km/12-km/4-km grid, shown in Figure 3.1. The episode period was August 22 - September 6, 2000. Meteorological inputs required by the model were based on results from the Mesoscale Meteorological Model, version 5, MM5 (TCEQ 2004c). The volatile organic compound (VOC) and Nitrogen Oxides (NOx) emission inventories used as input for the modeling episode were prepared by the Texas Commission on Environmental Quality (TCEQ) in accordance with U.S. EPA guidance. A MOBILE6-based inventory was developed for on-road mobile source emissions; emissions for non-road mobile and area sources were developed using emission factors and the U.S. EPA's NONROAD model, using local activity data when available. Biogenic emission inventories were estimated using the GLOBEIS emission model with locally developed landcover data (TCEQ 2004a). Point source emissions were developed through a special inventory survey and were also estimated based on ambient data collected in the source region. Details of the VOC and NOx emission inventory development are available at *TCEQ, Houston /Galveston Air Quality Science Evaluation* (2004b).

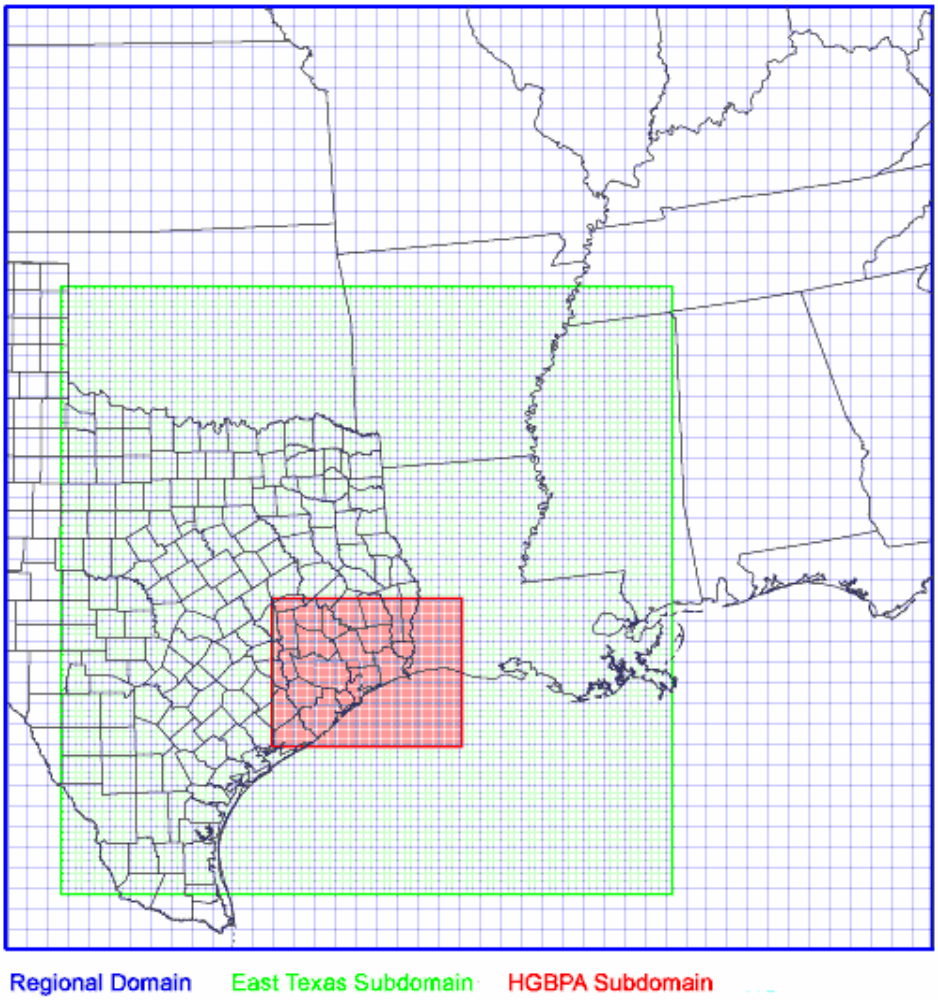


**Figure 3.1.** Modeling domain used in the study: The Regional, East Texas and Houston-Galveston-Beaumont-Port Arthur nested domains had 36, 12 and 4 km horizontal resolution, respectively.

For this work, emissions of $SO_2$ from all sources and particulate matter emissions from fires were added to the model inputs. The major sources of $SO_2$ were point sources. Data for point source $SO_2$ emissions in Texas for the year 2000 were obtained from the TCEQ point source database (TCEQ 2004a). For regions outside of Texas, $SO_2$ emissions were obtained from the US EPA 1999 National Emission Inventory (NEI99). (Available at http://www.epa.gov/ttn/chief/net/1999inventory.html#final3crit; accessed on 3/15/05). Annual emissions of some facilities in the NEI99 database were updated

with Louisiana Department of Environmental Quality's emission inventory dataset for the year 2000 (Available at http://www.deq.state.la.us/evaluation/eis/eisdata.htm; accessed on 3/15/05). The spatial distribution of these $SO_2$ point emissions in Texas and Louisiana is shown in Figure 3.2. $SO_2$ emissions from on-road and non-road mobile sources were also retrieved from the NEI99 database, and were adjusted to year 2000 values using growth factors.

Emissions from fires were based on the work of Junquera et al. (2005) and the locations of the fires on September 6, 2000 are shown in Figure 3.3. Wildfire emissions were uniformly distributed throughout the calculated plume rise height, which was based on the FIREPLUME model (Brown et al. 1999). Fire emissions were distributed uniformly throughout the day of the reported fire. If a fire burned for more than one day, the emissions were divided uniformly throughout the burning period. The original work of Junquera et al. (2005) did not include $SO_2$ emissions from fires. These emissions were added, based on an emission factor reported by Reddy and Venkataraman (2002b). The extent of $SO_2$ emissions from fires (Figure 3.3) was approximately 1% of the point source $SO_2$ emissions on days with high fire activity.

Both gas-phase and selected condensed phase $SO_2$ oxidation pathways mechanisms that are believed to be important in the atmosphere (Walcek and Taylor 1986) are incorporated in CAMx.

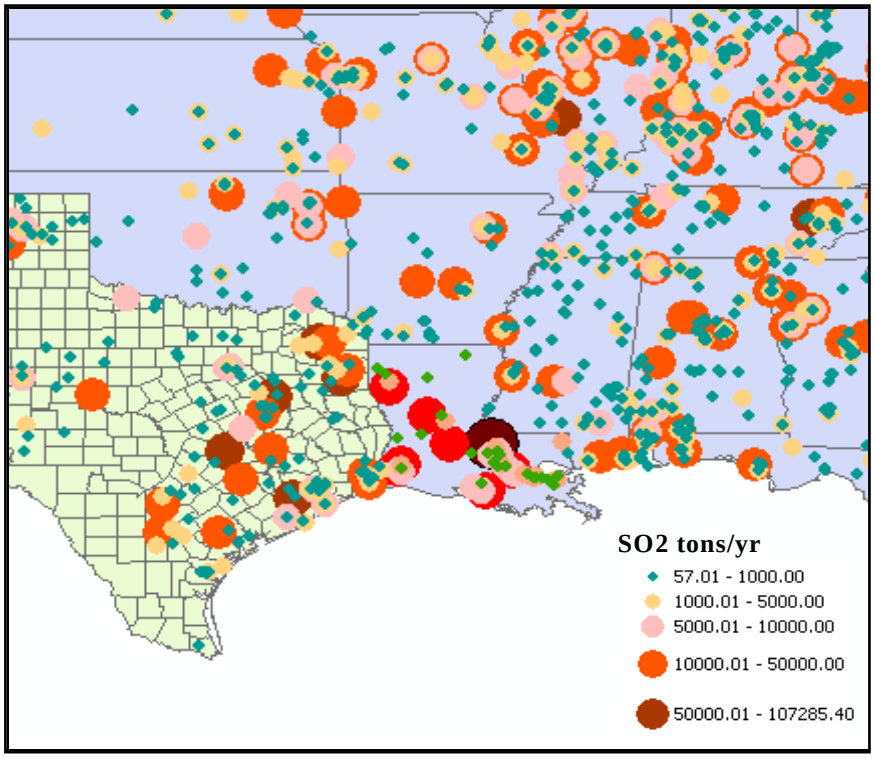


**Figure 3.2.** $SO_2$ point source emissions (tons/yr).

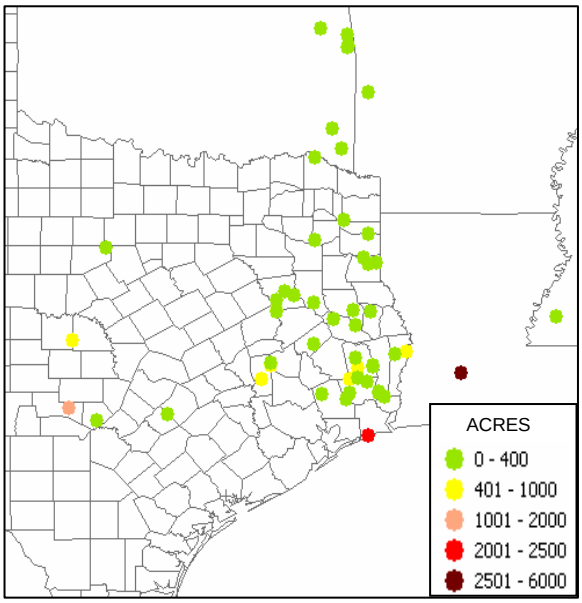


**Figure 3.3.** Fire locations on 6 September, based on the emission inventory of Junquera et al. (2005).

### *3.2 SULFATE FORMATION CHEMISTRY*

The oxidation of $SO_2$ in the gas phase occurs primarily via its reaction with hydroxyl (OH) radicals and water to form $H_2SO_4$, and $H_2SO_4$ condenses on available particles (Stockwell and Calvert 1983). The production of sulfuric acid in the gas phase is well quantified and can be modeled acceptably in current tropospheric chemistry models, including CAMx. Major aqueous-phase sulfate formation mechanisms in cloud or fog droplets include the reactions of dissolved $SO_2$ with $H_2O_2$, $O_3$ and $O_2$ (catalyzed by $Mn^{2+}$ and $Fe^{3+}$)(Seinfeld and Pandis 1998). These aqueous-phase reactions have been well studied and integrated in some air quality and cloud models, including those in CAMx (Walcek and Taylor 1986).

Conversion of $SO_2$ gas into sulfate aerosol has been observed on the surface of carbonaceous particles. A variety of mechanisms for $SO_2$ oxidation reactions on carbonaceous surfaces have been proposed, involving a variety of oxidizing species. It is difficult to generalize about the rates and extent of these reactions, however, since the reactions are sensitive to the chemical and physical nature of the surfaces and oxidants.

Because detailed mechanisms for sulfate formation on carbonaceous particles remain speculative, the approach that will be used in this work to estimate the rate of heterogeneous sulfate formation will be to multiply the surface impingement rate of gas phase $SO_2$ on wood smoke particle surfaces by an estimate of the fraction of the impinging molecules that adsorb and react. The fraction reacted is typically quantified in terms of a reactive uptake coefficient ($\gamma$) (Ullerstam et al. 2002; Ullerstam et al. 2003). The number of reactive collisions with the surface (the sulfate formation rate) is defined as the reactive uptake coefficient multiplied by the total number of surface collisions per unit time (Z).

$$d[SO_4^{2-}]/dt = \gamma \bullet Z \tag{3.1}$$

$$Z = \frac{1}{4} A[SO_2]\nu_{SO_2} \tag{3.2}$$

where v is the mean molecular velocity of $SO_2$, calculated as $\sqrt{8RT/\pi M_{SO_2}}$ and A is the effective particle surface.

CAMx codes were modified (see Appendix C) to account for these heterogeneous reactions and to distinguish the sulfate mass produced from the heterogeneous pathway. The rate of impingement of $SO_2$ onto fire particles was calculated for the modeling domain shown in Figure 3.1. The mass of fire particle emissions was taken from the emission inventory of Junquera et al. (2005) and the number of particles and available surface area was calculated by assuming a particle density of 1.5 g/cm$^3$ and an average particle diameter of 0.25 μm. The average particle diameter was based on the work of Reid et al. (2004), who listed aerosol volume median diameters for fresh smoke in the 0.25-0.3 μm range. Note that the hydration state of smoke particles was not distinguished here. The regional photochemical model was modified so that the rate of impingement of $SO_2$ onto fire particles was calculated for each one-hour time step in each grid cell. The magnitude and spatial distribution of sulfate formation via impingement predicted by the model with various reactive uptake coefficients was compared to observations during the wood smoke episode.

The fraction of $SO_2$ reacting to form sulfate, following impingement on carbonaceous particles, was calculated using a variety of reaction probabilities. In one set of simulations, γ was assumed to be constant over the entire modeling domain and the entire modeling period. However, it is possible that the reaction probability depends on the availability of other oxidant species such as $O_3$, $H_2O_2$ and $NO_2$. Therefore, values for γ were also scaled by the concentrations of each of these oxidants. In the scaling, a maximum value was established for the reaction probability and that maximum value was assumed to occur at the same time and location as the maximum value of the oxidant concentration during the simulation. Reaction probabilities for all other times and locations were assumed to be proportional to the ratio of the oxidant concentration at the time and location of interest, to the maximum oxidant concentration.

$$\gamma = \frac{\mathrm{Max}[\gamma]\,\mathrm{x}[\mathrm{Conc}_{\mathrm{oxidant}}]}{\mathrm{Max}[\mathrm{Conc}_{\mathrm{oxidant}}]} \tag{3.3}$$

For example, if the oxidant was assumed to be $H_2O_2$, the maximum concentration of $H_2O_2$ for the episode, over all locations, was identified. That grid cell, at the time of maximum concentration, was assigned a maximum reaction probability. If a particular model grid cell, at a particular time had a $H_2O_2$ concentration equal to half of the maximum value, the reaction probability for that grid cell would be assumed to be half of the maximum value.

### *3.3 MODELING RESULTS*

#### *3.3.1 MODEL PERFORMANCE EVALUATION*

Photochemical air quality model performance was assessed by comparing predicted ozone concentrations to observations and by comparing sulfate formation (on days without wood smoke) in power plant plumes to aircraft observations. Table 3.1 reports overall model performance in predicting ozone formation using standard EPA-recommended performance measures: relative bias, relative gross error, and unpaired peak accuracy. Model performance in predicting ozone concentrations was also evaluated by examining predicted and observed diurnal patterns in ozone concentration at specific sites. A time series of observed and modeled ozone concentrations at the La Porte site shown in Figure 3.4. Although there are discrepancies between observed and modeled peak ozone concentrations on some days, the overall performance was judged acceptable for air quality planning by the State of Texas.

**Table 3.1.** Base case model performance in Houston Galveston area (4km grid) (TCEQ 2004d)

| Episode Date | Data Pair w/ Observation > 60.0ppb | | *Site Daily Maximum* | | Area-wide Maximum ozone | | | | |
|---|---|---|---|---|---|---|---|---|---|
| | Normalized Bias (%) | Normalized Gross Error (%) | Normalized Bias (%) | Normalized Gross Error (%) | Accuracy (%) | Modeled | | Observed | |
| | | | | | | ppb | Hour (CST) | ppb | Hour (CST) |
| 08/24/2000 | -38.5 | 38.5 | -25.3 | 26.4 | -34.8 | 78.4 | 1300 | 120.1 | 1100 |
| 08/25/2000 | -9.9 | 20.9 | -5.9 | 20.3 | -19.3 | 156.5 | 1500 | 194.0 | 1300 |
| 08/26/2000 | 6.3 | 18.5 | 33.7 | 38.8 | 6.7 | 149.4 | 1500 | 140.0 | 1700 |
| 08/27/2000 | 25.2 | 25.2 | 25.7 | 25.7 | 29.0 | 112.3 | 1400 | 87.0 | 1700 |
| 08/28/2000 | 22.4 | 24.3 | 26.5 | 27.0 | 17.8 | 132.0 | 1500 | 112.0 | 1700 |
| 08/29/2000 | 8.1 | 15.8 | 16.9 | 21.1 | 3.1 | 151.2 | 1500 | 146.7 | 1500 |
| 08/30/2000 | -11.0 | 20.4 | -16.0 | 22.8 | -31.6 | 137.2 | 1600 | 200.5 | 1600 |
| 08/31/2000 | 4.6 | 15.8 | -5.1 | 13.6 | -1.4 | 173.0 | 1500 | 175.5 | 1600 |
| 09/01/2000 | 8.1 | 13.7 | 16.0 | 20.6 | -16.5 | 136.7 | 1500 | 163.7 | 1300 |
| 09/02/2000 | -2.7 | 17.2 | -0.8 | 12.4 | 21.7 | 152.7 | 1400 | 125.5 | 1400 |
| 09/03/2000 | -3.7 | 19.4 | 6.7 | 11.1 | 9.5 | 139.3 | 1400 | 127.2 | 1600 |
| 09/04/2000 | 5.5 | 20.4 | 16.5 | 21.2 | 8.9 | 158.0 | 1300 | 145.0 | 1200 |
| 09/05/2000 | 6.9 | 26.6 | 39.2 | 50.0 | 13.3 | 209.7 | 1400 | 185.0 | 1400 |
| 09/06/2000 | -5.1 | 18.9 | 3.2 | 18.0 | -2.0 | 152.9 | 1400 | 156.0 | 1300 |

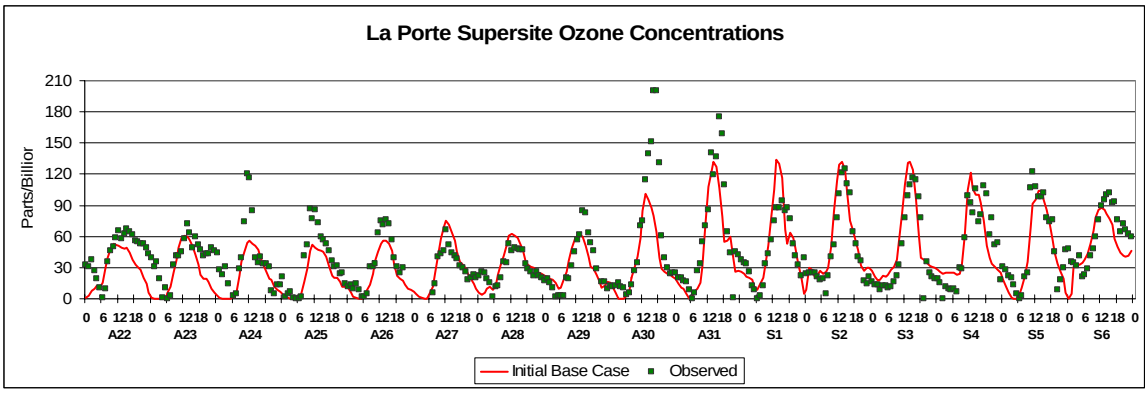


**Figure 3.4.** Modeled and observed surface layer ozone concentration at the La Porte monitoring site from August 22nd to September 8th, 2000 (TCEQ 2004d).

.

To assess the performance of the model in predicting sulfate formation via homogeneous and condensed-phase mechanisms, without addition of impingement

calculations, sulfate concentrations in a power plant plume were examined. Observations of volume concentrations of atmospheric particles ($\mu m^3 cm^{-3}$) from aircraft measurements (Brock et al. 2003) were compared to model predictions. The days examined were August 27th and 28th 2000; both of these days had few fire events. The aircraft data show a distinct plume from the Parish Power plant and it is assumed that the particulate in the plume will be dominated by sulfate. Characteristics of the plume transects made by the aircraft are shown in Table 3.2.

**Table 3.2.** Downwind distance of the plume transect, mean and maximum particle volume (V) concentrations, average $SO_2$ concentrations measured downwind of the Parish power plant and in background air southwest of Houston.

| Sources | Date | Distance (km) | Width (km) | Vmean[a] ($\mu m^3 cm^{-3}$) | Vmax[a] ($\mu m^3 cm^{-3}$) | $SO_{2,average}$ ppbv |
|---|---|---|---|---|---|---|
| Background | 27 August | NA[b] | NA | ~7 | NA | 0.50 |
| | 28 August | NA | NA | ~9 | NA | 0.75 |
| Parish | 27 August | 23 | ~ 11 | 9 | 12.2 | 10.8 |
| | 28 August | 18 | ~12 | 11.8 | 14.3 | 14.9 |

[a] Brock et al. (2003)
[b] NA = Not applicable

Figure 3.5(a) shows the location of the power plant source, the flight track of the NOAA/NCAR Electra aircraft on August 27, and the $SO_2$ measurements made by the aircraft. More detail of the $SO_2$ concentrations in the plume, across one of the transects made by the aircraft, is shown in Figure 3.5(b). Also shown in Figure 3.5(b) are modeled $SO_2$ concentrations in the plume. The model predicts a wider plume than indicated by observations and the modeled plume is displaced a few kilometers to the west of the observed plume at the measurement height of the aircraft. Nevertheless, both the model and the observational data indicate the same total quantity of $SO_2$ in the plume. The quantity of $SO_2$ in the plume was calculated using measured values of wind speed, mixing height and $SO_2$ concentration, shown in Table 3.3. The resulting $SO_2$ flux and total sulfur flux ($SO_2$ plus particulate sulfate based on particle volume measurements) agreed well with the emission rate used in the modeling.

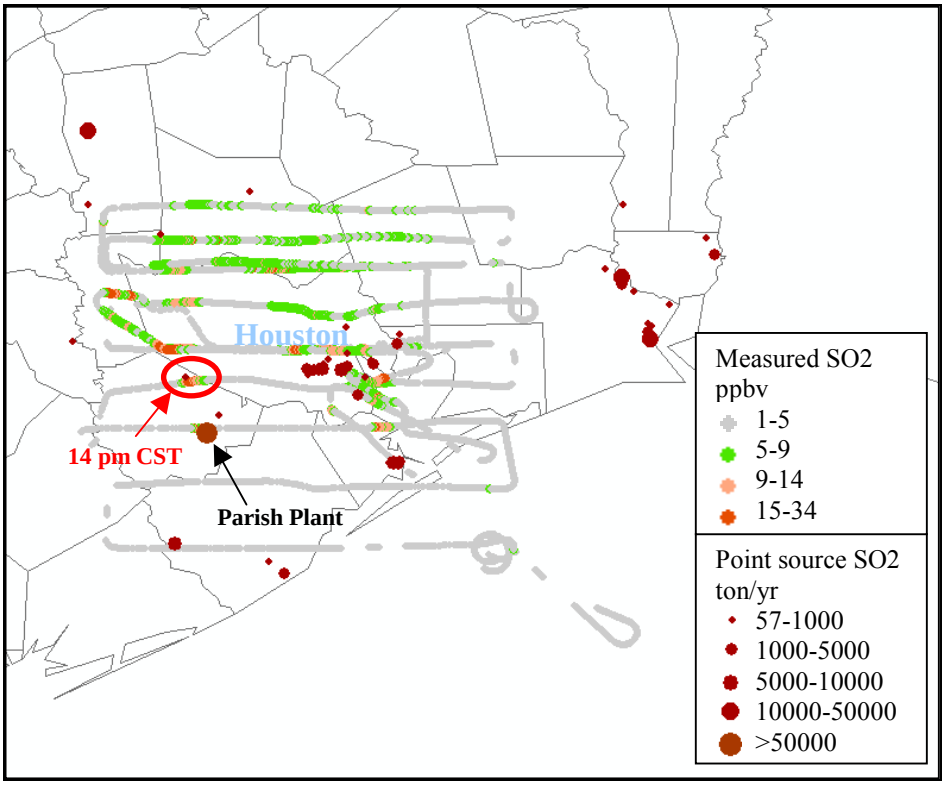


(a)

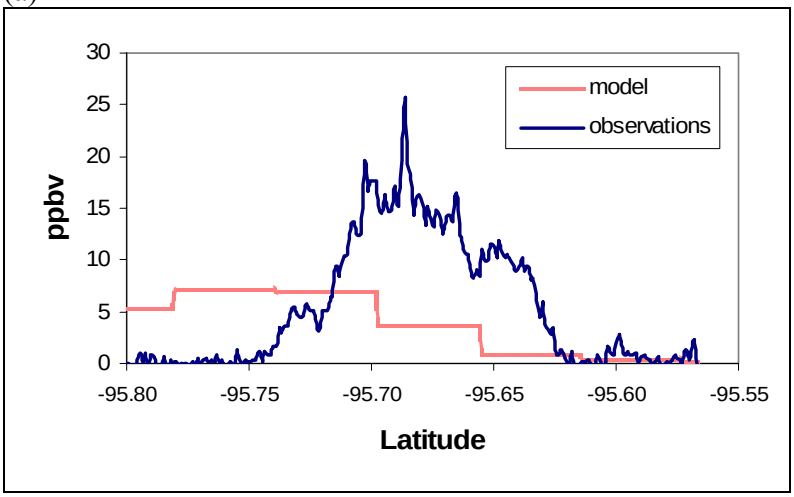


(b)

**Figure 3.5.** August 27, $SO_2$ concentrations measured by NOAA's Electra aircraft (a) $SO_2$ concentrations are presented in different colors, and $SO_2$ point sources are represented by different dot sizes. The Parish plume was detected by the aircraft at approximately 1400 hr. (b) Detail of the aircraft measurements and model predictions of $SO_2$ in the Parish plume

**Table 3.3.** Comparison of $SO_2$ in plume, based on aircraft measurements to emission inventory data used in modeling (PBL = Planetary Boundary Layer)

| Data | $SO_2$ ( kmol/hr ) |
|---|---|
| | 27-Aug |
| Emission rate used in modeling | 105.7 |
| Aircraft data | |
| Wind speed (m/s) | 3.5-4 |
| PBL(m.) | 1450-1850 |
| Mass flux of observed $SO_2$ | 105±20 |
| Mass flux of total sulfur species | 110±20 |

The fractional conversions of $SO_2$ to sulfate observed by the aircraft, assuming that all of the particulate observed in the plume, above background levels was sulfate, was 5% on the 27th. Similar values were observed for the 28th. CAMx predicts, for the elevation of the aircraft and the predicted location of the Parish plume, a fractional conversion of $SO_2$ of 6% on the 27th. Similar values were predicted for the 28th. Although the aircraft results assume that the entire observed aerosol volume is due to sulfate, which likely biases those values high, the results are very promising. It can be concluded that the model is predicting a fraction of $SO_2$ conversion to sulfate that is consistent with observations when wood smoke is not present.

In contrast, the sulfate produced by these conventional routes, through gas and aqueous phase chemistry, shown in Figure 3.6, does not replicate either the magnitude or the spatial and temporal distribution of sulfate concentrations on September 6th. The amount of sulfate formation that is predicted for most of the Houston area (2-6 $\mu g/m^3$) is consistent with observations on days without fire events, but is significantly less than the maximum observed sulfate concentrations (13-15 $\mu g/m^3$) observed on September 6. These simulations suggest that gas phase and non-catalytic aqueous phase sulfate formation mechanisms in CAMx cannot track sulfate formation under atmospheric conditions with high concentrations of wood smoke particles.

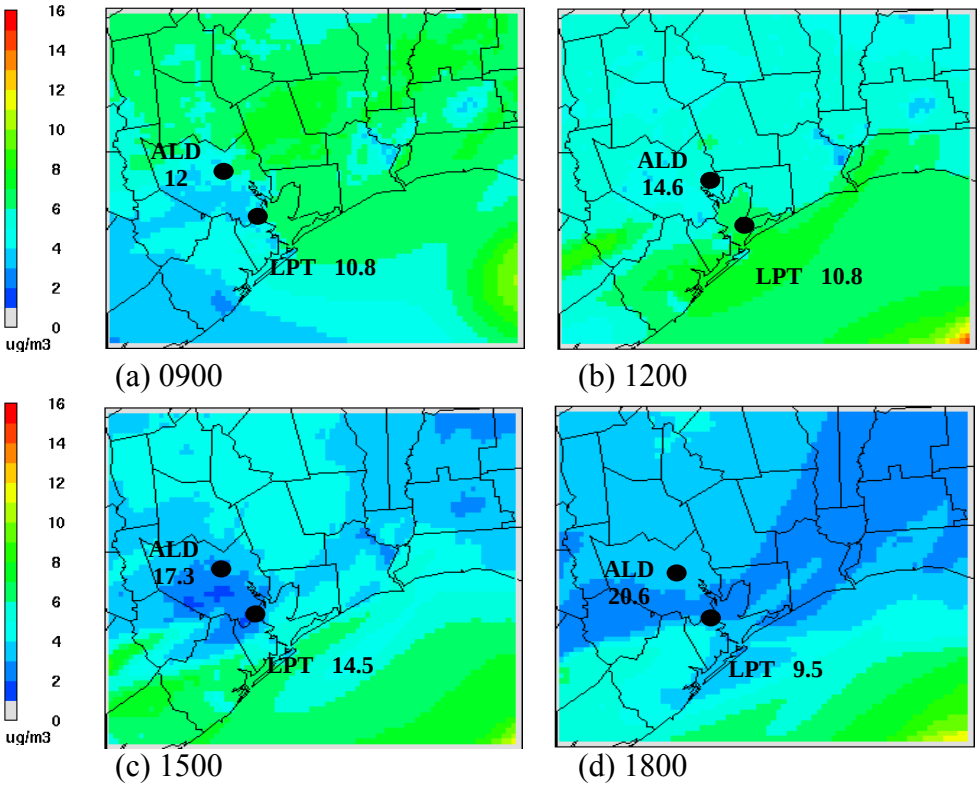


**Figure 3.6.** Ground level sulfate concentrations (μg/m$^3$) predicted by CAMx on Sep 6th at (a) 0900 h, (b) 1200 h., (c) 1500 h, and (d) 1800 h; simulations account for gas and aqueous-phase reaction pathways of $SO_2$ , but not surface reactions on wood smoke; observed sulfate concentrations (ug/m$^3$) at the La Porte (LPT) and Aldine (ALD) monitoring sites are also shown.

#### *3.3.2 GAS-PARTICLE-PHASE SURFACE REACTIONS MODELING*

Figure 3.7 shows the sulfate concentrations predicted when surface reactions on wood smoke particles are included. For the simulations reported in Figure 3.7, the reaction probability γ was assumed constant throughout the modeling domain, at all times of day. Values of 0.001, 0.01, 0.05 and 0.1 were assumed for γ. Relatively small amounts of sulfate are predicted via wood smoke mediated reactions for values of γ less than 0.01, but at values near or above 0.01, the magnitude of sulfate formation is consistent with observations. As shown in Figure 3.8, adding wood smoke mediated reactions to form sulfate also leads to temporal distributions in sulfate concentrations similar to observations. Figure 3.8 shows a large plume of sulfate, produced by wood

smoke mediated reactions, advecting to the west from Louisiana on the morning of September 6. Sulfate accumulates in the Houston area throughout the afternoon. By early evening the model predicts that the plume of sulfate from wood smoke mediated reactions will have left Houston, resulting in a diurnal profile of sulfate concentrations consistent with the observations at La Porte and Aldine. Even though the exact location of the predicted plumes is subject to uncertainty, the overall characteristics of these plumes are consistent with observations, particularly the time of onset of the high sulfate concentrations in Houston and the time at which the sulfate concentrations decrease.

The value of the reaction probability parameter $\gamma$ that leads to results most consistent with observations is approximately 0.01. It should be noted, however, that this parameter fitting is dependent on the assumed surface area of the wood smoke particles, the modeled locations of the wood smoke plumes, and other parameters. TEOM data, taken during the wood smoke episode, show very large peaks in smoke concentration (see Figure 2.1) that are not entirely matched by the simulations. It should also be noted that the dependence of sulfate formation on $\gamma$ is not linear. An increase by a factor of 10 in the reaction probability did not result in an order of magnitude increase in sulfate concentration. Therefore a reaction probability in the range of 0.01 may represent an upper bound. Nevertheless, the overall indications are that wood smoke mediated reactions did influence sulfate concentrations during this episode.

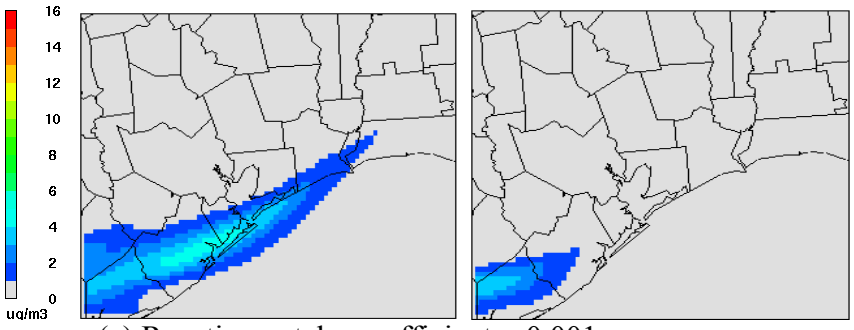


(a) Reactive uptake coefficient = 0.001

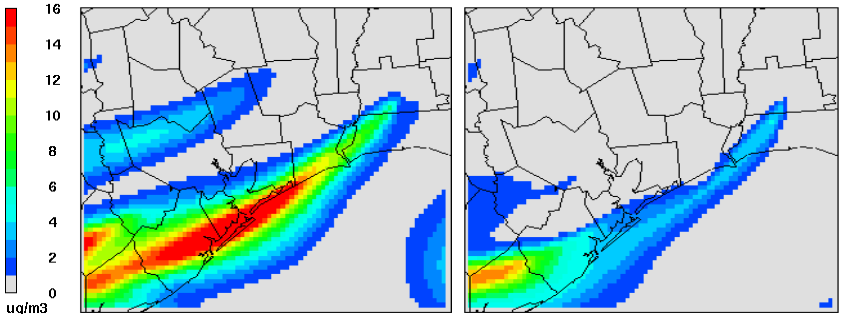


(b) Reactive uptake coefficient = 0.01

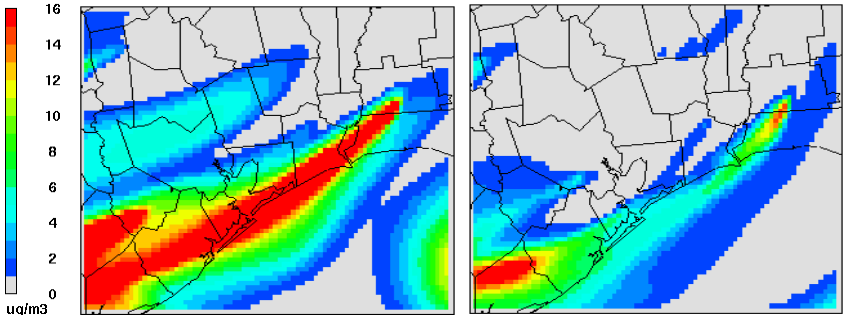


(c) Reactive uptake coefficient = 0.05

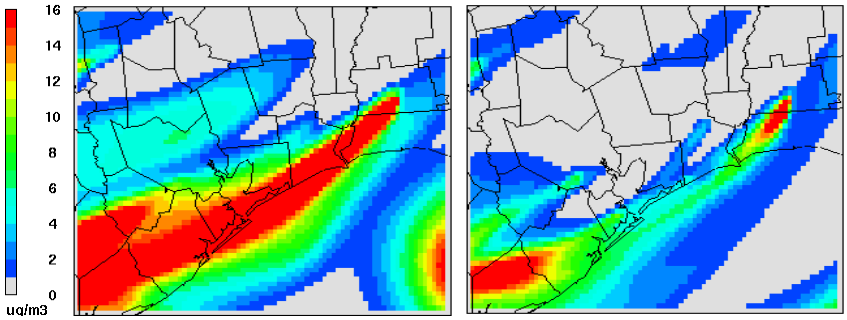


(d) Reactive uptake coefficient = 0.1

**Figure 3.7.** Predicted ground level sulfate concentrations ($\mu g/m^3$) on Sep 6$^{th}$ at 0800 h (left) and at 1400 h (right) due to impingement of $SO_2$, from sources within the domain, onto wood smoke particles, with a reactive uptake coefficient of (a) 0.001 (b) 0.01, (c) 0.05, and (d) 0.1.

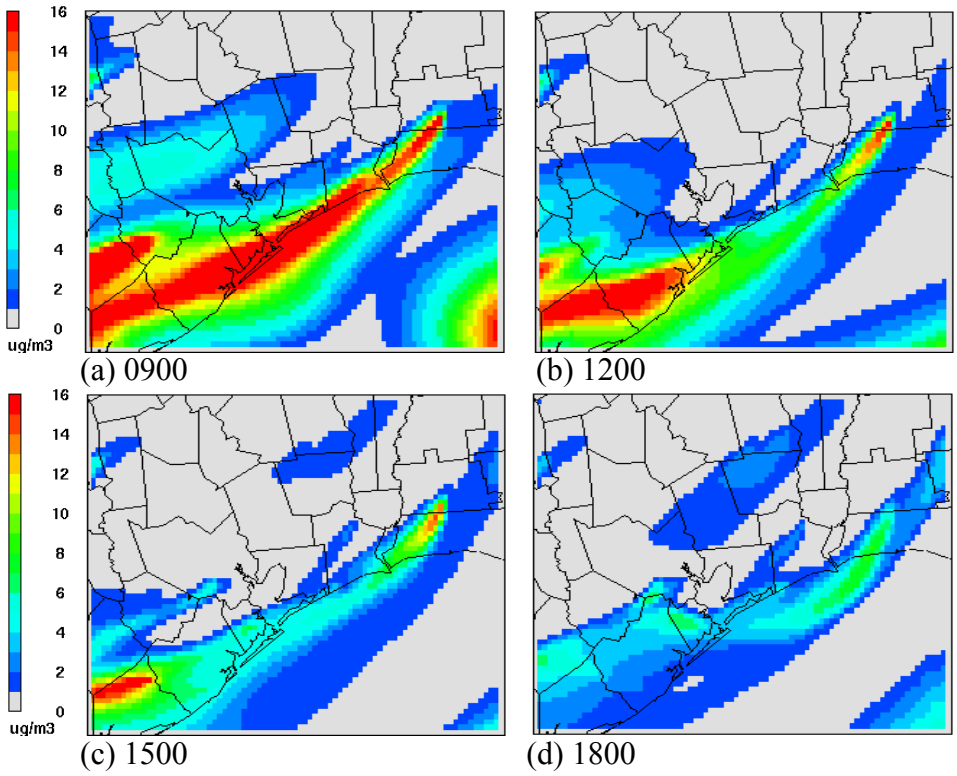


**Figure 3.8.** Predicted ground level sulfate concentrations ($\mu g/m^3$) due to impingement of $SO_2$, from sources within the domain, onto wood smoke particles, with a reactive uptake coefficient of 0.05 on Sep 6th at (a) 0900 h, (b) 1200 h, (c) 1500 h, and (d) 1800 h.

Assuming that the reaction probability, $\gamma$, is constant is equivalent to assuming that the reactions are limited by availability of $SO_2$, rather than by the availability of oxidants. To account for limited availability of oxidant species ($O_3$, $H_2O_2$ and $NO_2$), $\gamma$ was scaled according to concentrations of each of the oxidants for each hour in each grid cell. A maximum value of 0.05 was assumed and the reaction probabilities were scaled as described in Equation 3.3. Sulfate concentrations, assuming three different oxidant species, were predicted for the entire episode; results are reported for September 4$^{th}$, since the results on September 4$^{th}$ show different spatial distributions of sulfate formation for the different oxidants. Predicted sulfate with a constant reaction probability is shown in Figure 3.9. Figures 3.10, 3.11, and 3.12 report sulfate concentrations resulting from wood smoke mediated reactions, assuming that sulfate formation scales with the availability of three different oxidants - $O_3$, $NO_2$ and $H_2O_2$, respectively.

The spatial distributions of the predicted sulfate concentrations differ, depending on which oxidant is assumed to be limiting. For example, at 9 a.m., sulfate formation peaks broadly across a northeastern area of the domain if $O_3$ or $H_2O_2$ is limiting, while a maximum enhancement from $NO_2$ oxidation is shifted south of the area where the enhancement from $H_2O_2$ is observed and the extent of the enhancement is significantly reduced. These predicted variations in the spatial distribution of sulfate formation, with different limiting oxidant concentrations, suggest that it may be possible, in future field programs, to determine which oxidant potentially contributes to sulfate formation via heterogeneous pathways.

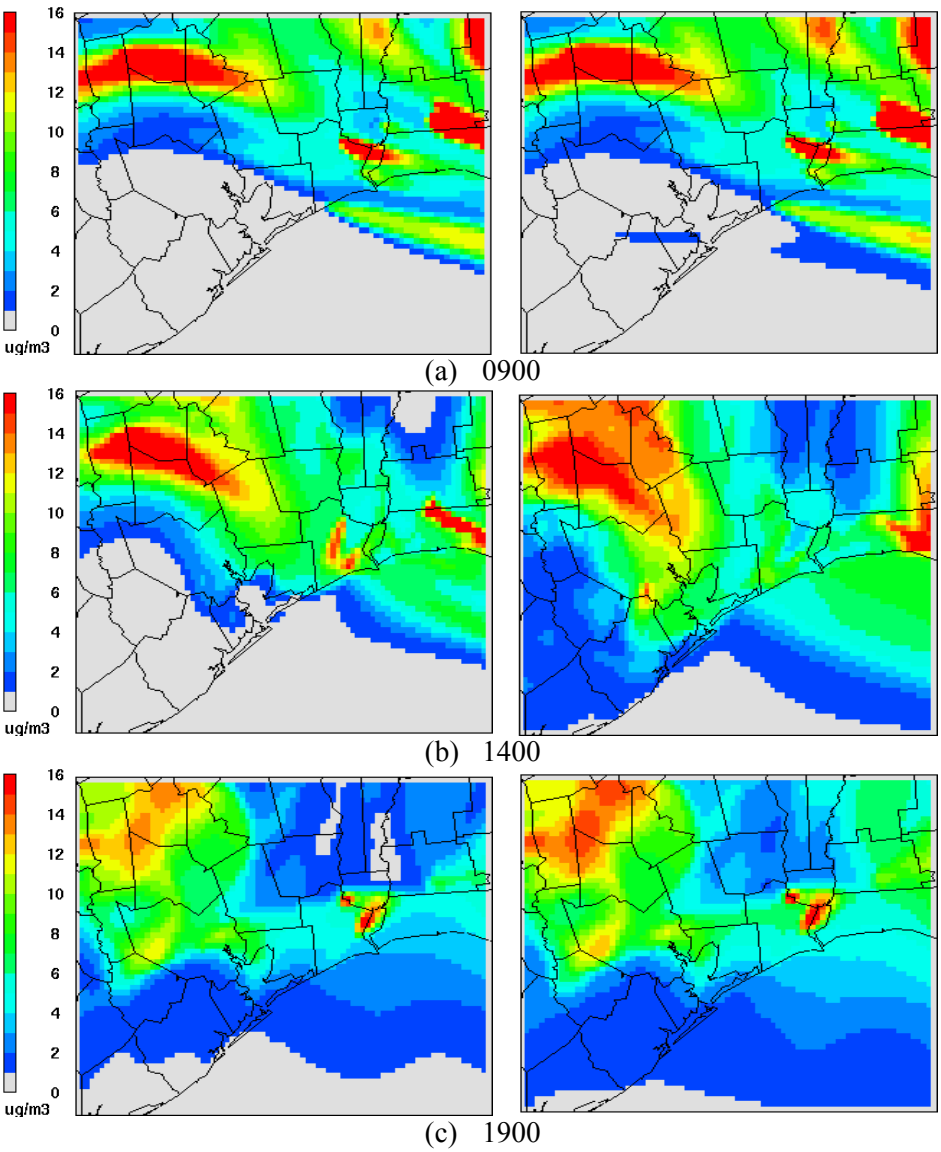


**Figure 3.9.** Predicted ground level sulfate concentrations ($\mu g/m^3$) due to impingement of $SO_2$ (left) and due to both conventional sulfate formation mechanisms and impingement of $SO_2$ on wood smoke particles (right) on Sep 4$^{th}$ at (a) 0900 h, (b) 1400 h, and (c) 1900 h; a constant reactive uptake coefficient of 0.05 is assumed.

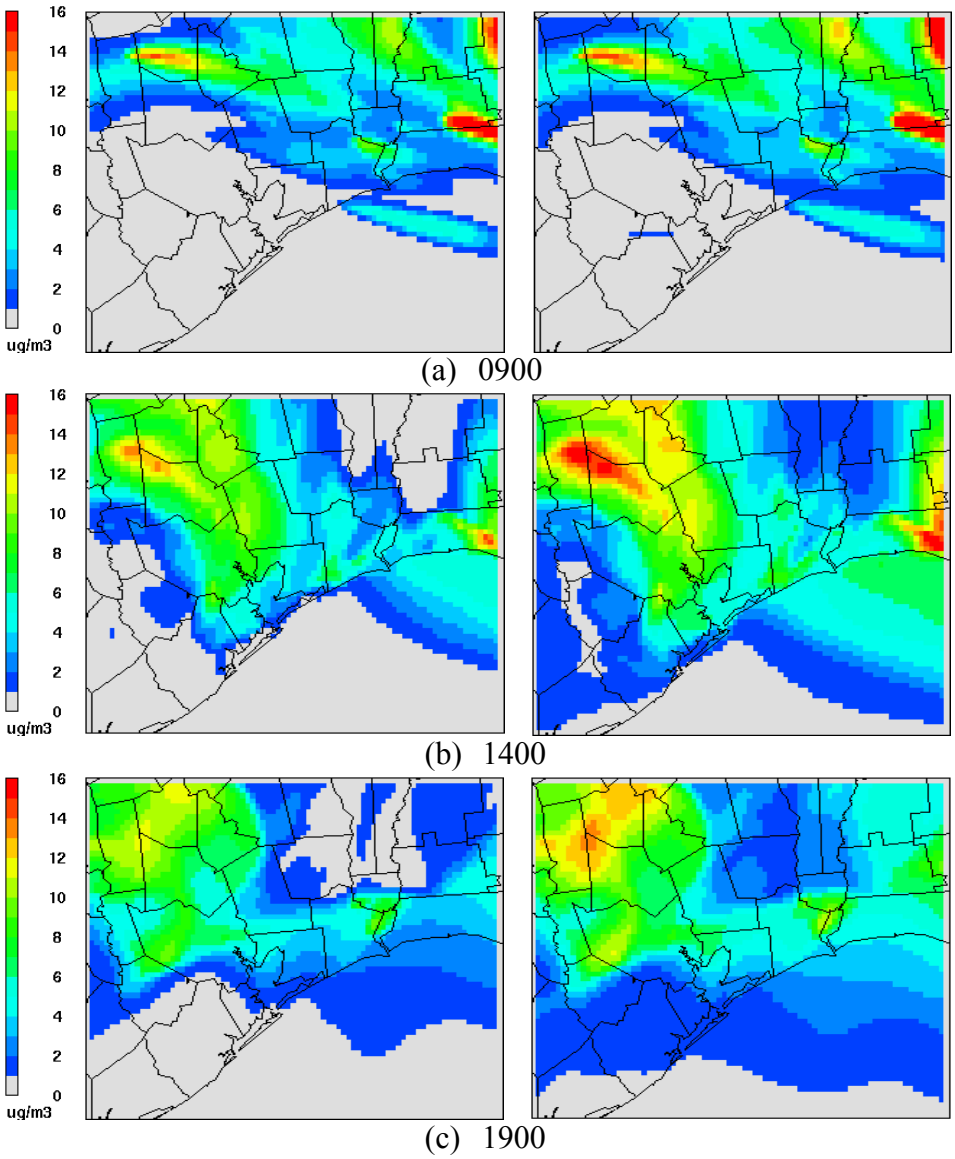


**Figure 3.10.** Predicted ground level sulfate concentrations ($\mu g/m^3$) due to impingement of $SO_2$ (left) and due to both conventional sulfate formation mechanisms and impingement of $SO_2$ on wood smoke particles (right) on Sep 4$^{th}$ at (a) 0900 h, (b) 1400 h, and (c) 1900 h; a reactive uptake coefficient dependent on $O_3$ concentrations is assumed.

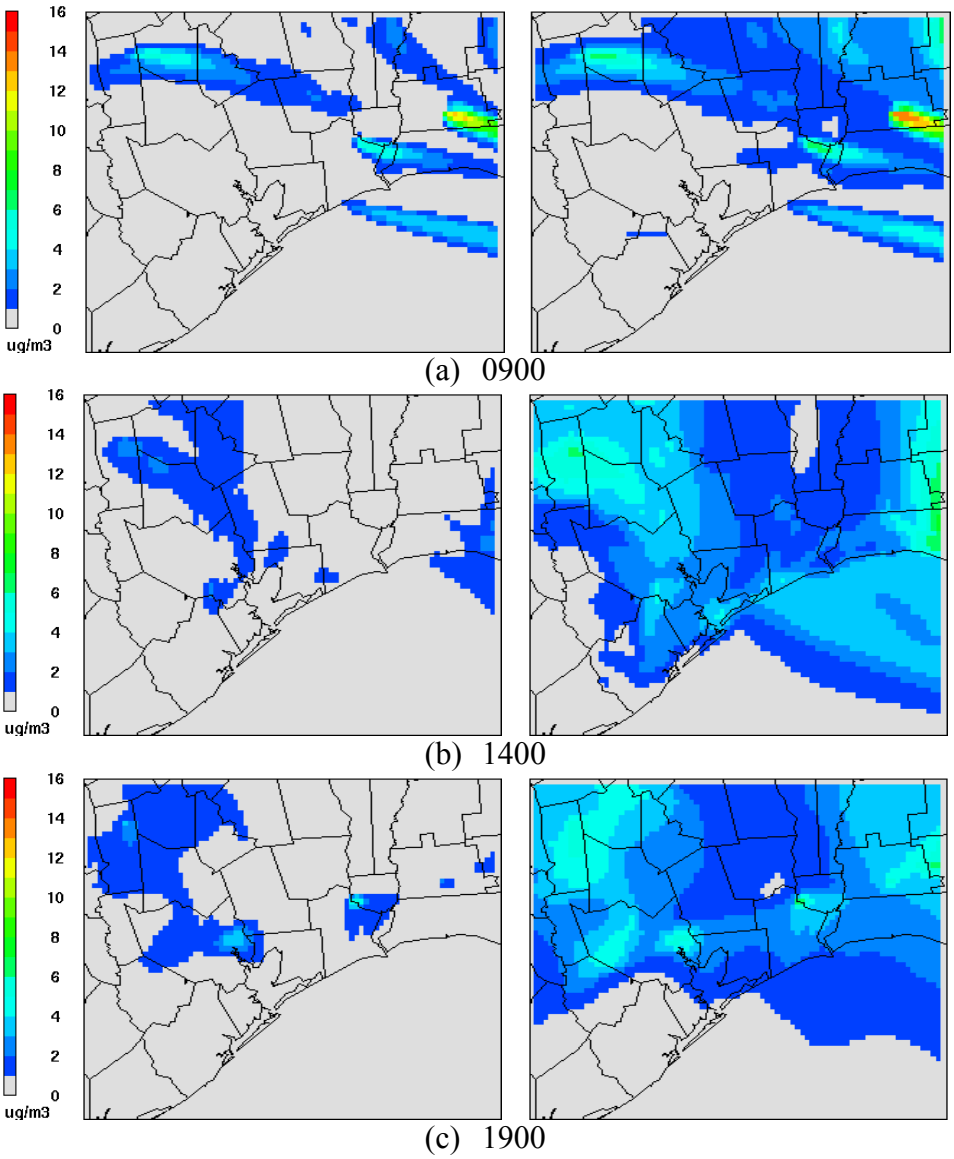


**Figure 3.11.** Predicted ground level sulfate concentrations (μg/m$^3$) due to impingement of $SO_2$ (left) and due to both conventional sulfate formation mechanisms and impingement of $SO_2$ on wood smoke particles (right) on Sep 4$^{th}$ at (a) 0900 h, (b) 1400 h, and (c) 1900 h; a reactive uptake coefficient dependent on $NO_2$ concentrations is assumed.

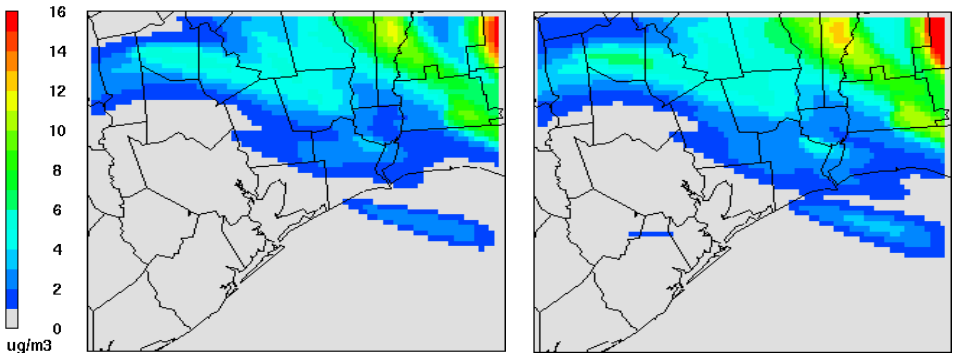


(a) 0900

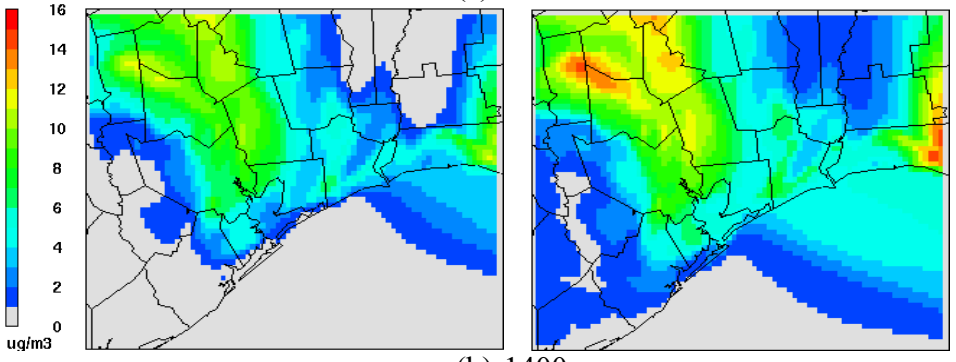


(b) 1400

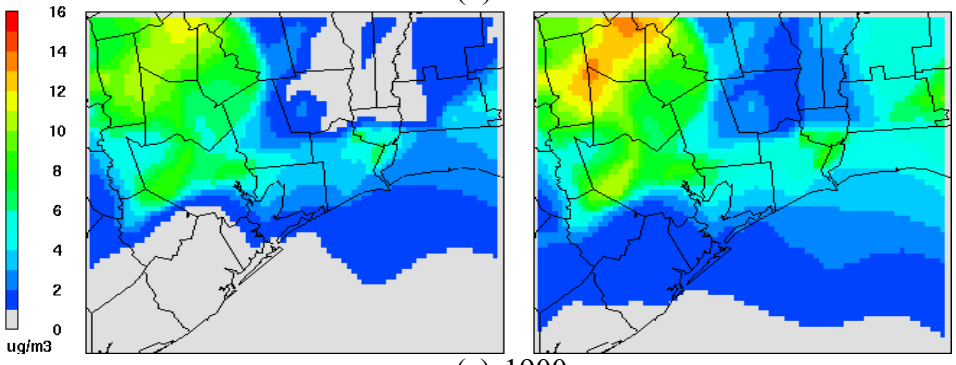


(c) 1900

**Figure 3.12.** Predicted ground level sulfate concentrations ($\mu g/m^3$) due to impingement of $SO_2$ (left) and due to both conventional sulfate formation mechanisms and impingement of $SO_2$ on wood smoke particles (right) on Sep 4$^{th}$ at (a) 0900 h, (b) 1400 h, and (c) 1900 h; a reactive uptake coefficient dependent on $H_2O_2$ concentrations is assumed.

### 3.4 Conclusion

A 3-D photochemical grid model was used to examine heterogeneous/surface sulfate formation reactions on wood smoke particles. An episode with significant wildfire emissions in the vicinity of sulfur dioxide sources was examined. Observational data during this episode indicated high particulate mass and sulfate concentrations on intense fire days. The high sulfate mass could not be explained using conventional sulfate formation pathways; previous analyses have indicated that heterogeneous/surface reactions may explain the high sulfate formation rates.

In the photochemical model, wood-smoke mediated sulfate formation was modeled by calculating the rate of impingement of $SO_2$ molecules on the wood smoke particles, and then assuming that a fraction of the impingements resulted in reaction. For reaction probabilities on the order of 0.01, the model predicted magnitudes, spatial distributions and temporal distributions of sulfate concentrations consistent with observations. Making the reaction probability dependent on oxidant availability did not change these overall findings. Observational data were not sufficiently detailed to be able to distinguish among the roles of different oxidants.

# Chapter 4
# Organic carbon during a wood smoke episode in Houston

This chapter will examine possible ambient evidence of acid catalyzed SOA formation during a wood smoke episode that occurred in southeast Texas during September 2000. As described by Buzcu et al. (2005) and Nopmongcol and Allen (2005), during this wood smoke episode, elevated concentrations of particulate sulfate were observed. Modeling calculations, described in this work, indicate that the sulfate was incompletely neutralized at some locations in the modeling domain, producing acidic aerosol at concentrations higher than normally observed in southeast Texas. These regions were also rich in gas phase organics that might participate in acid catalyzed condensation reactions, forming secondary organic aerosol (SOA). Modeling calculations will be used to assess the potential magnitude of SOA that might be expected from acid catalyzed organic condensation reactions in these regions.

### *4.1 SECONDARY ORGANIC AEROSOL OVERVIEW*

Organic carbon (OC) is a major component of atmospheric particulate matter (PM) and consists of primary organic compounds, emitted directly from anthropogenic and biogenic sources, as well as secondary organic aerosol (SOA), formed via reactions in the atmosphere. SOA is formed through the gas phase oxidation of precursor hydrocarbons; these reactions produce semi-volatile organic compounds (SVOC), which partition between gas and aerosol phases. SOA may also be formed via acid-catalyzed heterogeneous reactions of gas phase hydrocarbons with aerosols (Czoschke et al. 2003; Gao et al. 2004b; Iinuma et al. 2004; Jang and Kamens 2001a; Jang et al. 2002; Tolocka et al. 2004).

Specifically, it has been proposed that the acid-catalyzed SOA formation involves carbonyl reactants undergoing hydration, polymerization, hemiacetal and acetal formation, aldol condensation, ring opening of terpenoid carbonyls and cross-linking in acidic aerosol media, as shown in Figure 4.1 (Jang and Kamens 2001a; 2001b; Jang et al. 2002; Kamens and Jaoui 2001).

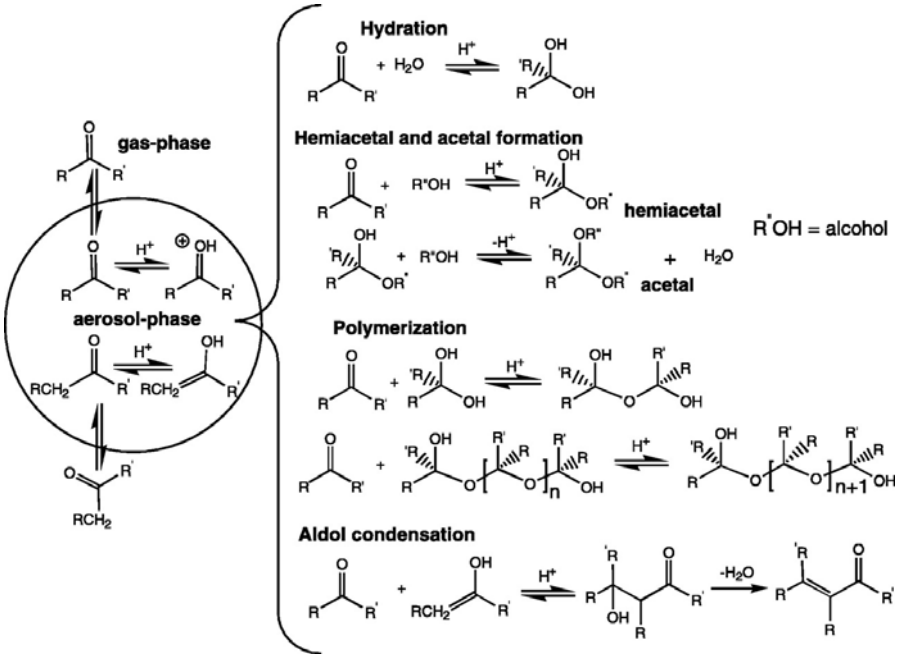


**Figure 4.1.** Acid-catalyzed heterogeneous reaction mechanisms of atmospheric carbonyls (Jang et al. 2002).

Isoprene and other biogenic emissions are among the atmospheric precursors of the carbonyl species that may lead to SOA formation through acid catalyzed reactions. Laboratory studies suggest that 2-methyl tetrols can be readily generated through acid-catalyzed reactions of isoprene (Claeys et al. 2004; Edney et al. 2005), and that acidic seed aerosols increase SOA formation from isoprene/ozone reactions (Jang et al. 2002). While these reports of acid-catalyzed reactions of carbonyl products suggest that the pathways could be important, much remains uncertain about the mechanisms and rates. Further, ambient data confirming the importance of these pathways has been limited.

#### *4.2 ORGANICS DURING WOOD SMOKE EPISODE*

As described in Chapter 2, during August and September 2000, air quality in the Houston area was significantly impacted by forest fires with the highest fire emissions occurring on September 4 and 6. In contrast to the intense fire activity that occurred from

August 30 through September 8, relatively little fire activity occurred from the beginning of August until August 28, in the Houston area. For comparison purposes, September 4, 6 and 8 will be selected to represent the wood smoke episode and August 21, 27, September 2 and 14 will represent non-wood smoke episode days (prior to and after the intensive fire period). September 2 is included as a non-wood smoke day, even though fires occurred on that day, because prevailing winds advected the fire emissions away from sampling sites (Buzcu et al. 2005).

24-hour average organic carbon concentrations in $PM_{2.5}$, from Federal Reference Method (FRM) samples, were available at many monitoring sites in Houston area during this period. The averaged OC and sulfate concentrations, for wood smoke and non-wood smoke episode days, from 9 monitoring stations, are shown in Table 4.1. The locations of the sites are shown in Figure 4.2. Sulfate concentrations on wood smoke days were, on average, 42% higher than on non-wood smoke days. OC and total $PM_{2.5}$ concentrations were 130% and 79% higher on wood smoke episode days than on non-wood smoke days, respectively, as reported in Table 4.1. These data indicate that OC, sulfate and total PM concentrations were all elevated during the wood smoke episode. The processes that lead to the enhanced sulfate concentrations have been examined by Buzcu et al. (2005) and Nopmongcol and Allen (2005), however, the processes that may be responsible for the elevated OC concentrations have not yet been quantitatively examined. The elevated OC concentrations may be due to direct emissions from fires, from increased partitioning of semi-volatile species into the particulate phase, or from heterogeneous reactions.

**Table 4.1.** Average OC, Sulfate and total $PM_{2.5}$ mass concentration ($\mu g/m^3$, measured using filter samples) for wood smoke (Sep 4-8) and non-wood smoke days (Aug 21, 27, Sep 2, and 14)

| Site Description | Wood Smoke | | | Non Wood Smoke | | |
|---|---|---|---|---|---|---|
| | OC | Sulfate | $PM_{2.5}$ | OC | Sulfate | $PM_{2.5}$ |
| Channelview | 6.68 | 8.74 | 22.50 | 2.89 | 5.87 | 12.95 |
| Conroe | 4.35 | 7.50 | 17.45 | 3.21 | 5.06 | 13.18 |
| Galveston Airport | 6.60 | 7.62 | 22.30 | 1.70 | 5.38 | 10.15 |
| Houston Aldine | 8.95 | 7.75 | 25.20 | 3.73 | 5.43 | 13.03 |
| Houston Bayland Park | 6.72 | 7.65 | 22.93 | 2.96 | 5.47 | 12.48 |
| Houston Deer Park 2 | 6.87 | 8.62 | 24.23 | 2.67 | 6.68 | 13.90 |
| HRM-3 Haden Road | 6.54 | 8.96 | 22.87 | 3.51 | 5.45 | 14.40 |
| La Porte Airport | 6.86 | 7.71 | 23.49 | 2.67 | 6.03 | 12.44 |
| Avg. of all sites | 6.70 | 8.07 | 22.62 | 2.92 | 5.67 | 12.62 |

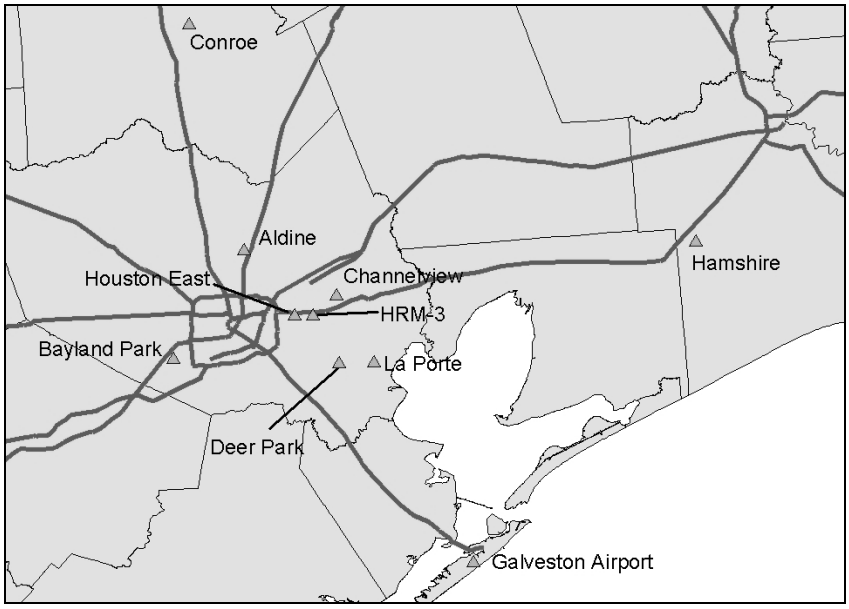


**Figure 4.2.** Southeast Texas monitoring sites

### *4.3 ESTIMATES OF PRIMARY OC EMISSIONS FROM FIRES*

One explanation for the elevated OC concentrations associated with the wood smoke episode is that the observed OC is due to primary emissions from the fires. Both molecular and atomic tracers have been used to estimate primary OC emissions from fires. Potassium (K) is sometimes used as a marker for wood combustion emissions,

since K typically accounts for 0.2 to 1.8 weight percent of fine particle mass emitted by fires (Fine et al. 2002; Hildemann et al. 1991). However, other sources, such as meat cooking (Schauer et al. 1999), and refuse incineration (Sheffield et al. 1994) can contribute to ambient potassium concentrations, so estimates of fire emissions based on K concentrations must be viewed with caution. More recent studies have used levoglucosan as a tracer for all types of wood smoke emissions (Fine et al. 2002; Simoneit et al. 1999). Levoglucosan emissions range from 40 to 1200 mg/kg of wood burned (Simoneit et al. 1999), and account for 3 to 16% of the fine particle organic mass emitted by fires (Fine et al. 2002). Levoglucosan is relatively stable in the atmosphere. A pathway that has been proposed as a possible sink for levoglucosan is the acid-catalyzed hydrolysis of levoglucosan to form β-D-glucose. However, Fraser and Lakshmannan (2000) found negligible degradation of levoglucosan under both non-acidic and acidic conditions (sulfuric acid), for up to 10 days. So, levoglucosan is generally regarded as a specific, stable and identifiable tracer of biomass combustion, but, its concentration in PM from biomass burning varies significantly, depending on the fuel type and the combustion conditions, making its use as a tracer species in quantitative source apportionment challenging.

Some of this variability in levoglucosan emissions from fires may be due to variability in the analytical methods used in quantifying the levoglucosan. The extraction and quantification procedures used in the studies selected for the calculations in this work are described in Table 4.2. Some of the variability in the analytical methods was addressed by applying a correction factor to the levoglucosan/OC mass fractions from the studies of both Oros and Simoneit (2001a) and Rinehart and Zielinska (2004), because the samples were extracted using only $CH_2Cl_2$. The correction factor assumes that the levoglucosan concentrations would be 10 times greater if a polar solvent was used (Oros and Simoneit 2001a; 2001b). This correction is, however, at best a rough approximation of the variability introduced by the use of different analytical methods.

**Table 4.2.** Extraction and quantification procedures used in the calculation of levoglucosan to OC mass fractions.

| Study | Extraction Solvent | Quantification |
|---|---|---|
| Schauer et al., 2001 | Hexane<br>Benzene/2-Proponal (2:1) | GC-MS (GC model 5890, MSD model 5972) |
| Oros and Simoneit, 2001a | Dichloromethane | GC-MS (GC model 5890A, MSD model 5973) |
| Fine et al., 2002 | Hexane<br>Benzene/2-Proponol (2:1) | GC-MS (GC model 5890, MSD model 5973) |
| Rinehart and Zielinska, 2004 | Dichloromethane/Acetone | GC-MS |
| Hildemann et al., 1991 | Hexane<br>Benzene/2-Proponol | GC-MS |

Additional variability in the mass fraction of levoglucosan in wood smoke OC is likely due to wood type. Levoglucosan emissions and levoglucosan to OC ratios in the PM emissions from the combustion of typical softwoods and hardwoods (Oros and Simoneit 2001a; 2001b) are shown in Figures 4.3 (a) and (b). The data show significant variability, with mass fractions of levoglucosan to OC ranging from less than 0.001 to more than 0.5, for both softwoods and hardwoods. Specifically, the mass fraction of levoglucosan to particulate OC from various types of softwood combustion vary from 0.001 to 0.075, with an average value of 0.024. For hardwood combustion, the mass ratio ranges from 0.0001 to 0.05 with an average value of 0.017.

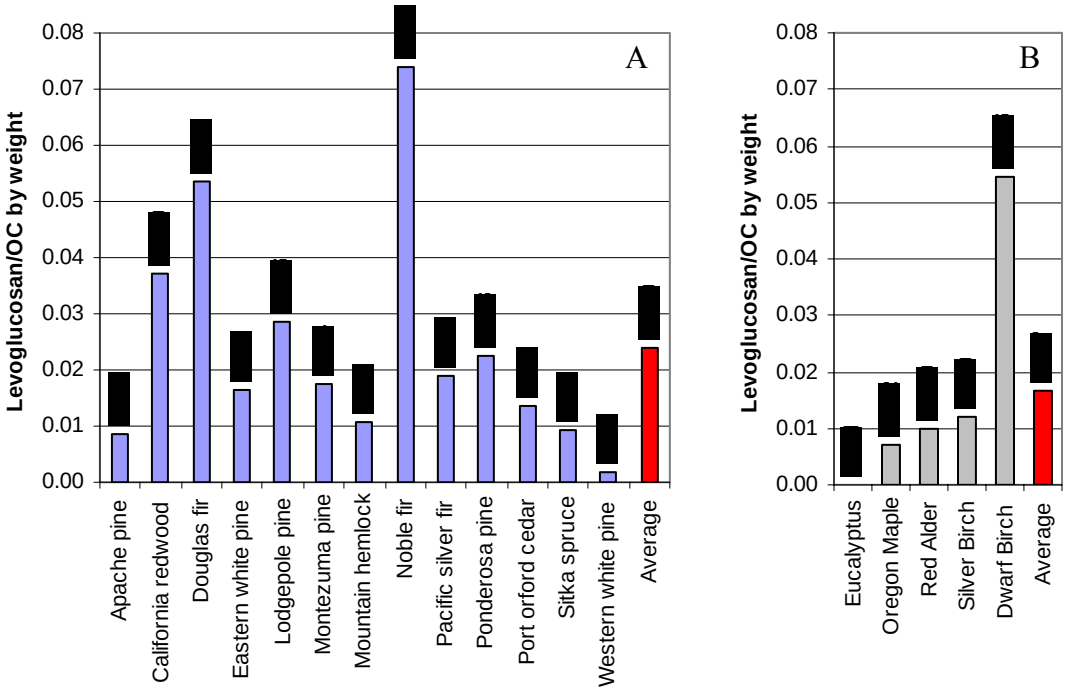


**Figure 4.3.** Mass fractions of levoglucosan/OC in combustion emissions from (a) softwood and (b) hardwood (Oros and Simoneit 2001a; 2001b)

Besides differences in analytical methods, and differences in wood type, differences in biomass combustion conditions such as temperature, wind velocity, and time of day can lead to differences in the composition of PM emissions. Table 4.3 shows the mass fractions of levoglucosan to OC and K to OC for PM emissions from a variety of types of combustion of pine. Pine was selected for this comparison since the fires that occurred during the episode considered in this work were mostly in pine forests. Results from the work of Schauer et al. (2001) conducted in a residential fireplace, located in a two-story house; yield the highest mass fraction of levoglucosan in OC (0.26). The lowest mass fractions (0.023-0.025) were obtained from the open-air wood combustion performed by the Desert Research Institute (DRI) and Oros and Simoneit (2001a).

**Table 4.3.** The estimated mass fraction of levoglucosan/OC and K/OC for residential fireplace and open air burning

| | | | mg/mg | |
|---|---|---|---|---|
| Referred code | Study | Condition | Levoglucosan/OC | K/OC |
| 1 | Schauer et al., 2001 | residential fireplace | 0.2584 | NA |
| 2 | Oros and Simoneit, 2001 | fireplace resemble wildfire | 0.0226[a] | NA |
| 3 | Fine et al., 2002 | residential fireplace | 0.0417 | 0.00018 |
| 4 | Rinehart and Zielinska, 2004 | open air burning | 0.025[a,b] | NA |
| 5 | Hildemann et al., 1991 | residential fireplace | NA | 0.0097 |

[a] factor of 10 is used to account for non-polar extraction solvent

[b] levoglucosan/total carbon

Levoglucosan concentrations in ambient PM were measured during the summer 2000 wood-smoke and non-wood smoke episodes by (Yue and Fraser 2004). Samples were extracted first by hexane then by mixture of 2:1 benzene/isoproponal. The extracts were converted to esters and each organic compound was quantified using GC-MS. The overall uncertainty in quantification was estimated to be ±20%. Air samples, collected at three sites; Aldine, HRM-3, and LaPorte, during September 6 and 8 were used for the wood smoke episode, and those collected during August 21, 27, September 2, and 14 represented the non-wood smoke episode. The averaged levoglucosan concentrations during the wood smoke and non-wood smoke episodes were 410 and 124 ng/m$^3$, respectively. Organic carbon concentrations due to the wood smoke (as shown in Figure 4 (a-b)) were estimated by multiplying observed levoglucosan concentrations by the mass fraction of levoglucosan to OC, based on data from the sources listed in Table 4.3.

In Table 4.3, the mass fraction from the work of Oros and Simoneit (2001a) represents data from Ponderosa Pine combustion, which dominates the forests in eastern Texas. As mentioned earlier, the mass fraction of levoglucosan/OC, however, can vary depending on wood species, ranging from as low as 0.0018 for Western white pine to as high as 0.074 for Noble fir. This variability could result in a substantial uncertainty (±200%) in the estimates of OC due to primary emissions. In addition to types of wood, the difference in combustion conditions, such as temperature, can lead to an additional uncertainty that is of order ±200%.

The variability in estimates of primary OC can be bounded somewhat by the use of potassium as a tracer. Potassium has been used as a wood combustion tracer, however its emission rate is small compared to levoglucosan and it can also be emitted from other

combustion sources such as cooking. Nevertheless, examining this tracer may bound the variability of employing the source apportionment technique. Previous studies reported that potassium contribute to 0.4-0.9% and 0.8-1.3% of aerosol mass from softwood combustion and hardwood combustion, respectively (Muhlbaier 1981). Figure 4.4 (b) shows estimates of OC from wood combustion using 0.0097 mg K/mg OC (Hildemann et al. 1991). The 24 hour averaged potassium ion concentrations collected during TexAQS 2000 at the three monitoring sites mentioned previously were utilized in the calculation. The averaged potassium concentrations for three sites were 0.13 and 0.063μg/$m^3$ during wood smoke and non-wood smoke episode, respectively. The results are shown in Figure 4.4 (b).

Observed OC concentrations are shown in Figure 4.4 (c). Comparison of predicted primary OC emissions to observed OC concentrations suggests that estimates of primary wood smoke OC concentrations, based on levoglucosan and K tracers, are high. All of the primary OC estimates, with the exception of the estimates based on the data of Schauer, et al. (2001), lead to estimated primary emissions that are larger than the total OC on both the wood smoke and non-wood smoke periods. Since other tracers (e.g., for diesel exhaust and cooking) clearly indicate that biomass burning is not the only source contributing to OC concentrations, especially on non-wood smoke days (Buzcu et al. 2005), and because use of the (Schauer et al. 2001) source profile for wood smoke leads to good mass closure on all sources of OC on non-wood smoke days, the Schauer et al. (2001) source profiles were used in this work. It should also be noted that the analytical techniques used in the ambient sampling were identical to the methods used by Schauer et al. (2001).

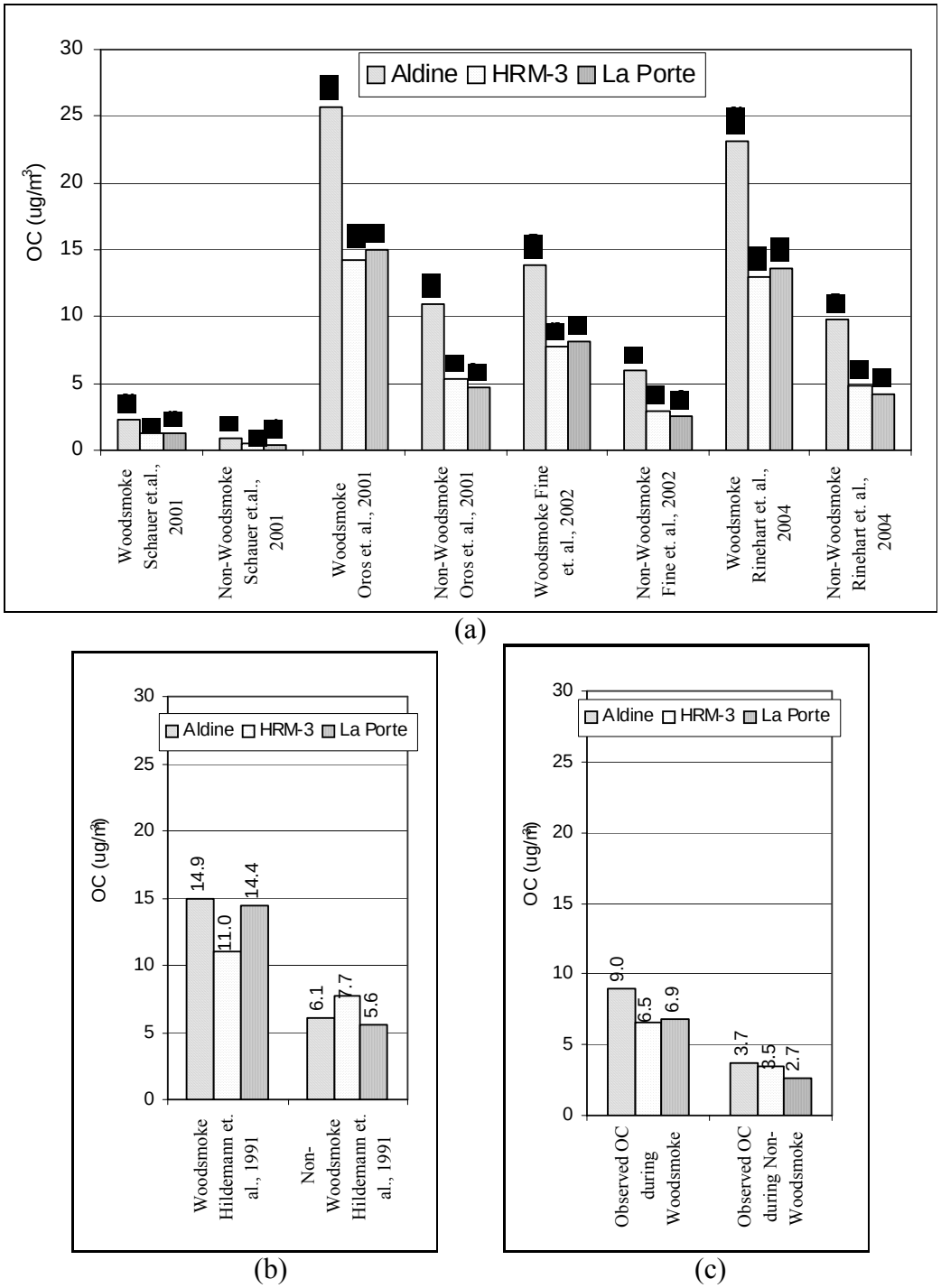


**Figure 4.4.** OC concentrations due to primary biomass combustion emissions (a) estimated by using Levoglucosan as a tracer and (b) estimated by using Potassium as a tracer; (c) observed OC concentrations during wood smoke and non-wood smoke episodes at three sites in Houston; Individual captions specify the episode and the referred literature in Table 4.2.

If the source data of Schauer et al. (2001) are used, the fraction of OC that can be attributed to primary sources can be estimated. Buzcu et al. (2005) have performed this assessment for wood smoke and non-wood smoke episodes. Secondary organic aerosol and primary organics from sources not were not attributed in the analysis are referred to as other organics. During non-wood smoke episode, other organics contributed 33%, 31%, and 36% of the organic carbon at Aldine, HRM-3 and La Porte, respectively (Table 4.4), indicating reasonable mass closure. The apportionment of organic carbon in $PM_{2.5}$ for the wood smoke case (Table 4.5) showed that the contribution of the primary wood combustion sources to organic carbon concentrations are higher but not comparable to the other organics which contributed to 50-70% of observed OC mass. The results for the two cases (non-wood smoke and wood smoke) are compared in Figures 4.5. These analyses suggest that other organics cannot be explained by direct emissions from biomass burning.

**Table 4.4.** Source contributions at three sites to ambient $PM_{2.5}$ mass and organic carbon (OC) concentrations ($ug/m^3$) for the days not affected by wood smoke. Organic carbon masses have not been scaled to represent mass of organic compounds (Buzcu et al. 2005).

| | *Aldine* | | *HRM-3* | | *La Porte* | |
|---|---|---|---|---|---|---|
| *Source Categories* | *$PM_{2.5}$Mass* | *$PM_{2.5}$ OC* | *$PM_{2.5}$Mass* | *$PM_{2.5}$ OC* | *$PM_{2.5}$Mass* | *$PM_{2.5}$ OC* |
| Gasoline Vehicles | 2.51± 0.94 | 1.10 ± 0.41 | 2.02± 0.67 | 0.89 ± 0.29 | 1.00± 0.40 | 0.44 ± 0.18 |
| Diesel Vehicles | 3.16± 0.44 | 1.01 ± 0.14 | 3.77± 0.45 | 1.21 ± 0.14 | 2.19± 0.28 | 0.70 ± 0.09 |
| Vegetative Detritus | 0.59± 0.09 | 0.19 ± 0.03 | 0.32± 0.05 | 0.10 ± 0.02 | 0.31± 0.04 | 0.10 ± 0.01 |
| Meat Cooking | 1.14± 0.26 | 0.39 ± 0.09 | 0.52± 0.14 | 0.18 ± 0.05 | 0.71± 0.16 | 0.24 ± 0.05 |
| Wood Combustion | 0.74± 0.18 | 0.41 ± 0.10 | 0.84± 0.15 | 0.47 ± 0.08 | 0.44± 0.10 | 0.25 ± 0.06 |
| Road Dust | n.i. | n.i. | 0.17± 0.04 | 0.05 ± 0.01 | n.i. | n.i. |
| Sum of Apportioned $PM_{2.5}$ Mass | 8.14± 1.09 | | 7.64± 0.83 | | 4.65± 0.52 | |
| Sum of Apportioned OC | | 3.11 ± 0.46 | | 2.90 ± 0.34 | | 1.73 ± 0.21 |
| Measured OC | | 4.70 | | 4.20 | | 2.70 |
| *Other Organics | | 1.57 | | 1.30 | | 0.97 |
| Secondary Sulfate | 5.28 | | 5.40 | | 5.30 | |
| Sum of $PM_{2.5}$ mass apportioned to primary sources, other organics and secondary sulfate | 14.99 | | 14.34 | | 10.92 | |
| Measured $PM_{2.5}$ mass | 15.00 | | 16.99 | | 11.00 | |

n.i. = not included

*Other organics represent secondary organic aerosol or primary organics from sources not included in the model calculations

**Table 4.5.** Source contributions at three sites to ambient $PM_{2.5}$ mass and organic carbon (OC) concentrations (ug/$m^3$) for the days during the wood smoke episode. Organic carbon masses have not been scaled to represent mass of organic compounds (Buzcu et al. 2005).

| | *Aldine* | | *HRM-3* | | *La Porte* | |
|---|---|---|---|---|---|---|
| *Source Categories* | *$PM_{2.5}$Mass* | *$PM_{2.5}$ OC* | *$PM_{2.5}$Mass* | *$PM_{2.5}$ OC* | *$PM_{2.5}$Mass* | *$PM_{2.5}$ OC* |
| Gasoline Vehicles | 1.68± 0.59 | 0.74 ± 0.26 | 3.18± 0.99 | 1.40 ± 0.43 | 1.56 ± 0.47 | 0.69 ± 0.18 |
| Diesel Vehicles | 3.48± 0.43 | 1.11 ± 0.14 | 3.63± 0.48 | 1.16 ± 0.15 | 2.91 ± 0.35 | 0.93 ±0.09 |
| Vegetative Detritus | 0.72± 0.09 | 0.23 ± 0.03 | 0.67± 0.09 | 0.21 ± 0.03 | 0.54 ± 0.07 | 0.17 ± 0.01 |
| Meat Cooking | n.i. | n.i. | 0.05± 0.01 | 0.02 ± 0.00 | n.i. | n.i. |
| Wood Combustion | 2.02± 0.27 | 1.13 ± 0.15 | 2.32± 0.37 | 1.30 ± 0.21 | 1.54 ± 0.21 | 0.86 ± 0.12 |
| Sum of Apportioned $PM_{2.5}$ Mass | 7.90± 0.78 | | 9.85± 1.16 | | 6.55± 0.63 | |
| Sum of Apportioned OC | | 3.21± 0.33 | | 4.09± 0.51 | | 2.65± 0.26 |
| Measured OC | | 10.12 | | 7.96 | | 8.13 |
| Other Organics | | 6.91 | | 3.87 | | 5.45 |
| Secondary Sulfate | 8.80 | | 9.45 | | 8.68 | |
| Sum of $PM_{2.5}$ mass apportioned to primary sources, other organics and secondary sulfate | 23.61 | | 23.17 | | 20.68 | |
| Measured $PM_{2.5}$ mass | 28.45 | | 25.30 | | 26.85 | |

n.i. = not included

*Other organics represent secondary organic aerosol or primary organics from sources not included in the model calculations

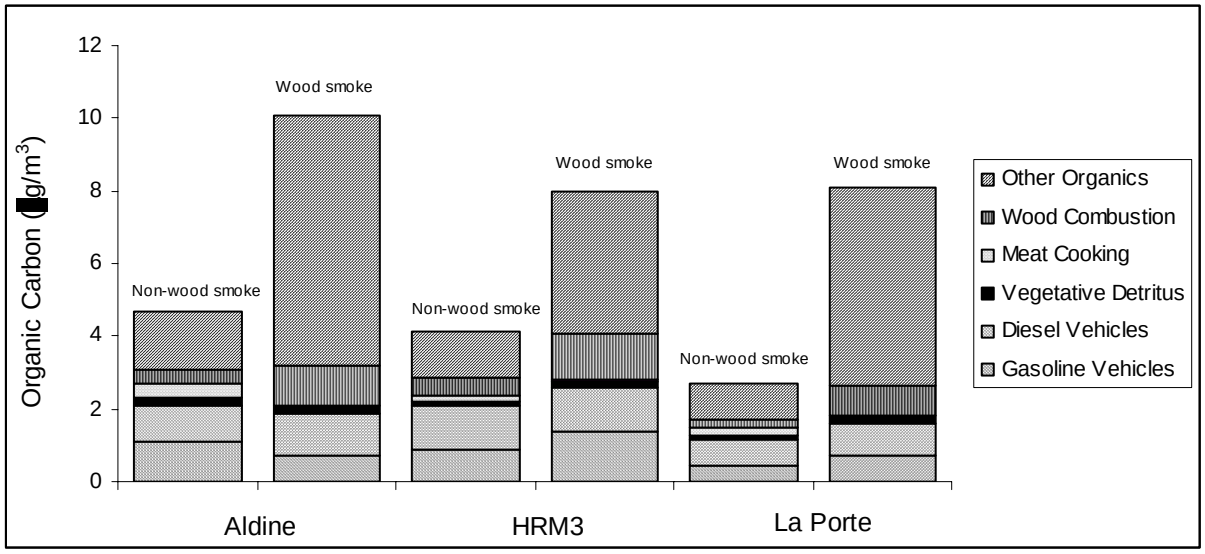


**Figure 4.5.** Comparison of the source contributions to OC in $PM_{2.5}$ in two cases (Buzcu et al. 2005).

### *4.4 PHOTOCHEMICAL MODELING*

While some of the additional OC observed during the wood smoke episode, as compared to the non-wood smoke episode, is undoubtedly due to primary emissions, some may be due to additional partitioning of semi-volatiles into the particulate phase, due to the additional primary particulate matter available in the atmosphere. In addition, acid-catalyzed organic condensation reactions may lead to additional organic carbon formation. Both of these pathways will be examined through photochemical modeling.

#### *4.4.1 MODELING FRAMEWORK*

Although any comparable photochemical grid model could be used, the comprehensive air quality model with extensions (CAMx) (ENVIRON, 2005) was selected for this study because it is currently being used by the State of Texas for attainment demonstrations in areas that have violated the National Ambient Air Quality Standards for ozone. The episode period used in the modeling was August 22 - September 6, 2000, which included the wood smoke event. The modeling domain was a nested regional/urban scale 36-km/12-km/4-km grid, shown in Figure 3.1.

Meteorological inputs and Emission inventories were described in modeling section in Chapter 3.

#### *4.4.2 SOA FORMATION*

Because a primary focus of this work is on estimating secondary organic aerosol formation, the modeling approaches used for estimating SOA formation are described in detail here. SOA formation modeling approaches used in regional photochemical air quality models have primarily assumed a gas-particle (G/P) equilibrium partitioning (Odum et al. 1996; Odum et al. 1997; Pankow 1994), in which a reactive hydrocarbon (HC) undergoes atmospheric oxidation to produce n semivolatile (condensable, SVOC) products $G_1$ to $G_n$ as shown in Equation (4.1)

$$HC + oxidant \rightarrow \alpha_1 G_1 + \alpha_2 G_2 + ... + \alpha_n G_n \quad (4.1)$$

where $\alpha_i$ is the stoichiometric yield of $G_i$. In a G/P partitioning model, the mass balance for each SVOC satisfies:

$$C_{t,i} = C_{g,i} + C_{aer,i} \quad (4.2)$$

where $C_{t,i}$ is the total concentration of species *i*, $C_{g,i}$ is the gas-phase concentration, and $C_{aer,i}$ is the aerosol-phase concentration (all in $\mu g\ m^{-3}$ of air). The total concentration can be expressed using stoichiometry as

$$C_{t,i} = \alpha_i \frac{M_i}{M_{HC}} \Delta HC \quad (4.3)$$

where $M_i$ is a molecular weight. Assuming that the aerosol species form an ideal organic solution, their gas-phase concentrations will satisfy

$$C_{g,i} = x_i \frac{P_{L,i} M_i}{RT} = x_i C_i^* \quad (4.4)$$

where $x_i$ is the mole fraction of the species i in the solution, $P_{L,i}$ is the liquid vapor pressure of pure organic compound i, and $C_i^*$ is the effective saturation concentration in $\mu g\ m^{-3}$ of pure i which can be determined from laboratory experiments.

Combining the above equations yields a set of n equations with n unknowns:

$$C_{aer,i} = \alpha_i \frac{M_i}{M_{HC}} \Delta HC - \frac{C_{aer,i} C_i^* / M_i}{\sum C_{aer,i} / M_i + POA / M_{POA}} \qquad \text{for i=1, n} \qquad (4.5)$$

where POA [ug $m^{-3}$] represents any initially present absorbing organic mass. SOA concentrations can then be obtained by solving this system (Odum et al. 1996; Odum et al. 1997). This approach does not account for heterogeneous reactions.

As shown in Equation 4.5, estimates of SOA formation rely on concentrations of POA. Previous work has shown that primary organic carbon in southeast Texas is substantial (Russell and Allen 2004a) and can serve as a medium in absorbing condensable oxidation products. Unfortunately, the primary OC inventory available for southeast Texas has substantial uncertainty associated with it. One approach to dealing with an unknown or uncertain inventory of POA is to assume negligible primary OC as an absorbing mass and to assume that condensable products will partition only to a solution of SOA. This approach results in under prediction of SOA formation, especially when primary OC is particularly high, such as during the wood-smoke episode. An alternative approach, that has been used by Russell and Allen (2005), is to use observed values of organic aerosol in the photochemical modeling calculations. This approach allows a direct and accurate characterization of the organic aerosol phase available for SVOCs to partition into, and was the approach used in this work.

24-hour average organic carbon concentrations in $PM_{2.5}$ were available at many monitoring sites, as shown in Figure 4.6. It was assumed that the total amount of OC in $PM_{2.5}$ was a good approximation of total organic absorbing mass. Absorbing mass was then obtained by interpolating time resolved $PM_{2.5}$ data to model grid cells within the 4-

km domain (see Figure 3.1). Details of the methodology have been described by Russell and Allen (2005). Briefly, hourly measurements of total $PM_{2.5}$ using Tapered Element Oscillating Microbalances (TEOM) were used to distribute average daily OC mass, at specific sites into specific hours. The kriging interpolation method was chosen for the interpolation (point kriging, linear variogram, slope = 1, no drift). These spatially resolved hourly OC concentrations were assumed to uniformly distribute over the planetary boundary layer (PBL). An example of an OC interpolation is shown in Figure 4.7.

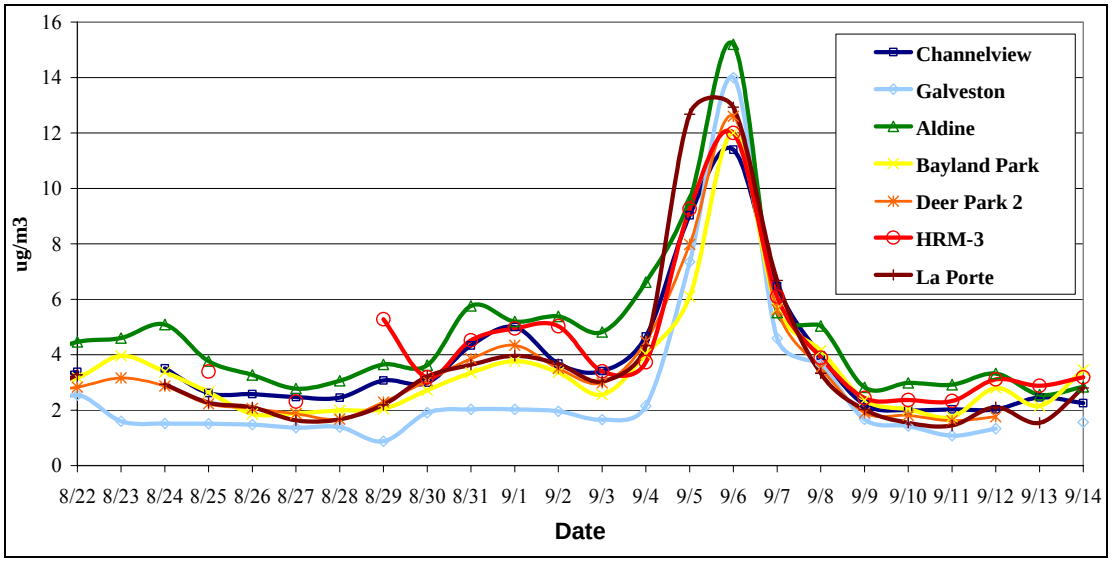


**Figure 4.6.** Daily average organic carbon concentrations measured at La Porte during the wood smoke episode (Russell et al. 2004b).

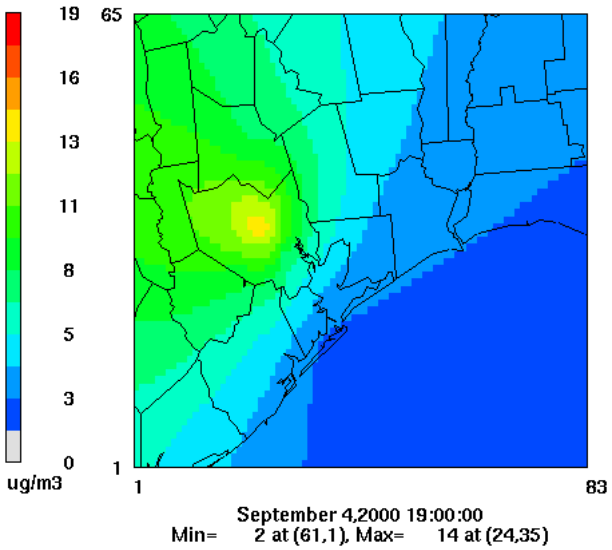


**Figure 4.7.** Interpolated OC concentrations (ug/m$^3$) at 1900 for September 4$^{th}$, 2000, within 4-km grid.

Although there is uncertainty associated with interpolation in general and the domain chosen here was extended beyond bounds of PM monitoring sites to cover the North area of Houston where biogenic emissions are significant, the approach has less uncertainty than the inventory of primary carbonaceous aerosol. Note that the interpolated OC mass does not represent primary organic aerosol, but total absorbing mass. It is, however, the primary organic (POA) that is required in the model formulation described by Equation 4.5. CAMx codes were modified to read the interpolated OC mass and internally estimate POA mass for each hour (see Appendix C). POA was approximated as a mass difference between interpolated OC and predicted SOA from the last hour. For example, if the interpolated OC at 900 hr was 16 ug/m$^3$ and the predicted SOA at 800 hr was 9 ug/m$^3$ the POA at 900 hr would be 7 ug/m$^3$.

To model acid catalyzed SOA formation, an impingement/reactive uptake calculation approach was used. An impingement model, rather than an explicit mechanism, was used because a variety of mechanisms have been proposed for the acid-catalyzed organic condensation reactions on acidic aerosol, and because quantitative information on the rates and extent of these reactions are not yet available. In this approach, the SOA formation rate is defined as the product of the total number of

collisions per unit time between catalytic surfaces gas phase reactants, multiplied by the probability that a collision results in a condensation reaction.

$$d[SOA]_{i,het} / dt = \gamma \bullet Z_i \tag{4.6}$$

$$Z_i = \frac{1}{4} A[C_i]\nu_i \tag{4.7}$$

where i represents the reacting species, $\nu_i$ is the mean molecular velocity, calculated as $\sqrt{8RT/\pi M_i}$ and A is the surface area potentially associated with acid-catalyzed reactions. Available acidic particle surface was calculated by assuming a particle density of 1.5 g/cm$^3$ and an average acidic particle diameter of 0.25 μm. The degree of neutralization was represented by hydrogen ion concentration, [H+].

Hydrogen ion concentration was estimated by performing a cation-anion balance. In this work, the degree of neutralization was represented as (molar basis):

$$[H+] = 2[SO_4^{2-}] + [NO_3^-] - [NH_4^+] \tag{4.8}$$

In order to convert this degree of neutralization into an estimate of available acidic aerosol surface area required in Equation 4.7, several assumptions were made. Specifically, it was assumed that for each mole of [H+], there would be 0.5 mol of sulfate (48 μg per μmol of [H+]). Since sulfate accounts for 30%, of aerosol mass, on average, there would be (1/0.3)x48 μg of total aerosol per μmol of [H+] (Russell et al. 2004; Tropp et al. 1998). Thus, one μmol of [H+] would be associated with 160 μg of PM mass. Further assuming an average particle density of 1.5 g/cm$^3$ and an average acidic particle diameter of 0.25 μm, then allows for calculation of acidic aerosol mass.

The tools used to estimate aerosol sulfate should also be noted. Observational data indicated that during the wood smoke episode sulfate could form via heterogeneous sulfate formation on carbonaceous surfaces with reaction probabilities on the order of 0.01 (Nopmongcol and Allen 2005). So, in addition to conventional sulfate formation

mechanisms (see Chapter 2), in this work heterogeneous mechanisms for sulfate formation were considered. The approach used in estimating the rate of heterogeneous sulfate formation was to multiply the surface impingement rate of gas phase $SO_2$ on wood smoke particle surfaces by an estimate of the fraction of the impinging molecules that adsorb and react. The fraction reacted is typically quantified in terms of a reactive uptake coefficient ($\gamma$). The number of reactive collisions with the surface (the sulfate formation rate) is defined as the reactive uptake coefficient multiplied by the total number of surface collisions per unit time (Z).

$$d[SO_4^{2-}]/dt = \gamma \bullet Z \tag{4.9}$$

$$Z = \frac{1}{4} A[SO_2]\nu_{SO_2} \tag{4.10}$$

where v is the mean molecular velocity of $SO_2$, calculated as $\sqrt{8RT/\pi M_{SO_2}}$ and A is the effective particle surface. The number of fire generated particles and available surface area available was calculated by assuming a particle density of 1.5 g/cm$^3$ and an average particle diameter of 0.25 μm. A reactive uptake coefficient ($\gamma$) value of 0.01 was assumed. More details of the modeling approach are available in Chapter 3.

Once the available acidic surface has been calculated, the concentrations of potential gas phase reactants participating in acid catalyzed concentrations must be determined. The gas-phase chemical mechanism used within CAMx in this work was the Carbon Bond-IV Mechanism (CBIV). The aldehydes (ALD2) species in the CBIV mechanism possesses carbonyl groups with two or more C atoms, and so was chosen as one potential reactant. Isoprene (ISOP), which is treated explicitly in the mechanism, was also considered as a potential precursor. For each mole of ALD2 that was assumed to react via an acid catalyzed mechanism, it was assumed that 32 g (the assumed molecular weight of ALD2) was added to SOA. For each mole of isoprene that was assumed to react via an acid catalyzed mechanism, it was assumed that 68 g (the molecular weight of ISOP) was added to SOA. Note that this assumed molecular weight is about half of 120 g (the molecular weight of 2,3 dihydroxymethacrylic acid, a typical

isoprene photoxidation product). CAMx codes were modified (see Appendix C) to account for these acid-catalyzed heterogeneous reactions.

#### *4.4.3 MODEL PERFORMANCE*

Model performance for this episode has been evaluated by comparing observed and predicted ozone, sulfate, formaldehyde, and VOC concentrations.

Ozone modeling performance statistics were performed by the Texas Commission on Environmental Quality (TCEQ) (TCEQ, 2004d). Although there are discrepancies between observed and modeled peak ozone concentrations on some days, the overall performance was judged acceptable for air quality planning by the State of Texas. Previous work demonstrated that the model could accurately predict a fraction of $SO_2$ conversion to sulfate that is consistent with observations when wood smoke is not present and excess sulfate observed with the presence of wood smoke could be explained by heterogeneous reaction pathways (Nopmongcol and Allen 2005).

Model performance in predicting VOC concentrations was also evaluated by TCEQ, by examining predicted and observed diurnal patterns in VOC concentration at specific sites. Time series of observed and modeled isoprene, formaldehyde and aldehydes (ALD2) concentrations during August 22$^{nd}$-September 6$^{th}$, 2000, at the La Porte site are shown in Figure 4.8. Observed species were transformed to CB-IV for this purpose. There are overestimations of isoprene concentrations during daytime throughout the episode period (shown in Figure 8(a)). This overestimation has been examined in detail by Song et al. (2005). Consequently, care will be taken when interpreting predictions of heterogeneous reactions with isoprene as a reactant. On the other hand, discrepencies between observed and modeled peak aldehyde concentrations exist on some days, however, the overall aldehyde predictions shown in Figure 4.8(b) are consistent with observations and judged acceptable.

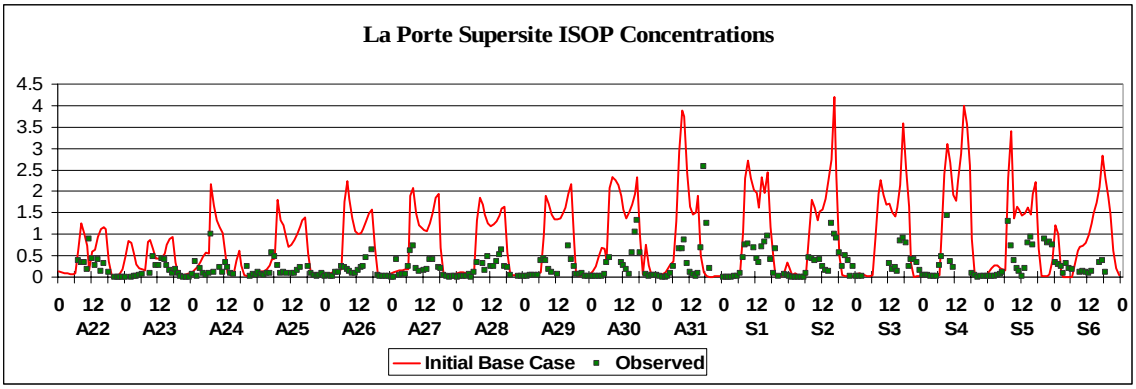


(a)

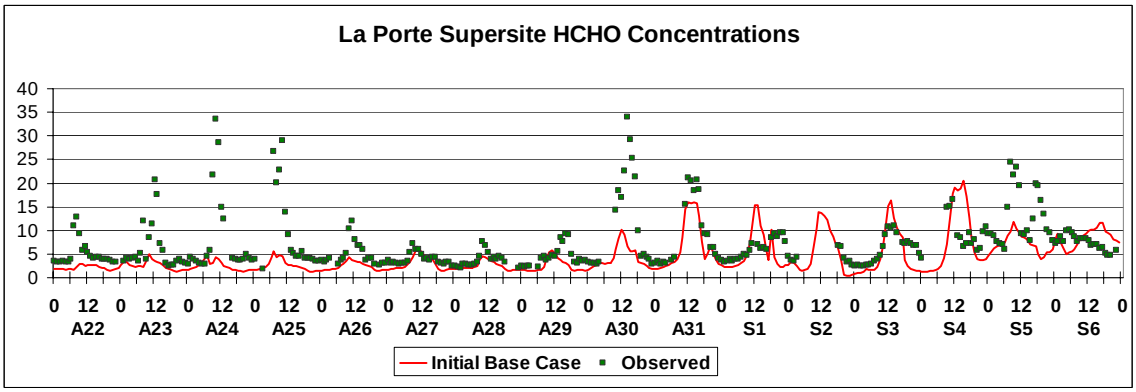


(b)

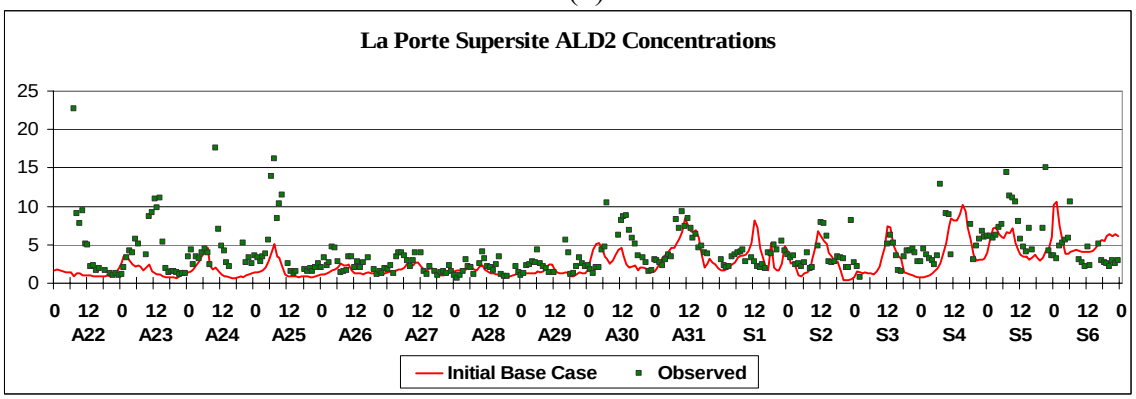


(c)

**Figure 4.8.** Modeled and observed surface layer (a) isoprene and (b) aldehydes (ALD2) concentration at the La Porte monitoring site from August 22nd to September 6th, 2000 (TCEQ, 2005d).

#### *4.4.4 RESULTS AND DISCUSSION*

A regional photochemical grid model was used to simulate the extent to which SOA formation would be enhanced due to acid catalyzed carbonyl condensation reactions and due to the availability of additional primary OC particulate emissions as a condensation medium. Three model simulations were performed:

Case 1: Basecase – There is no modification to CAMx (no acid-catalyzed reactions) and no primary particulate OC (POA).

Case 2: CAMx codes were modified to take into account additional primary particulate OC (POA) emissions as a condensation medium but the acid-catalyzed reactions are not included.

Case 3: CAMx codes were modified to take into account additional primary particulate OC (POA) emissions as a condensation medium and the acid-catalyzed reactions are included.

To examine whether the availability of additional primary particulate OC emissions affected SOA formation by providing additional volume of condensation media, simulations with and without this additional absorbing mass (Case 2 and Case 1) were compared. These simulations did not include any acid catalyzed carbonyl condensation reactions. The results, shown in Figure 4.9 (b), indicate that the maximum enhancement of SOA formation due to additional condensation volume was 0.24 ug/$m^3$ (less than 10% of the predicted SOA). This magnitude of mass is considered insignificant especially on a day with intense fire activities. These simulations suggest that SOA formation was not limited by availability of absorbing mass but rather limited by availability of semivolatile species.

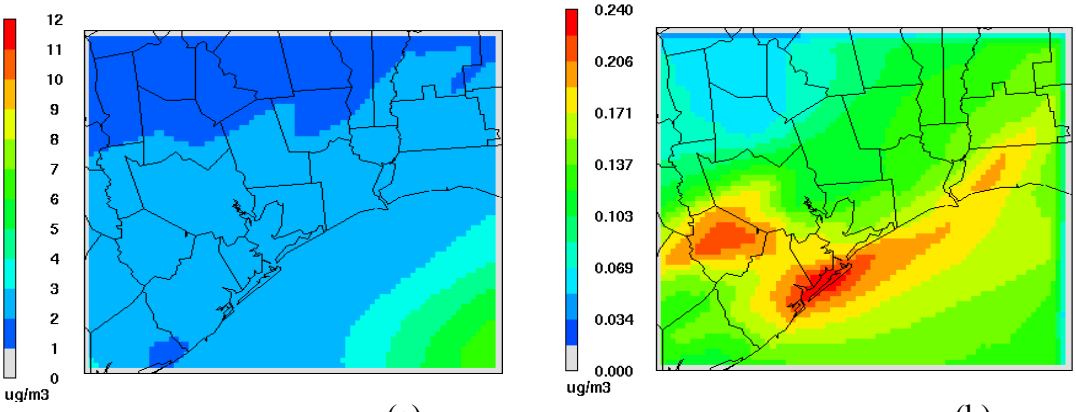


**Figure 4.9.** (a) Ground level SOA concentrations (μg/m$^3$) predicted with the presence of additional absorbing mass (Case 2) and (b) difference between SOA concentrations in Cases 1 and 2 (Case 2 – Case 1) predicted by CAMx at 10 am (the time when the maximum difference between two cases is observed) on September 6. Note that different scales are applied.

The next step in examining SOA formation pathways was to determine which hydrocarbon precursors led to SOA formation in the base case model formulation. Russell and Allen (2005) found that biogenic emissions, particularly of monoterpenes, were the main source of SOA precursors. Simulations performed as part of this work confirmed this finding. In CAMx, four condensable organic gas species (CG1- CG4) represent reaction products that contribute to four secondary organic aerosol species (SOA1-SOA4). CG1-CG3 that form SOA1-SOA3 are from anthropogenic VOCs and CG4 that form SOA4 are from biogenic terpenes (OLE2). Figure 4.10 shows predicted total SOA mass (SOA1-4) and SOA mass from biogenic contributions (SOA4). The figure demonstrates that biogenic emissions are a major contributor to SOA observed in Houston area. Specifically SOA4 contributed to 85% of total SOA mass domain wide in Case 2.

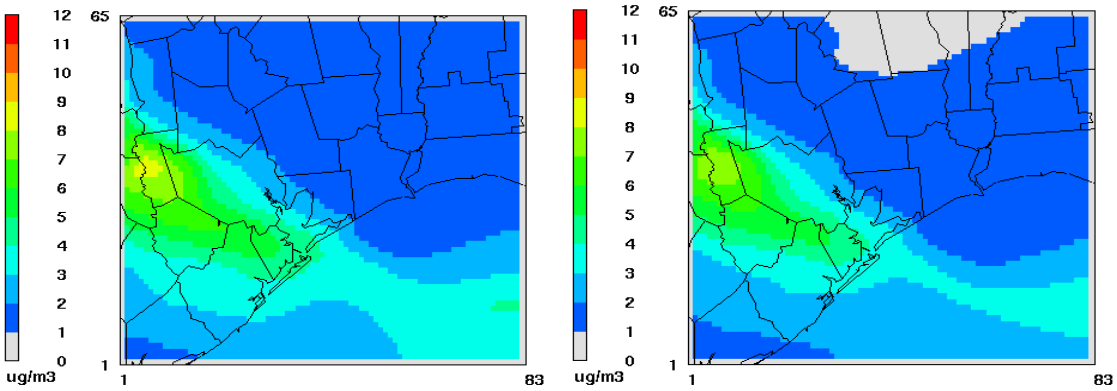


**Figure 4.10.** Ground level concentrations of (a) total SOA (SOA1-4) and (b) SOA from biogenic sources (SOA4) (µg/m$^3$) predicted by CAMx at 3 am (the time when peak OC concentration was observed at La Porte) on September 6; simulations account for gas/particle partitioning pathways of SOA with additional absorbing mass.

Recognizing that biogenic emissions are likely to be the dominant precursors in SOA formation, a next step in evaluating the potential importance of SOA formation via acid catalyzed routes is to estimate the extent biogenic precursor impingement on acidic aerosol. Figure 11(a-c) shows the degree of neutralization in terms of hydrogen ion (µmol/m3 air). Note also that although the location of the predicted peak non-neutralized plume is slightly south of the La Porte site, the general features are consistent with OC observations shown in Figure 11(d), particularly the time of onset of the non-neutralized plume and the time at which the plume dissipates. The temporal consistency of acid plume and observed OC concentrations at La Porte site strongly suggests that increase in OC concentrations during this wood smoke episode had a temporal pattern similar to the temporal pattern of acidity at the site.

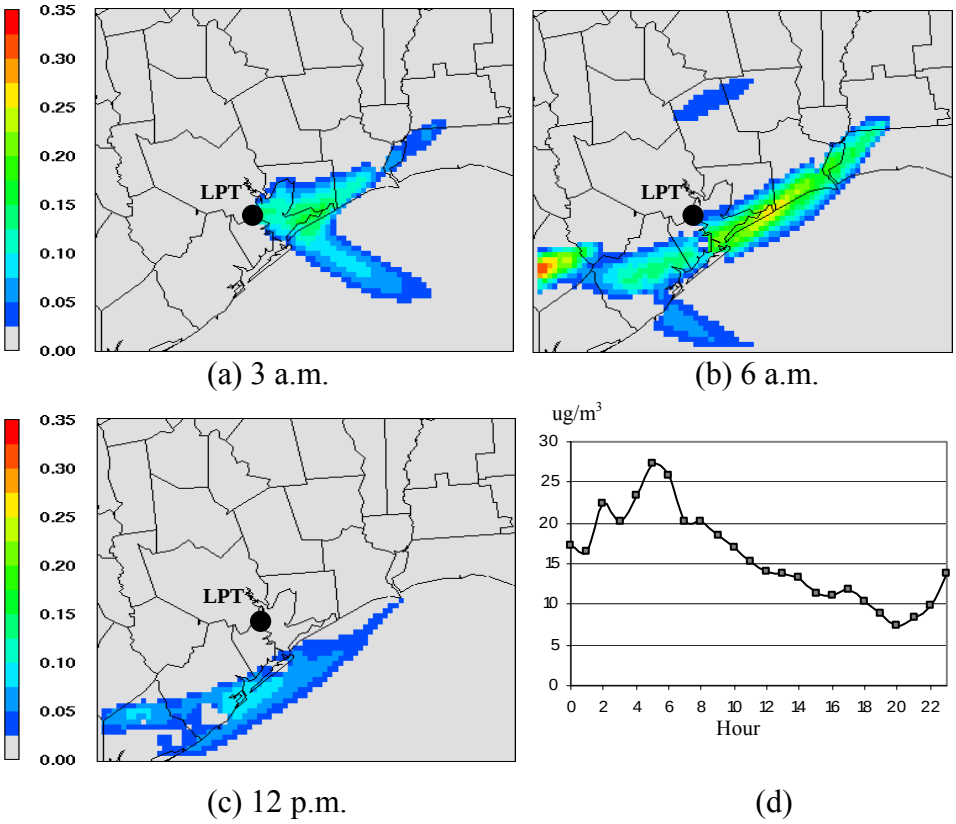


**Figure 4.11.** Degree of neutralization, [H+] (μmol/m$^3$), on September 6 at (a) 3 a.m., (b) 6 a.m., and (c) 12 p.m.; and (d) diurnal distribution of OC measured on September 6 at La Porte site (LPT) during the Texas Air Quality, in a unit of ug/m3 (Canagaratna et al. 2005).

The rate of SOA formation due to impingement of isoprene and aldehydes on the acidic aerosol was initially assessed by calculating total impingement rates, and assuming a reactive uptake fraction (conversion to SOA) of 1. This calculation provides an upper bound on potential SOA formation. Figure 4.12 shows isoprene concentrations and the post-processing impingement calculations of isoprene with acidic particles. Note that isoprene concentrations were over predicted by a factor of 2-3 in the model and thus, one should discount the predicted magnitudes by a factor of two to three. Isoprene concentrations were low at night and in early morning hours and therefore rates of heterogeneous reactions due to isoprene were low during the nighttime until early in the morning. In contrast, observations indicated that the OC that might be attributed to acid

catalyzed reactions may peak at night. Based largely on this difference in temporal patterns, the remaining modeling work will focus on the ALD2 species.

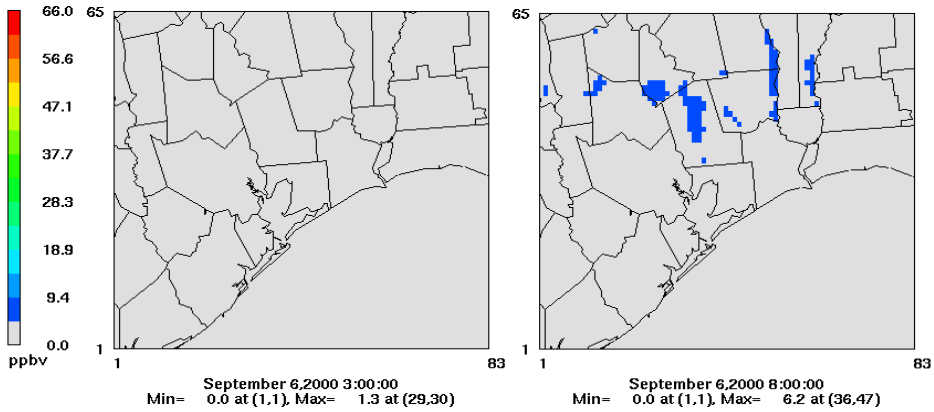


(a) Isoprene (ppbv)

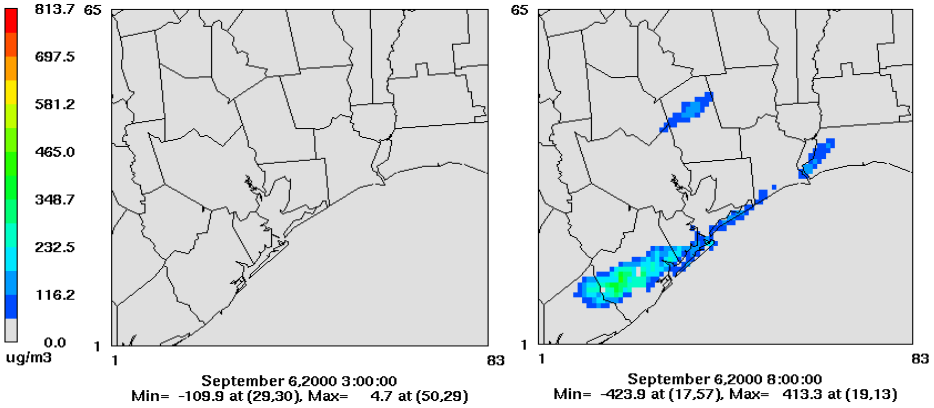


(b) Impingement calculations

**Figure 4.12.** Predicted ground level (a) isoprene concentrations (ppbv) and (b) secondary organic aerosol (ug/m3) due to impingement of isoprene, from sources within the domain, onto unneutralized particles, with a reactive uptake coefficient of 1 on Sep 6$^{th}$ at 0300 h (left) and at 0800 h (right).

In contrast to the case for isoprene, aldehyde concentrations (shown in Figure 4.13(a)) were significant at night. The acid-catalyzed heterogeneous reactions of ALD2 on acidic particles were incorporated in CAMx. CAMx simulations with various reaction

probabilities were performed and the results are depicted in Figure 4.14. The reaction probability γ was assumed constant throughout the modeling domain, at all times of day. Values of 0.0001, 0.0005, 0.005 and 0.001 were assumed for γ. Relatively small amounts of SOA are predicted via acid catalyzed reactions for values of γ less than 0.0005, but at values near or above 0.0005, the magnitude of SOA formation is more consistent with observations. Figure 4.15 compares the concentrations of SOA formed through partitioning theory and the concentrations of SOA formed via heterogeneous reactions on unneutralized particles.

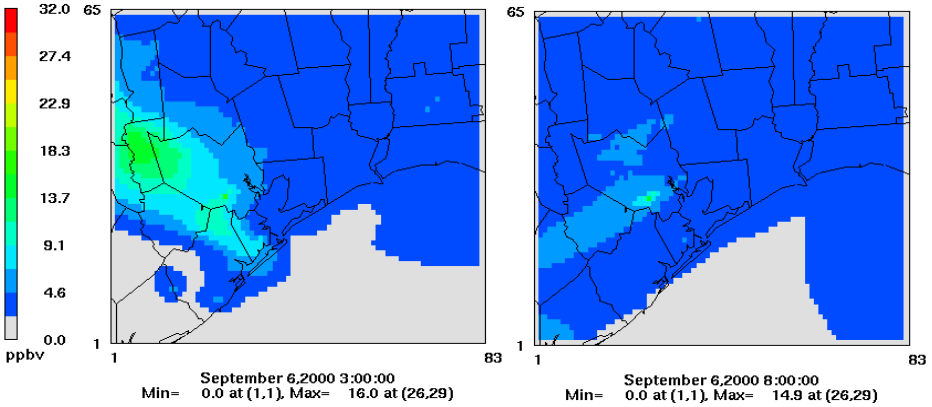


(a) Aldehydes (ppbv)

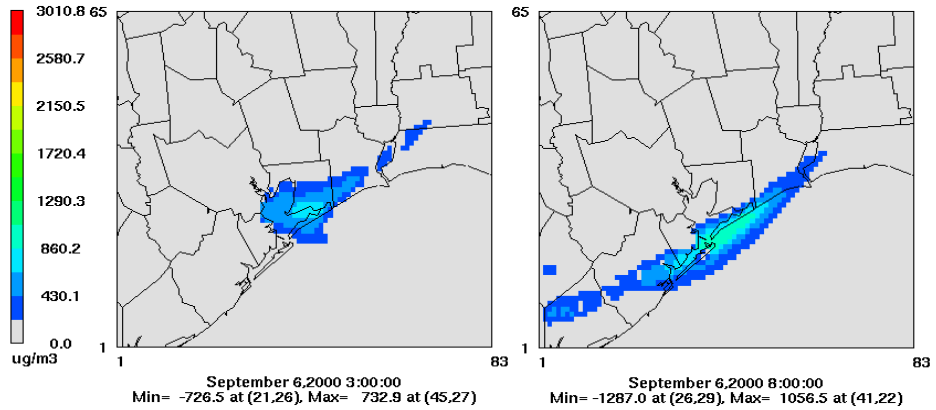


(b) Impingement calculations

**Figure 4.13.** Predicted ground level (a) aldehydes (ALD2) concentrations (ppbv) and (b) secondary organic aerosol (ug/m3) due to impingement of ALD2, from sources within the domain, onto unneutralized particles, with a reactive uptake coefficient of 1 on Sep 6$^{th}$ at 0300 h (left) and at 0800 h (right).

The right hand side of Figure 4.15 shows the temporal evolution of a large plume of SOA, produced by heterogeneous oxidation on unneutralized particles. The plume pronounces similar pattern with sulfate plume from wood smoke mediated reactions, i.e. the plume forms in Louisiana on the morning of September 6, advects toward Houston and passes the Houston measurement sites by the evening. Shown also in Figure 4.16 is the predicted SOA formation partitioning of condensible SVOCs and the acid heterogeneous reactions of aldehydes. The time of onset of the plume and the time at which the plume dissipates are consistent with temporal pattern of the organic compound measurements made at La Porte (also shown in Figure 4.15). In contrast, the SOA produced by condensible pathway (through partitioning theory), shown in the left hand side of Figure 4.15, does not replicate the spatial and temporal distribution of organic compound concentrations on September 6$^{th}$.

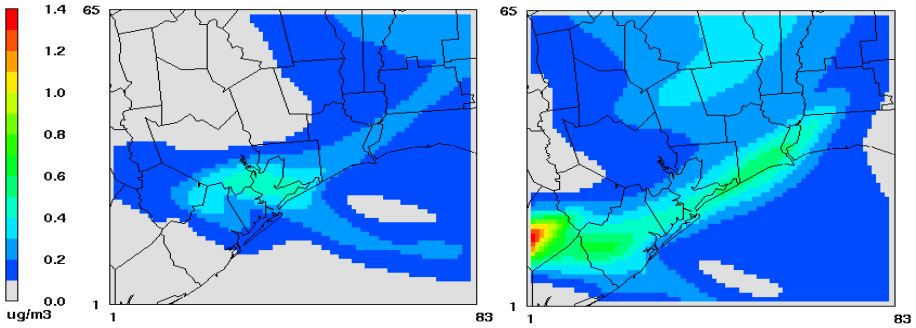


(a) Reactive uptake coefficient = 0.0001

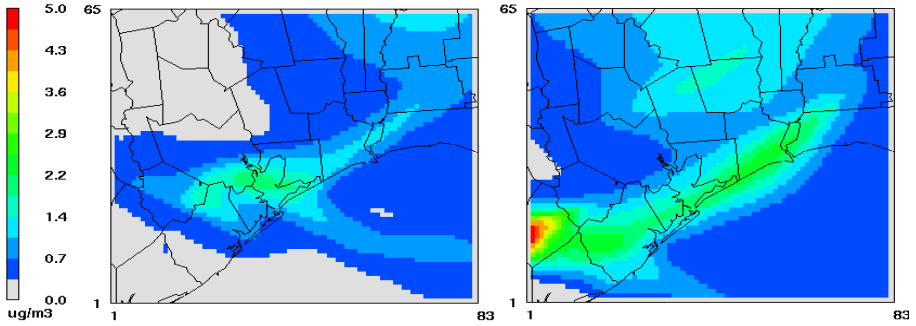


(b) Reactive uptake coefficient = 0.0005

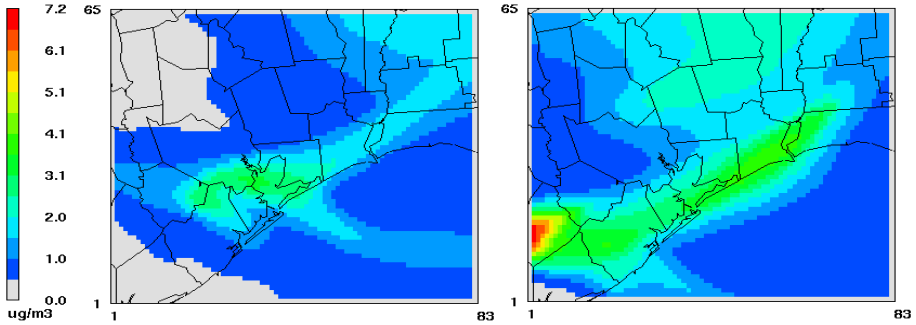


(c) Reactive uptake coefficient = 0.001

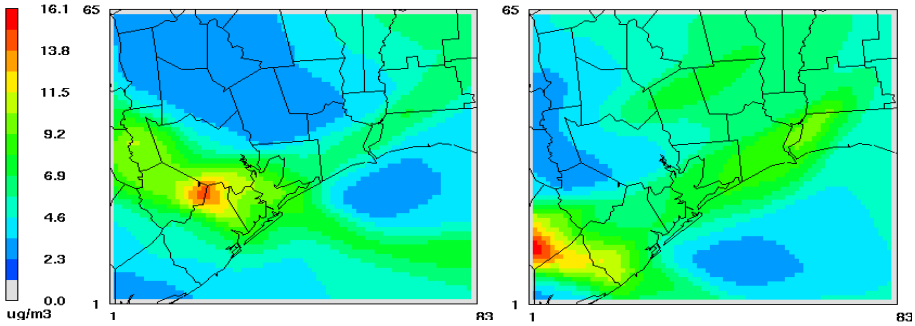


(d) Reactive uptake coefficient = 0.005

**Figure 4.14.** Predicted ground level SOA concentrations (μg/m$^3$) on Sep 6$^{th}$ at 0300 h (left) and at 0600 h (right) due to impingement of ALD2, from sources within the domain, onto acidic particles, with a reactive uptake coefficient of (a) 0.0001 (b) 0.0005, (c) 0.001, and (d) 0.005.

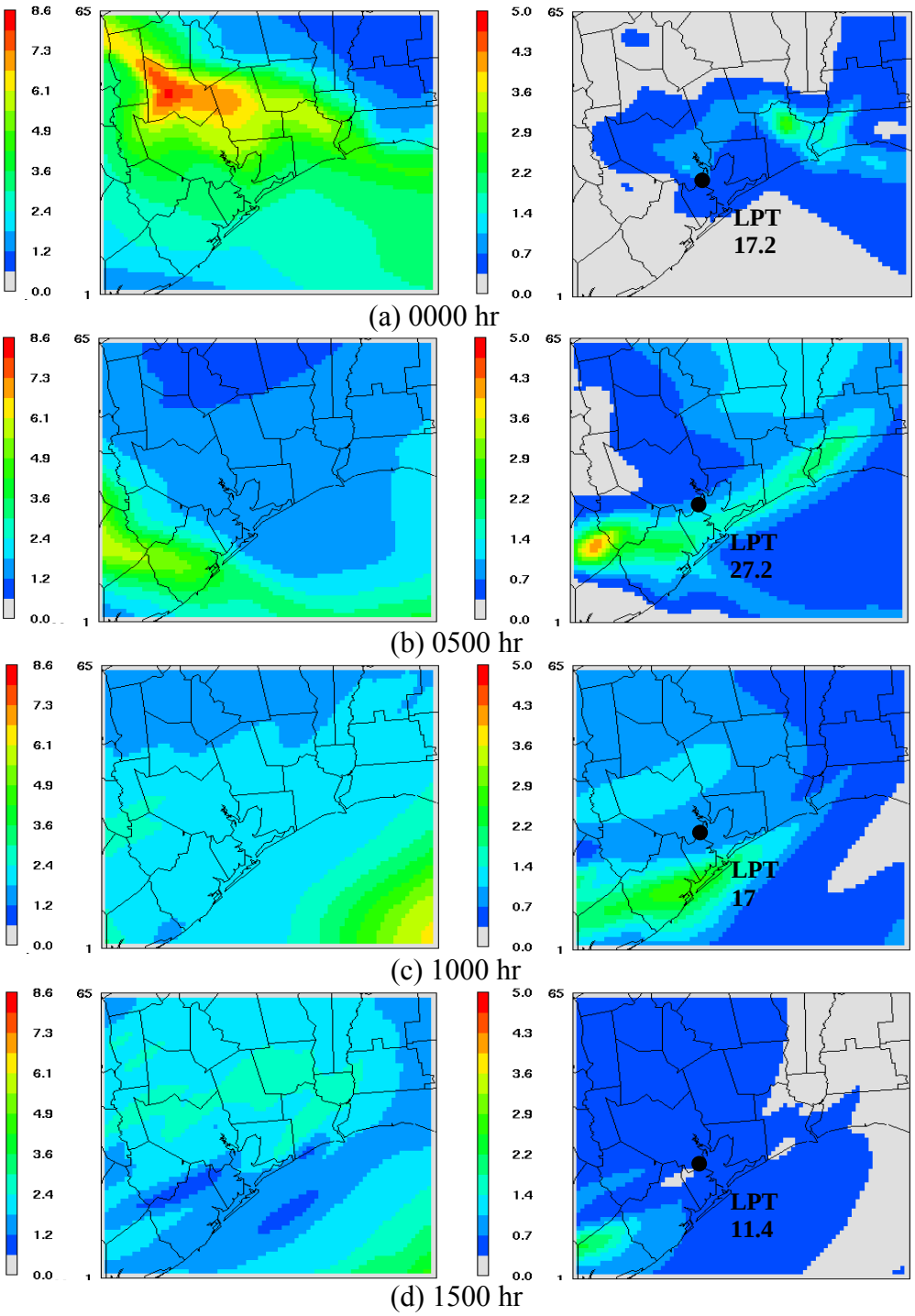


**Figure 4.15.** Ground level SOA concentrations (μg/m$^3$) on 6 September predicted by CAMx via partitioning theory (Left) and via impingement of ALD2, from sources within the domain, onto unneutralized particles, with a reactive coefficient of 0.0005 (Right) at (a) 0000 h (b) 0500 h (c) 1000 h, and (d) 1500 h; observed organic compound concentrations (μg/m$^3$) at the La Porte (LPT) monitoring site are shown (Canagaratna et al. 2005).

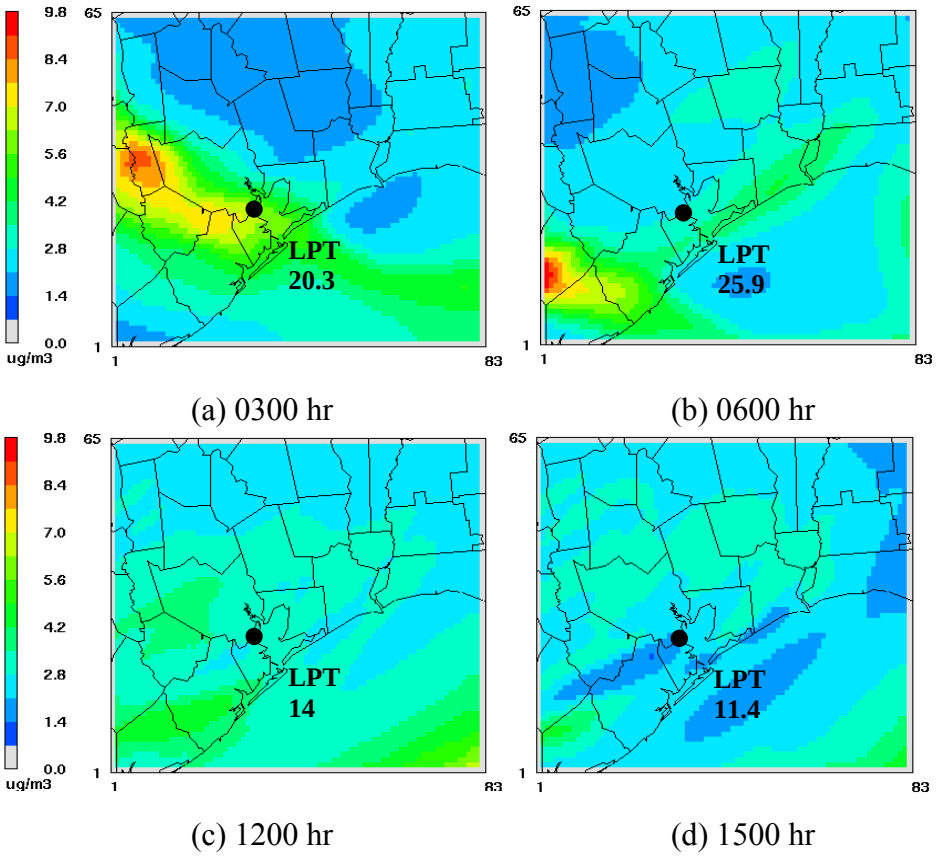


**Figure 4.16.** Predicted ground level total SOA concentrations (μg/m$^3$) due to partitioning of condensible SVOCs and the acid heterogeneous reactions of aldehydes with a reactive uptake coefficient of 0.0005 on September 6 at (a) 0300 hr, (b) 0600 hr, and (c) 1200 hr and (d) 1500 hr; observed organic compound concentrations (μg/m3) at the La Porte (LPT) monitoring site are shown (Canagaratna et al. 2005).

It is difficult to pinpoint the value of the reaction probability parameter γ that leads to results most consistent with observations due to limitations in estimating the observed secondary organic concentrations, as described earlier. Nevertheless, the overall indications are that the acid-catalyzed heterogeneous reactions of aldehydes did influence organic carbon concentrations during this episode. Even a small reaction probability value of only 0.0005 can contribute up to 5 μg/m$^3$ of SOA. It should be noted, however, that this parameter finding is dependent on the assumed surface area of the wood smoke particles and molecular weight of the impingement product, the modeled locations of the wood smoke plumes that influence acidity, and other parameters. As

mentioned earlier, neutralized sulfate was excluded in approximated unneutralized particle mass and the molecular weight was assumed as a lower bound. It should also be noted that the dependence of SOA formation on $\gamma$ is not linear, as was true in the case of heterogeneous sulfate formation.

### *4.5 CONCLUSION*

Observational data, collected during a wood smoke episode in Houston, Texas, indicated that wood smoke enhanced SOA formation in the area. Previous study used the source apportionment technique to quantify contributions from primary sources including wood combustion during the episode. In this work it was shown that such technique could lead to a significant bias due to the variability of biomass marker and the limitation of sample frequency, i.e. daily samples instead of hourly samples. Thus, more experimental work and field studies are in critical needed to reconcile such limitations. Other approach in evaluating SOA mass is via photochemical simulations.

A 3-D photochemical grid model was used to examine SOA formation based on the partitioning theory when available absorbing mass increases. Results suggest that the domain of interest was not limited by availability of absorbing mass but rather limited by availability of SOA precursors. Observational data during this episode indicated high particulate mass, sulfate concentrations and organic carbon concentrations on intense fire days. Our hypothesis is that high sulfate productions could potentially influence the degree of neutralization and thus the acid-catalyzed heterogeneous reactions could play a significant role in OC enhancements during the wood smoke episode. The acid-catalyzed heterogeneous reactions can drive low molecular weight organic gases that are generally not favorable according the partitioning theory into low vapor pressure products, resulting in SOA mass. Our simulations have shown that Houston area during this wood smoke episode had acidic environment during the day with intensive fire activities. This finding is very important, as it is the first time to show potentials of the acid-catalyzed heterogeneous reactions using photochemical grid simulation.

In the photochemical model, the acid-catalyzed heterogeneous reaction of SOA formation was modeled by using the impingement calculation approach similar to the

assessment of wood-smoke mediated sulfate formation. Two VOC species were examined, namely isoprene and aldehydes. The post-processing analysis suggested that isoprene itself did not play a major role in the heterogeneous formation of secondary aerosol. Its photo-oxidation products and aldehydes that contain carbonyl group, however, might play a part.

The acid-catalyzed SOA formation of aldehydes was modeled by calculating the rate of impingement of aldehydes molecules on the unneutralized particles, and then assuming that a fraction of the impingements resulted in reaction. For reaction probabilities on the order of 0.0005, the model predicted up to 5 $\mu g/m^3$ with promising temporal distributions of SOA concentrations consistent with observations.

# Chapter 5 Conclusions and Recommendations

There are three major accomplishments of this research:

1) *Identification of an observable effect of heterogeneous (gas/particle) atmospheric reactions in ambient data* The Evidence for heterogeneous chemistry was strongest during a wood smoke episode that occurred in August and September 2000 in the Houston area. During this episode high concentrations of both sulfate and organic carbon were observed; the work reported in this theses found that, for the sulfate: a) direct primary emissions from wildfire smoke did not play a role in creating high sulfate concentrations in ambient particulate matter, b) chloride concentrations in oak and pine wood smoke are not sufficient to account for the observed sulfate enhancements via chloride displacement reactions, c) observed $SO_2$ and $OH\cdot$ concentrations were not particularly elevated during days of intense fire activity and modeling suggests this route does not account for observed sulfate concentrations on days with fire, d) the volume of aqueous phase condensed onto wood smoke particles led to an insignificant sulfate formation, and e) heterogeneous reactions are the only explanation left for enhancement of sulfate during the wood smoke episode. For the organic carbon, the work presented in this thesis demonstrated: f) observed organic carbon concentrations cannot be explained entirely by direct emissions from biomass burning.

2) *Incorporation of heterogeneous atmospheric reactions into a widely used eulerian photochemical model* The approach used in this work to estimate the rate of heterogeneous sulfate and SOA formation was to multiply the surface impingement rate of gas phase $SO_2$ or SOA precursors on wood smoke particle surfaces or acidic particle surfaces. This rate of impingement was multiplied by an estimate of the fraction

of the impinging molecules that adsorb and react, referred to as a reactive uptake coefficient/reaction probability.

3) *Demonstration of qualitative agreement between model predictions and observed concentrations of sulfate and organic carbon, produced by heterogeneous reactions in Southeast Texas*. Using reasonable reaction probabilities ($10^{-4}$ to $10^{-2}$), the predicted rates of heterogeneous sulfate and SOA formation and accumulation showed magnitudes, temporal distributions and spatial distributions that were qualitatively similar to ambient observations.

This research has successfully implemented heterogeneous reactions for sulfate and organic carbon formation into a regional grid model. A similar procedure could be applied to other heterogeneous reactions, such as the heterogeneous $N_2O_5$ hydrolysis.

Global model studies by Dentener and Crutzen (1993) and Tie, et al. (2001) show that heterogeneous $N_2O_5$ hydrolysis can significantly reduce the NOx budget and result in 10-20% $O_3$ reduction in the Northern Hemisphere. Currently, this heterogeneous $N_2O_5$ hydrolysis does not exist in CAMx and inclusion of the reaction is in critical need. The model tool developed in this research is ideal for this purpose.

Nitrogen oxides ($NO_x$) play a critical role in tropospheric chemistry. They influence the cycle of odd hydrogen (HOx) and react catalytically to produce ozone ($O_3$). A major atmospheric sink of $NO_x$ is the formation of $HNO_3$, which is eventually removed by wet or dry deposition. During the day, the formation of $HNO_3$ occurs via the reaction of $NO_2$ and OH. At night, the heterogeneous hydrolysis of $N_2O_5$ on aerosol surfaces and cloud droplets leading to $HNO_3$ formation is the dominant removal mechanism for NOx (Dentener and Crutzen 1993; Platt et al. 1984).

$$N_2O_5 + H_2O_{aerosol} \rightarrow 2HNO_3 \qquad (5.1)$$

One way to quantify reaction rate of the hydrolysis of $N_2O_5$ on particles (Equation 5.1) is to use the reaction probability, $\gamma_{N2O5}$. Its value may differ by orders of magnitudes

on different aerosol surfaces and is typically in the range of 0.001 to 0.1. Recent laboratory studies found that $\gamma_{N2O5}$ value depends on relative humidity (RH) and temperature. Table 5.1 shows some reported $\gamma_{N2O5}$ values on different aerosol surfaces under varying atmospheric conditions.

**Table 5.1.** Reaction probabilities for $N_2O_5$ Hydrolysis on aerosol surfaces

| Aerosol Type | Reaction Probability | Reference |
|---|---|---|
| $(NH_4)_2SO_4$ | $\gamma = \alpha \times 10^{\beta}$<br>$\alpha = 2.79 \times 10^{-4} + 1.3 \times 10^{-4}RH - 3.43 \times 10^{-6}RH^2 + 7.52 \times 10^{-8}RH^3$<br>$\beta = 4 \times 10^{-2} (T-294)$ $(T \geq 282K)$<br>$\beta = -0.48$ $(T < 282K)$ | (Evans and Jacob 2005; Hallquist et al. 2003; Kane et al. 2001) |
| $(NH_4)_2SO_4$ | $\gamma = 2.07 \times 10^{-3} - 1.48 \times 10^{-4}RH - 8.26 \times 10^{-6}RH^2$ | (Kane et al. 2001) |
| $H_2SO_4$ | $\gamma = 0.052 - 2.79 \times 10^{-4}RH$ | (Kane et al. 2001) |
| Organic Carbon | $\gamma = 5.2 \times 10^{-4}RH$ $(RH \leq 57\%)$<br>$\gamma = 0.03$ $(RH > 57\%)$ | (Evans and Jacob 2005; Thornton et al. 2003) |
| Black Carbon | $\gamma = 0.016$<br>$\gamma = 4 \pm 2 \times 10^{-5}$ (dry), $2 \pm 1 \times 10^{-4}$ (50% RH) | (Longfellow et al. 2000; Saathoff et al. 2001) |

Several attempts have been made to implement the heterogeneous $N_2O_5$ hydrolysis in chemical transport models. A constant $\gamma_{N2O5}$ value of 0.1 measured by Mozurkewich and Calvert (1988) has been the standard used in many global models (Dentener and Crutzen 1993; Tie et al. 2001; Wang et al. 1998). However, some modeling studies with analyses of field observations suggested that $\gamma_{N2O5}$ is less than 0.1(Schultz et al. 2000; Tie et al. 2003). Recently, Evans and Jacob (2005) introduced a new parameterization of $\gamma_{N2O5}$ in a global model by taking account to aerosol composition, relative humidity, and temperature. This author found increases in mass-averaged NOx and $O_3$ of 7% and 4%, respectively, relative to a model simulation with a uniform $\gamma_{N2O5}$ (0.1). Although the majority of work on this reaction has been on global scale, there have been few observations to compare the global model assessments of the impact of $N_2O_5$ hydrolysis on tropospheric chemistry. Regional scale models when summer episodes are investigated are recommended.

One of a few studies on $N_2O_5$ hydrolysis in regional scale was performed by Riemer et al. (2003) using a European model. This work employed a chemical composition weighting approach by scaling two base values $\gamma_{N2O5} = 0.02$ for sulfate and 0.002 for nitrate according to the sulfate and nitrate mass concentrations in the aerosol. The author found that the impact of this reaction on ozone is small, but it remarkably affects aerosol surface area and nitrate content. More studies on this reaction with a focus in regional scale models in the area where active field measurements are available, such as Texas, are necessary.

Currently, this heterogeneous $N_2O_5$ hydrolysis does not exist in CAMx and incorporation of the reaction is in critical need. The model tool developed in this research is ideal for this purpose. Although the implementation of this reaction is out of scope of this research, a preliminary analysis on contributions of $N_2O_5$ hydrolysis to Texas areas was performed here. The Community Multiscale Air Quality (CMAQ-MADRID) (EPRI 2002) was selected for this study because it already includes the heterogeneous $N_2O_5$ hydrolysis. In addition, there are extensive CMAQ-MADRID modeling data sets available for previous air quality study, BRAVO[1]. The modeling domain was a regional scale 36-km grid, shown in Figure 5.1. The episode period was September 10-20, 1999. Meteorological inputs required by the model were based on results from the Mesoscale Meteorological Model, version 5, MM5 (Seaman and Stauffer 2003). Emission inventories of NOx, VOC, CO, SO2, NH3, PM2.5 and PM10 for this episode were developed elsewhere (Kuhns et al. 2005).

[1] [1] The Big Bend Regional Aerosol and Visibility Observational Study (BRAVO) was undertaken in 1999. The study included sampling of aerosols at 40 locations to investigate the cause of visibility reducing hazes at Big Bend National Park. The reader is referred to http://www.epa.gov/ttn/chief/net/mexico.html[1]


**Figure 5.1.** Modeling domain used in the BRAVO study.

Two simulations were performed. The first simulation uses a uniform $\gamma_{N2O5} = 0.1$ for all aerosol types and conditions. The result can serve as upper-bound contribution from this reaction to atmospheric conditions in Texas. For comparison purposes, the heterogeneous reactions were turned off for the second simulation. Figure 5.2 (a-b) show predicted maximum percentage reduction of $O_3$ and NOx respectively, relative to a model simulation with a uniform $\gamma_{N2O5}$. The maximum percentage reduction (max $\%O_{3\ \text{reduction}}$) is defined as the maximum of $[O_{3\ \text{without heterogeneous reactions}} - O_{3\ \text{with heterogeneous reactions}}]/\ O_{3\ \text{without heterogeneous reactions}}$ x 100 at any given time during one day period.

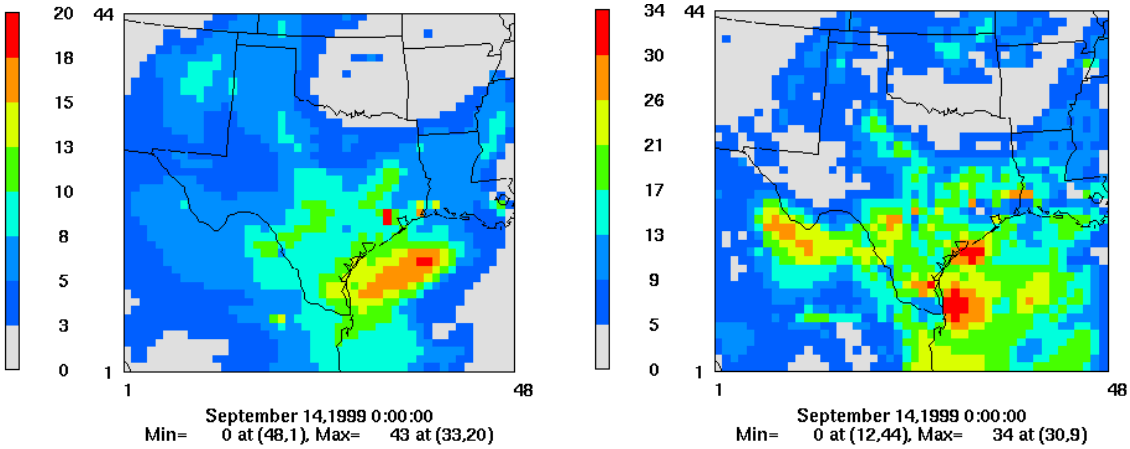


(a) $O_3$ (b) NOx

**Figure 5.2.** Predicted maximum percentage reductions of ground level (a) $O_3$ and (b) NOx on September 14, 1999.

Simulations results in Figure 5.2 suggest that $N_2O_5$ hydrolysis could reduce mass-averaged of $O_3$ and NOx up to 43% and 34% respectively. On average 10% maximum reduction of $O_3$ was predicted for the Southeastern area of Texas. This magnitude of difference is significant that the author suggests further investigation on contribution of this $N_2O_5$ hydrolysis.

***Recommendations***

Future development of more detailed emission inventories is also a fundamental need. Since the heterogeneous reactions can be significant, it is recommended that primary emissions inventory of PM be developed. This PM inventory should carry detailed speciation and size segregation information. For some gas species that can contribute to particulate formation, such as $NH_3$, more field measurements should be made available to allow emission inventory evaluation and modeling assessment on these gases. Note also that $NH_3$ emissions were observed during fires (Trebs et al. 2005) and thus it is important to include $NH_3$ in fire emission inventories.

Future SOA modeling work needs to more fully integrate inorganic and organic chemistries. Development of inorganic equilibrium models that are based on pH calculations need to integrate the acidity from organics. In addition, more quantitative

analysis of reaction rates and detailed mechanisms of acid catalyzed carbonyl condensation pathways are needed.

# APPENDIX A: Secondary sulfate formation

In order to characterize the magnitude sulfate formation both homogeneous and heterogeneous reaction mechanisms must be accounted for. This appendix describes the homogeneous and heterogeneous sulfate formation mechanisms used in this thesis.

**Sulfate formation through homogeneous gas phase Mechanisms**

In the gas phase, radicals; e.g., HO, $HO_2$, and $CH_3O_2$, are the principal species responsible for the homogeneous oxidation of sulfur dioxide. First order rates of oxidation of sulfur dioxide, due to these homogeneous reactions during daylight hours can be as high as 4%/h (Calvert et al. 1978). Among these pathways, reaction of $SO_2$ with $OH^{\bullet}$ is dominant (Stockwell and Calvert 1983). $SO_2$ reacts with OH radical in the presence of oxygen and water to form $HSO_3$ as shown in Equation (A.1).

$$SO_2 + OH^{\bullet} + M \longrightarrow HOSO_2^{\bullet} + M \qquad (A.1)$$

M is a non-reacting species that is able to stabilize active species by collision. This step is followed by the regeneration of the chain-carrying $HO_2$ radical.

$$HOSO_2^{\bullet} + O_2 \longrightarrow HO_2^{\bullet} + SO_3 \qquad \textbf{(A.2)}$$

Sulfur trioxide, in the presence of water vapor, is converted rapidly to sulfuric acid,

$$SO_3 + H_2O + M \longrightarrow H_2SO_4 + M \qquad (A.3)$$

The sulfuric acid then condenses rapidly into the particle phase. The reaction of sulfur dioxide with hydroxyl radical (A.1) is the rate-limiting step in this sequence (Gleason et al. 1987).

**Sulfate formation via Chloride displacement reaction**

Particulate matter from fires is emitted at high temperature, and at these temperatures, many inorganic elements volatize (Gaudichet et al. 1995; Knudsen et al. 2004; Robinson et al. 2004; Sander B. et al. 2000). Observations show that the elements Potassium (K), Chlorine (Cl), and S are emitted from biomass burning in the gas phase mainly as KCl, KOH, $SO_2$, and HCl (Christensen et al. 1998; Sander B. et al. 2000). KOH can react with HCl, adding more KCl into the system. As the emissions are mixed with cooler ambient air, some of the KCl mass may condense as KCl on particle surfaces. However, $SO_2$ and atmospheric $O_2$ can react with KCl (both in gas and particle phases) forming particulate phase $K_2SO_4$ and gaseous HCl. The chloride displacement reaction has been shown to predominantly take place in the gas phase (Boonsongsup et al. 1997; Christensen et al. 1998; Dayton et al. 1995; Jensen et al. 2000) shown in Equation (A.4):

$$2KCl + SO_2 + \frac{1}{2}O_2 + H_2O \Leftrightarrow K_2SO_4 + 2HCl \qquad (A.4)$$

This chloride displacement occurs rapidly with fresh particles that originally have a high Cl/S ratios. Li et al. (2003) reported that more than 90% of the KCl particles were completely converted to potassium sulfate or nitrate during a 24 minute transport time to a receptor site 16 km down wind.

**Sulfate formation through condensed phase reactions**

Sulfate formation is generally believed to occur in aqueous aerosol, so formation of sulfate through condensed phase reactions will involve the conversion of wood smoke particles to hydrophilic materials and subsequent aqueous reactions. Each of these processes is described below.

Wood smoke particles are initially emitted as dry and relatively hydrophobic materials; these hydrophobic particles can then undergo atmospheric reactions and $O_2$ physisorption to become hydrophilic. Examples of the atmospheric reactions that can make wood smoke particles hydrophilic are $SO_2$ oxidation on dry surfaces producing $H_2SO_4$, and reaction of $O_3$ with particle carbon resulting in formation of surface carboxylic groups (Smith and Chughtai 1995).

Hygroscopicity measurements have commonly been performed using a tandem differential mobility analyzer (TDMA). In the TDMA technique, one first measures the size distributions of ambient particles using a DMA. The DMA creates samples of monodisperse aerosols; these monodisperse samples of the ambient aerosol are exposed to a higher relative humidity and a second DMA measures their new size. Results from this technique are expressed in terms of the growth factor, $D_p/D_p^*$ as a function of particle size, where the growth factor is the ratio of the hydrated particle diameter, $D_{p,}$ to the monodisperse dry diameter, $D_p^*$.

Previous studies of the hygroscopicity using TDMA technique have shown that 1) sub-micrometer atmospheric particles mostly exhibit bimodal (or even multi-modal) growth patterns, suggesting an externally mixed aerosol population, and 2) particle hygroscopicity increases with increasing dry size (Gasparini et al. 2004; Kerminen 1997; Swietlicki et al. 1999). The observed groups of particles are normally denoted the less-hygroscopic mode and the more-hygroscopic mode, having average growth factors of 1.11-1.15 and 1.38-1.69 respectively when taken from a dry state to a relative humidity of 90% (Swietlicki et al. 1999). Inorganic substances, such as NaCl and $(NH_4)_2SO_4$, generally uptake water and dissolve (deliquescence) under sub-saturated humidity conditions. The dissolution of these particles is thermodynamically favorable since it lowers the free energy. Therefore, those particles that contain soluble inorganic salts, acids, and oxidized organics grow significantly in response to increased relative humidity

(RH), while those composed of water insoluble species such as soot, many organic compounds, and dust exhibit little hygroscopic growth.

Particles from biomass burning have a complex mixture of inorganic and organic components. Reported data indicate that, on average, organic components account for about 80% mass of the fresh dry smoke particles, followed by 5-9% black carbon, and 12-15% of trace inorganics (Reid et al. 2004). Much organic carbon making up smoke particles is believed to be water-soluble since cellulose is water-soluble, yet, knowledge of the water uptake of the overall organic portion of atmospheric aerosol has been limited. Although these biomass burning particles are believed to contain large amounts of soluble material (Simoneit et al. 1993), Zhou (2001) reported that the hygroscopic behavior of sub-micrometer aerosol particles in the Amazon pristine rain forest is essentially mono-modal with quite low growth factors (1.17-1.32, from dry $D_p$ of 0.035-0.265 microns to 90% RH). Similarly, Hämeri et al. (2001) performed observations for the Finnish boreal forest in Finland and found higher growth factors(1.16-1.59, from dry $D_p$ of 0.01-0.264 microns to 90% RH) and that the hygroscopic behavior is rather mono-modal as well.

In summary, smoke particles are usually internally mixed, typically with a core of black carbon and alkali earth compounds coated with organic compounds. Hygroscopicity of these particles, although measurable, is very complex. This is because the hygroscopicity depends strongly on particle composition and size distributions, both of which depend on fuel composition and fire chemistry. Atmospheric RH also plays an important role in this property.

The process of converting gas phase $SO_2$ into aqueous phase sulfate involves the following steps: 1) transport of gas to the surface of the particles, 2) transfer of the gas across the air-liquid interface, 3) formation of aqueous equilibria and 4) transport of the dissolved species from the surface to the bulk aqueous phase of the droplet, and 5) reaction of the dissolved species in the bulk aqueous phase. Schwartz and Freiberg (1981) have calculated characteristic time associated with these processes, and Schwartz (1988) suggested that under most conditions mass transport is not a limitation, and the chemical reaction rate will be rate determining in the S(IV) aqueous-phase oxidation (Finlayson-Pitts 1999).

S(*IV*) Aqueous Equilibria

When gas phase sulfur dioxide dissolves in water, it forms the following equilibrium species:

$$SO_{2(g)} + H_2O \Leftrightarrow SO_2 \cdot H_2O_{(aq)} \quad \text{(A.5)}$$

$$SO_2 \cdot H_2O_{(aq)} \Leftrightarrow HSO_3^- + H^+ \quad \text{(A.6)}$$

$$HSO_3^- \Leftrightarrow SO_3^{2-} + H^+ \quad \text{(A.7)}$$

The predominant form dissolved in solution depends on the acidity of the solution. Because different forms exists in solution, the oxidation state (i.e., +4) is often used to denote all these dissolved $SO_2$, that is,

$$S(IV) = SO_2 \cdot H_2O + HSO_3^- + SO_3^{2-} \quad \text{(A.8)}$$

The oxidized form of sulfur is in the +6 oxidation state, common referred to as S(VI). The individual reactions in (A.5)-(A.7) are relatively fast (Martin 1984), thus, regardless of which of the three species on the right hand side of Eq.(A.8) is the actual reaction, the equilibrium will be reestablished rapidly.

S(IV) Oxidations in aqueous solutions

There are several pathways for S(IV) oxidations involving reactions of $H_2O_2$, $O_3$, $O_2$, OH, $SO_5^-$, $HSO_5^-$, $SO_4^-$, PAN, $CH_3COOH$, $CH_3C(O)OOH$, $HO_2$, $NO_2$, $NO_3$, HCHO and $Cl_2^-$. We summarize below only a few of the most important reactions for oxidizing S(IV) into S(VI) in solution by individual atmospheric oxidants.

*Oxidation by hydrogen peroxide ($H_2O_2$)*: $H_2O_2$ has been shown to oxidize S(IV) relatively rapidly because it is highly soluble in water with high ambient concentrations compared to other oxidants. The reaction with sulfur is more or less pH independent but happens preferably between pH 2 and 8 (Martin and Damschen 1981). The mechanism is thought to be a nucleophilic displacement reaction by hydrogen peroxide on $HSO_3^-$ as the reactive species.

$$HSO_3^- + H_2O_2 \rightarrow SO_2OOH^- + H_2O \quad (A.9)$$

$$SO_2OOH^- + H^+ \rightarrow H_2SO_4 \quad (A.10)$$

*Oxidation by ozone ($O_3$)*: Even though the Henry's law constant for ozone is fairly small, there is sufficient ozone in the troposphere to drive reaction with $SO_2$ in solution, making it a potential oxidant. The rate is pH dependent in that it is inhibited in more acidic solution. Hence, this reaction is particularly important in sea salt particles or when pH of the aqueous phase exceeds about 4.

$$S(IV) + O_3 \rightarrow S(VI) + O_2 \quad (A.11)$$

*Oxidation by oxygen ($O_2$) catalyzed by $Mn^{2+}$, $Fe^{3+}$*: Uncatalyzed reaction of $O_2$ is too slow to be important (Finlayson-Pitts 1999; Seinfeld and Pandis 1998). Of more concern is the catalyzed oxidation with $Mn^{2+}$ and $Fe^{3+}$, which are both common constituents of tropospheric aerosols. The mechanism and kinetics are very complex and very sensitive to variety of factors, including pH, and ionic strength. The reactions are likely to be significant at pH values near neutral, i.e., in the range of 6-7 (Finlayson-Pitts 1999).

*Oxidation by organic peroxides*: Methylhydroxyperoxide (MHP) reacts with $HSO_3$ after the following scheme with an overall rate that is pH independent:

$$HSO_3^- + CH_3OOH + H^+ \rightarrow SO_4^{2-} + 2H^+ + CH_3OH \quad \text{(A.12)}$$

Peroxyacetic acid (PAA) proceeds with high rate constants at pH 3-6 with the overall rate increasing with increasing pH:

$$HSO_3^- + CH_3C(O)OOH \rightarrow SO_4^{2-} + H^+ + CH_3OOH \quad \text{(A.13)}$$

*Oxidation by oxides of nitrogen*: The reaction of nitrogen dioxide ($NO_2$) is in general of minor importance because $NO_2$ has limited water solubility, resulting in low aqueous-phase concentration. However, it can become important in areas with high $NO_2$ concentrations like in urban clouds. The suggested reaction is:

$$2NO_2 + HSO_3^- \xrightarrow{H_2O} 3H^+ + 2NO_2^- + SO_4^{2-} \quad \text{(A.14)}$$

Estimates have shown that $H_2O_2$ is expected to be the most important oxidant for S(IV) in clouds at pH< 4.5. The rate of oxidation can exceed 500% $h^{-1}$ assuming cloud conditions with 1 g $m^{-3}$ of liquid water content (Seinfeld and Pandis 1998). At higher pH values, both $O_3$ and the iron-catalyzed $O_2$ oxidation can compete. These aqueous-phase reactions have been well studied and integrated in some air quality and cloud models (Walcek and Taylor 1986). In CAMx, S(IV) oxidants in the current modeling configuration are $H_2O_2$, $O_3$, $O_2$(catalyzed by $Mn^{2+}$, $Fe^{3+}$),MHP and PAA.

**Sulfate formation through heterogeneous gas/particle phase reactions**

The reactions of $SO_2$ to form sulfate have been studied on a variety of surfaces and with a variety of oxidants. It is difficult to generalize about the rates and extent of these reactions, however, since the reactions are sensitive to the chemical and physical nature of the surfaces and oxidants. These processes could be limited by availability of $SO_2$ in the atmosphere, availability of surface sites, and/or reaction rate processes.

One of the pioneering works indicating the appearance of sulfate on the surface of various particles was done by Novakov et al. (1974). They suggested that atmospheric $O_2$ can be important in $SO_2$ oxidation. Following this work, many laboratory studies were conducted to find the rate of removal of gaseous $SO_2$ over many solids. Judeikis et al. (1978) used a particle-coated laminar flow reactor to produce experimental data for a number of solids (ash, MgO, charcoal etc.) which suggested very high initial reactions rates. However, the surface saturation behavior and limited available surface area makes the initial rates difficult to sustain. Liberti et al. (1978) and Tartarelli et al. (1978) examined the adsorption and reaction of $SO_2$ on atmospheric particles from a variety of sources. The extent of adsorption and reaction depends upon the particles' chemical composition and their nature, which can be defined in terms of pH, surface area, humidity and degree of surface coverage by adsorbed components. The presence of $O_2$ strongly enhanced sulfate formation on carbonaceous particles.

Britton and Clarke (1980) saw an enhancement of the rate of $SO_2$ transformation due to the presence of $NO_2$ with insignificant change in the total amount of $SO_2$ that can be adsorbed. Reaction of $NO_2$ with adsorbed $SO_2$ can be significant at atmospheric concentrations and could be dominant in plume situations. Baldwin (1982) concluded that in surface-catalyzed oxidation of $SO_2$ (with concentration in ppm range) the rate-limiting step is the surface reaction, not the adsorption of the $SO_2$. He added that the adsorption of $SO_2$ on active carbon was not affected by $NO_2$; however, the surface oxidation was enhanced by $NO_2$. Desantis and Allegrini (1992) concluded that such enhancement depends on the nature of sample chosen; *i.e.*, $NO_2$ has no effects on samples from an urban combustor while it affected strongly a sample from an industrial combustor.

This brief literature review suggests that these heterogeneous pathways occur but the extent of their contributions is unknown. Lacking of detailed mechanisms and knowledge of limiting-steps hinders incorporation of these pathways into current air quality models.

# APPENDIX B: Secondary organic aerosol formation

Carbon in atmospheric particulate matter (PM) has been traditionally categorized as organic carbon (OC) and elemental carbon (EC). EC is the largely graphitic component of soot emissions from primary sources. OC in aerosols can be primary, emitted directly into the atmosphere, and secondary, formed in the atmosphere via chemical reaction. Particulate OC is made up of numerous compounds varying in volatility, chemical properties and thermodynamic properties. This appendix describes mechanisms for secondary organic aerosol formation pathways.

Formation of secondary organic aerosol (SOA) occurs through two processes: oxidation of precursor hydrocarbons in gas phase and partitioning of semi-volatile products (SVOC) into the aerosol phase. The major hydrocarbon oxidants leading to SVOC formation are OH•, ozone, and the nitrate radicals. SVOCs are generally formed only from the oxidation of hydrocarbon molecules containing six or more carbon atoms (Grosjean and Seinfeld 1989). More specifically, aromatics (from anthropogenic sources), terpenes (from biogenic sources) and high molecular weight alkanes and alkenes are suspected to form SOA based on the ability of their reaction products to partition to aerosol phase.

In the case of a single SVOC, no SOA will form if the reaction product has not reached its vapor pressure in the gas phase. Once the threshold is reached, SOA may initially form via nucleation or the SVOCs may condense onto any available absorbing mass. Organic vapors tend to dissolve in the organic particulate phase. Thus, the gas-particle partitioning of SVOC depends on the molecular properties of the species and the organic phase and the amount of the particulate organic phase available for SVOC to dissolve into (Seinfeld and Pandis 1998). In the absence of an organic particulate phase, adsorption can served as the method to initiate gas-particle partitioning (Pankow and Bidleman 1991; Yamasaki et al. 1982).

**SOA formation via partitioning theory**

Models describing SOA formation presume a thermodynamic equilibrium of organic compounds between the gas and the aerosol phase. SOA partitioning is typically modeled assuming that a reactive hydrocarbon undergoes atmospheric oxidation to produce n condensable products $G_1$ to $G_n$ as shown in Equation (B.1)

$$HC + oxidant \rightarrow \alpha_1 G_1 + \alpha_2 G_2 + ... + \alpha_n G_n \quad (B.1)$$

where $\alpha_i$ is the stoichiometric yield of $G_i$.

It has been suggested that partitioning may be occurring via absorption of these semi-volatile organics into a pre-existing organic on particulate matter organic phase at concentrations below their saturation concentrations (Bowman et al. 1997; Odum et al. 1996; Odum et al. 1997). This absorptive partitioning is governed by gas/liquid equilibrium of a non-ideal organic solution (Raoult's Law in non-ideal solution):

$$P_i = \gamma_{OM} x_i P_{L,i} \quad (B.2)$$

$P_i$ = partial pressure of i in gas phase (atm)
$x_i$ = mole fraction of i in absorbing organic matter
$\gamma_{OM}$ = activity coefficient of the species in the absorbing organic matter
$P_{L,i}$ = is liquid vapor pressure of pure organic compound (Pa)

Partitioning of any compound between gas and aerosol phase is frequently modeled using equation (B.3) (Pankow 1994)

$$K_p = \frac{F_{OM} / TSP}{A} = \frac{RTf_{OM}}{10^6 M_{OM} \gamma_{OM} P_L} \quad (B.3)$$

$K_p$ = gas - particle partitioning coefficient ($m^3/\mu g$)
$F_{OM}$ = aerosol organic phase species concentration ($ng/m^3$)
A = gas phase species concentration ($\mu g/m^3$)
TSP = total suspended particle matter concentration ($\mu g/m^3$)
$f_{OM}$ = fraction of organic matter in the aerosol

$M_{OM}$ = mean molar mass of the organic matter (g/mol)

SOA formation depends on reactivity of the parent compound and the volatility of the product species. The reactivity can be directly measured. However atmospheric reaction pathways for large hydrocarbon molecules are complex because SVOC products generally result from multi-step reactions and these products are difficult to identify and quantify; a more indirect measure productivity, SOA yield (Y) which relates how much PM is produced when a certain amount of a parent gaseous VOC is oxidized, has been used. Yield coefficients (Y) are defined as:

$$Y = \frac{\Delta M_o}{\Delta HC} \tag{B.4}$$

$\Delta HC$ = the amount of hydrocarbon reacted ($\mu g/m^3$)

$\Delta M_o$ = the organic aerosol mass produced ($\mu g/m^3$)

Experiment studies (Odum et al. 1996) and gas/particle partitioning theory (Pankow 1994) have demonstrated that by using an aerosol yield approach an increment of SOA formation can be expressed in terms of partitioning coefficient, stoichiometric yield and the total organic aerosol mass, Mo. The total aerosol yield will be the sum of the yield for each compound i ($Y_i$) over all i:

$$Y = \sum_i Y_i = M_o \sum_i \left( \frac{\alpha_i \, K_{om,i}}{1 + K_{om,i} \, M_o} \right) \tag{B.5}$$

$M_o$= total absorbing organic aerosol mass ($\mu g/m^3$)

$K_{om,i}$ = the partitioning coefficient of i to the organic phase, i.e. defined as $K_{OM,i} = \frac{F_{OM,i} / M_O}{A_i}$

For most VOCs, SVOC reaction products are not known; therefore, $\alpha_i$ and $K_{om,i}$ values cannot be explicitly calculated. Equation (B.5) has been used extensively in

fitting yield data (measured Y and Mo) in laboratory smog chamber experiments to obtain $\alpha_i$ and $K_{om,i}$ values using the assumption that two hypothetical first-generation reaction products were formed, i.e. obtaining four fitting parameters: $\alpha_1$, $\alpha_2$, $K_{om,1}$ and $K_{om,2}$. These parameters are available for a small number of VOCs that are known to produce SOA when oxidized. Seinfeld and Pankow (2003) summarized laboratory studies of overall yields of SOA formation from various hydrocarbons and oxidants carried out over the last decade.

This approach can be replaced here with the more physically meaningful pseudo-ideal solution theory. The mass balance for each SVOC satisfies

$$C_{t,i} = C_{g,i} + C_{aer,i} \tag{B.6}$$

where $C_{t,i}$ is the total concentration of species i, $C_{g,i}$ is gas-phase, and $C_{aer,i}$ is aerosol-phase concentration. The total concentration can be expressed using stoichiometry as

$$C_{t,i} = \alpha_i \frac{M_i}{M_{HC}} \Delta HC \tag{B.7}$$

where Mi is a molecular weight. Assuming that the aerosol species form an ideal organic solution, their gas-phase concentrations will satisfy

$$C_{g,i} = x_i \frac{P_{L,i} M_i}{RT} = x_i C_i^* \tag{B.8}$$

where $C_i^*$ is the effective saturation concentration in $\mu g/m^3$ of pure i which can be determined from laboratory experiments comparative to $K_{Pi}$ in Equation (B.2). The temperature dependence of $C_i^*$ can be assumed to follow the form of the Clausius-Clapeyron equation:

$$\frac{C_i^*(T_2)}{C_i^*(T_1)} = \frac{T_1}{T_2}\exp\left[\frac{-\Delta H}{R}\left(\frac{1}{T_1}-\frac{1}{T_2}\right)\right] \qquad \text{(B.9)}$$

Combining the above equations yields a set of n equations with n unknowns:

$$C_{aer,i} = \alpha_i \frac{M_i}{M_{HC}}\Delta HC - \frac{C_{aer,i}C_i^*/M_i}{\sum C_{aer,i}/M_i + POA/M_{POA}} \qquad \text{for i=1, n} \qquad \text{(B.10)}$$

where POA (ug/m$^3$) represents any initially present absorbing organic mass. We can also present this in term of mol fraction:

$$x_i\left[\Sigma\,\alpha_i \frac{M_i}{M_{HC}}\Delta HC - \Sigma\, x_i C_i^* + \frac{POA}{M_{POA}}\right] = \alpha_i \frac{M_i}{M_{HC}}\Delta HC - x_i C_i^* \qquad \text{for i=1, n} \qquad \text{(B.11)}$$

This set of equations can be solved for secondary organic aerosol concentrations. Note that this approach is mathematically equivalent to the approach with the semi-empirical partitioning coefficient (Odum et al. 1996; Odum et al. 1997) as shown in Equation (B.5).

The accuracy of this method is limited by the fact that the fitting parameters are empirical, while in reality they will depend on many environmental variables. Moreover, they are approximations of the average stoichiometric yields (which depend on the availability of oxidants in the individual reactions of parent and intermediate VOC's) and partitioning coefficients (which depend on the temperature and composition of absorbing medium) of several SVOC species. Until reaction mechanisms are better characterized for more SOA precursors, using empirical $\alpha$ values will remain an important limitation to predicting SOA.

$K_P$ and $C_i^*$ are typically estimated from smog chamber data with low relative humidity and no presence of pre-existing organic aerosol. Some studies, however, have shown that water content directly affects the partitioning of organic compounds (Cocker et al. 2001a; Cocker et al. 2001b; Edney et al. 2005; Saxena et al. 1995), mainly via decreasing the mean molecular weight of the absorbing mixture, $M_{OM}$ (Seinfeld et al. 2001). Other studies suggested that aerosol composition can significantly affect $K_P$ and

$C_i^*$ values (Bowman and Karamalegos 2002; Jang et al. 1997); it is unclear how to account for this dependency using empirical values. Temperature is another important factor in the partitioning of SVOC (Kamens et al. 1999; Yamasaki et al. 1982) and should be accounted for when modeling SOA formation.

**SOA formation in a regional grid model**

In version 4.11x, CAMx features a treatment for particulate matter. Special modules were introduced for aqueous chemistry (RADM-AQ), inorganic aerosol thermodynamics/partitioning (ISORROPIA), and secondary organic aerosol formation/partitioning (SOAP). The particulate chemistry mechanism utilizes products from the gas-phase photochemistry for production of sulfate, nitrate, condensable organic gases, and chloride. For particle size distributions, the scheme employs a sectional approach that models the size evolution of each aerosol constituent among a number of fixed size sections. The characteristic time associated with the mass transfer is short compared to the timescale required for the production/removal of VOC. Therefore thermodynamic equilibrium is applied at each time step.

In CAMx, four condensable organic gas species (CG1- CG4) represent secondary organic aerosol (SOA) precursors. CG1-CG3 are formed from anthropogenic VOCs and CG4 is formed from terpenes (OLE2). The CG yields are expressed as ppm of aerosol precursor formed per ppm of VOC reacted so that CG concentrations follow the CAMx convention for gases and are in ppm. The SOAP module performs gas/solid partitioning equilibrium calculations based on Equation (B.11) to obtain SOA mass.

**Table B.1.** Properties of condensable organic gases (CG1-CG4) that are precursors to secondary organic aerosols (SOA1-SOA4) (Environ 2004)

| CB4 VOC Precursor | Condensable Gas Species | Aerosol Yield (ppm/ppm) | Saturation Concentration ($\mu g\ m^{-3}$ at 281.5 K) | Heat of vaporization $H_{vap}$ ($J\ mole^{-1}$) | Molecular Weight ($g\ mole^{-1}$) |
|---|---|---|---|---|---|
| PAR | CG3 | 0.0024 | 0.007 | 0 | 150 |
| OLE | CG3 | 0.0024 | 0.007 | 0 | 150 |
| TOL | CG1 | 0.07 | 0.023 | 156250 | 150 |
| TOL | CG2 | 0.137 | 0.674 | 156250 | 150 |
| XYL | CG1 | 0.044 | 0.023 | 156250 | 150 |
| XYL | CG2 | 0.192 | 0.674 | 156250 | 150 |
| CRES | CG3 | 0.036 | 0.007 | 0 | 150 |
| OLE2 | CG4 | 0.136 | 0.008 | 0 | 180 |

**SOA formation via the acid-catalyzed heterogeneous reactions**

There is an increasing body of laboratory evidence indicating that acid-catalyzed (e.g. $H_2SO_4$) processes substantially increase SOA formation and enhance stability of the particle organics. These reactions are essentially interactions between the multifunctional organic and inorganic portions of aerosols. The acid-catalyzed reactions of gas phase carbonyls were reported to possibly be a major class of heterogeneous reactions in urban areas where concentrations of particulate matter are high (Jang and Kamens 2001a; Jang et al. 2002; Jang et al. 2003b).

The widely accepted thermodynamic gas/particle partitioning theory discussed in the previous section, does not account for these heterogeneous reactions. Evident discrepancies between measured and model $K_P$ values of carbonyl-containing products were observed in many studies (Chandramouli et al. 2003; Jang and Kamens 2001b; Lee et al. 2004). In two extreme cases: (1) Lee et al. (2004) reported that pinalic-4-acid, α-pinene photochemical product, had an empirical $K_P$ 3000 times higher than its theoretical value, and in accordingly (2) Jang and Kamens (2001b) observed an empirical $K_P$ of 2-hydroxy-1,3-propanedial, a toluene photochemical product, that was three orders of magnitude higher than predicted. It is plausible that heterogeneous reactions could explain these variations.

Indirect evidence of acid-catalyzed heterogeneous reactions was also shown as a comparison of the yields between acidic and non-acidic seeds (Czoschke et al. 2003; Jang et al. 2002; Jang et al. 2003b). For example, Czoschke et al. (2003) observeed as much as a factor of 3 increase of SOA yields from biogenic organics (i.e. isoprene, α-pinene) produced on acidic seeds.

Besides laboratory studies, some field observations that were not understood previously may now be explained by these acid-catalyzed mechanisms. For example, Fourier transform infrared (FTIR) spectra of field sample collected in the Smokey Mountains at Look Rock, TN, during a Southeastern Visibility Study (Blando et al. 1998) show similar peaks with laboratory FTIR spectra of organic aerosols from glyoxal and from reaction of ozone with isoprene in the presence of acid (Jang et al. 2002). In this thesis, field measurements from the TeXAQs2000 study in the Houston area were investigated.

It has been proposed that the acid-catalyzed carbonyls chemistry includes hydration, polymerization, hemiacetal and acetal formation, aldol condensation, ring opening of terpenoid carbonyls and cross-linking in the aerosol media (Jang et al. 2002). Such chemistry takes place on the acidic particles and transforms carbonyls in the particle phase into low vapor pressure products. These products favorably reside in the particle phase and their formation drives additional aerosol phase partitioning of their parent compounds resulting in more SOA mass. Although low molecular weight aldehydes had previously been considered insignificant in contributing to SOA mass in troposphere, deviations from expected partitioning behavior and FTIR spectra that illustrate aldehyde transformation on particles suggest that aldehydes can contribute to SOA mass in the presence of acid (Jang and Kamens 2001a; 2001b; Jang et al. 2002; Kamens and Jaoui 2001).

Recently, the presence of high molecular structures like oligomers or polymers from SOA products, previously unresolved by gas chromatography–mass spectrometry (GC-MS) along with infrared spectroscopy, was identifiable by using less destructive techniques such as electrospray ionization (ESI) and laser desorption ionization (LDI). For example, Kalberer et al. (2004) reported polymerization results from reactions of

carbonyls and their hydrates from photooxidation of 1,3,5-trimethybenzene in the absence of seed particles. High molecular masses up to 1000 m/z of polymeric materials were approximately 50% of the aerosol mass after 20 hours. Tolocka et al. (2004) reported the SOA produced by ozonation of α-pinene in the presence of inorganic acid seeds to have oligomeric structures as large as tetramers. Docherty et al. (2005) proposed that a large fraction of SOA from monoterpene with $O_3$ was organic peroxides and suggested that the oligomers were mostly peroxyhemiacetals formed through heterogeneous reactions of hydroperoxides and aldehyde. Study on natural SOA from Amazonian rain forest identified 2-methyltetrols, an oxygenated compound, resulting from photooxidation of isoprene (Claeys et al. 2004). Other studies also reported the presence of polymeric structures from SOA products (Gao et al. 2004a; Gao et al. 2004b; Iinuma et al. 2004; Limbeck et al. 2003). Although these oligomeric/polymeric structures are formed on particles, detailed mechanisms describing the formation processes are still unclear and quantitative analysis for reaction rates is not yet available. Further studies are still necessary to qualitatively and quantitatively explain an unresolved organic fraction of aerosol in the atmosphere.

There are various sources of acid in the atmosphere. Many of which are associated with fossil fuel combustions sources, such as diesel exhaust and power plants (Reddy and Venkataraman 2002a; Tobias et al. 2001). $SO_2$ from these sources can be oxidized to $H_2SO_4$ as described earlier. $HNO_3$ is abundant in the atmosphere making it another plausible candidate for an acid catalyst, although it is much more volatile than $H_2SO_4$. These acids are neutralized by ammonia forming ammonium sulfate and nitrate. In an area where ammonia, nitric acid, sulfuric acid and water are all present, a complex equilibrium of materials in the gas and particle phases exists. Since the equilibrium favors the formation of ammonium sulfate over ammonium nitrate, under ammonia-poor conditions (not enough ammonia to neutralize the sulfuric acid) the sulfate will tend to drive nitrate to the gas phase, as nitric acid (Seinfeld and Pandis 1998). The molar ratio of $NH_3/H_2SO_4$ will define acidity and the potential for acid catalyzed heterogeneous reactions.

Besides inorganic acids, organic acids may as well play a role in the acid-catalyzed reactions. Gao et al. (2004b) found that oligomers were formed regardless of the initial particle acidity which is consistent with the finding by Kalberer et al. (2004). This suggests that the acidity of organic products from gas-phase oxidation itself may sufficiently accommodate catalytic reactions. The authors also reported that as the particle acidity increased larger oligomers were formed in a greater extent. Although organic acids may provide enough acid to initiate the catalyzed reactions, it is most likely that inorganic acids play a major role in driving the chemistry due to their abundance in the atmosphere.

Humidity is related directly to particle acidity by water content of particle. In the absence of acid, the log of aerosol yield was not sensitive to RH (Jang et al. 2003a). In contrast, strong linearity between the yield and RH was observed for SOA formations via heterogeneous acid-catalyzed reactions. The effect of increase of SOA mass in the presence of acid inorganic aerosol appears to be even greater at low RH (Czoschke et al. 2003; Jang et al. 2003a). This may be explained by the Hammet Deyrup relationship (Hammett and Deyrup 1932) in which higher acidity occurs at low RH. This higher acidity (more available $H^+$) can drive the heterogeneous reactions in a greater extent, yielding more SOA mass.

It is clear that acid-catalyzed SOA formations can potentially increase SOA mass. Little is known about chemical transformations that take place in the particle phase. They are believed to be very complex and involve many intermediate steps; therefore, currently it is difficult to assess the influence of heterogeneous reactions on SOA growth quantitatively. Detailed studies of the acid on organic aerosol yields and the kinetic mechanisms especially a rate-determining step are critically needed.

# APPENDIX C: Modification of CAMx4.11

This Appendix summarizes the code development used to include an impingement calculation into the Comprehensive Air Quality Model with Extensions version 4.11 (CAMx4.11x). CAMx4.11 software is available at www.camx.com (ENVIRON 2005).

There were three major modifications made to CAMx4.11:

1) Addition of the impingement calculations for heterogeneous formation of sulfuric acid on carbonaceous particles
2) Modifications of routines to read additional absorbing mass (Mo) and Planetary Boundary Layer (PBL) used in partitioning calculations for secondary organic aerosol (SOA)
3) Addition of the impingement calculations for acid catalyzed condensation reactions of low molecular weight aldehydes

## C.1 Impingement calculations for heterogeneous reactions of sulfuric acid

Modifications of CAMx for this case include adding/modifying shared parameter files, modifying some existing routines that involve chemistry, and adding an impingement calculation routine.

**Table C.1.** Modifications and additions to the CAMx411x source code for the sulfate formation via impingement calculation (pso4h).

| Subroutine | Function | Modifications/Description |
|---|---|---|
| camx_aero.inc | Includes aerosol module parameters | Added a pointer for a new specie |
| aerpar.inc | Includes aerosol paramters | Added a concentration vector for a new specie |
| camx.prm | Main model parameters | Changed number of species used in a model and number of species' names |
| chmstry.com | Includes chemistry variables | Declared new species name and re-index output species names |
| CAMx4.1.chemparam.4_CMU | Chemistry parameter file | Changed number of aerosol species used and added a new specie name |
| readchm.f | Reads chemistry parameters | Added new species name |
| aeroset.f | Sets up aerosol routine | Added new species pointer |
| fullaero.f | Drives aerosol module with CMU scheme | Calls impingement calculation routine |
| impingement.f (New.Called by fullaero.f) | Calculates sulfate formation via impingement | Calculates sulfate formation via impingement using so2 and fire PM concentrations for every chemistry time step |

The impingement calculation routine, impinge.f, is shown below. Inputs for this routine include concentrations of gas and aerosols, temperature, pressure and chemistry time step. The impingement routine calculates the sulfate formation from heterogeneous reaction and updates gas and aerosol concentrations.

```
subroutine impinge(mxspec_c,tempk,pres_pa,con,dt_sec,Dso4)
c     Input arguments:
c        mxspec_c       maximum number of species
c        con            species concentrations (ppm,ug/m3)
c        dt_sec         time step (sec)
c        tempk          cell temperature (K)
c        pres_pa        cell pressure (Pa)
c
c     Output arguments:
c        con            species concentrations (ppm,ug/m3)
c        Dso4           heterogeneous sulfate formation
c                       in this time step (ug/m3)
c     Called by fullaero.f
```

```
      include 'section.inc'
      include 'section_aq.inc'
      include 'camx_aero.inc'
      include 'camx_aero.com'
      include 'camx.prm'
      include 'filunit.com'

      real*4 con(mxspec_c+1)
      real*4 totCRST,pres_pa,tempk,conv    !ug/m3,Pa,K
      real*4 so20                          !ppm
      real*4 Dso4_Dt,Dso4,Dso2             !ug/m3.s,ug/m3,ppm
      real*4 dt_sec
      integer nsec
      real react_coef, gasconst, velocity, MWso4, density, Dpvrm
      parameter (react_coef = 0.01)
      parameter ( gasconst = 8.314472)
      parameter ( velocity = 314.0)        ! m/s
      parameter (MWso4 = 96.0)             ! g/mol
      parameter (density = 1.5)            ! g/cm3
      parameter (Dpvrm = 0.25)             ! average mean volume Dp (um)

c------Calculate some conversion units
c       PV=nRT  ; n/V = P/RT
c       conv    ; ppm * conv = mol/m3
        conv = pres_pa*1.e-6/(gasconst*tempk)

c------Calculate total CRST mass
        totCRST = 0.0
        do knsec=1,nsec
          totCRST = totCRST + con(kcrst_c+(knsec-1))
        enddo
c------Clear sulfate formation
        Dso4_Dt = 0.0
c------Perform impingement calculation
        Dso4_Dt =0.25*con(kso2_c)*conv*totCRST*(6.0/(density*Dpvrm))*
     &            velocity*MWso4*react_coef
       Dso4 = Dso4_Dt*dt_sec
c-----Update SO2 concentrations
c     Dso2 (ppm)
        Dso2 = Dso4*1e-6/(MWso4*conv)
```

## C.2 Modifications of partitioning calculations for secondary organic aerosol (SOA)

Modifications of CAMx for this case include adding/modifying shared parameter files, modifying some existing routines that involve organic chemistry, and adding a new routine, Moprep.f, to read Mo and PBL values from inputs.

**Table C.2.** Modifications and additions to the CAMx411x source code for the SOA modeling with additional absorbing mass.

| Subroutine | Function | Modifications/Description |
|---|---|---|
| Startup.f | Reads CAMx.in file and calls routines to read in information files (chemparam etc.) | Added a read and message for SOA flag. If SOA=TRUE, call Moprep. |
| openfils.f | Opens file units for input and output data | If SOA=TRUE, open an output file with .mo extension, and open Mo fields file and PBL fields file. |
| filunit.com | Includes model file units | Added file unit numbers for Mo and PBL field files and the output file with .mo extension |
| Moprep.f (New. Called by startup.f) | Opens file units for input and output data. Read Mo fields file, PBL fields file. | • Prints SOA absorbing mass information to .out file.<br>• Writes header information to Mo output file.<br>• Passes Mo and PBL information to starup.f |
| mochem.com (New) | Includes file with arrays and parameters for SOA modeling with Mo mass. | Added several new global variables for modeling SOA formation with Mo mass |
| flags.com | Includes model flags | Added "lsoa" flag if Mo is present |
| Soap.com | Includes common parameters for SOAP module | Set "pflag" to be 1 indicating presence of pre-existing organic aerosol |
| fullaero.f | Drives aerosol module with CMU scheme | • Included mochem.com<br>• Passes Mo value to SOAP module |
| aerchem.f | Checks aerosol chemistry mode (EQUI, MADM, HYBR) | Passes Mo value to to eqpart.f |
| eqpart.f | Main partitioning routine | Passes Mo value to eqparto.f |
| eqparto.f | Equilibrium partitioning of consensible gases | • Assigns a value for a variable "cpre" (primary organic aerosol) [cpre = Mo – total SOA mass from the last hour]<br>• Assumed equally distributed cpre mass between bin 1 and 2. |
| CAMx.f | Main simulation routine | If SOA=TRUE, call new routine wrtmo.f at the end of each hour. |
| Wrtmo.f (New. Called by CAMx.f) | Write Mo output | Writes the hourly Mo fields [ug/m3] in the 4km domain to the .mo output file. |

The format for SOA parameters file, the Mo field file and the PBL field file are shown in Table C.3 and C.4, respectively. Note that the size of Mo and PBL field matches with the size of the finest 4-km domain.

**Table C.3.** Format of Mo fields file.

| Line # | Description |
|---|---|
| 1 | x-coordinate of lower left corner of Mo field (in the same coordinate system as the model 4-km domain) in meters |
| 2 | y-coordinate of lower left corner of Mo field (in the same coordinate system as the model 4-km domain) in meters |
| 3 | number of columns in Mo field |
| 4 | number of rows in Mo field |
| 5 | grid cell size in meters |
| Repeat the following information 24 times, once per hour: | |
| 6 | hour for the Mo information to follow |
| 7+ (# rows) | Mo value for each column in $\mu g/m^3$ [space delimited] |

**Table C.4.** Format of PBL layer fields file.

| Line # | Description |
|---|---|
| 1 | x-coordinate of lower left corner of PBL field (in the same coordinate system as the model 4-km domain) in meters |
| 2 | y-coordinate of lower left corner of PBL field (in the same coordinate system as the model 4-km domain) in meters |
| 3 | number of columns in PBL field (must be in the same as model 4-km grid) |
| 4 | number of rows in PBL field (must be in the same as model 4-km grid) |
| 5 | grid cell size in meters (must be in the same as model 4-km grid) |
| repeat the following information 24 times, once per hour: | |
| 6 | hour for the PBL information to follow |
| 7+ (# rows) | PBL value for each column indicating the vertical modeling layer above which is the top of the PBL [space delimited] |

## C.3 Impingement calculations for acid catalyzed condensation reactions of low molecular weight aldehydes

Modifications of CAMx for this case include adding/modifying shared parameter files, modifying some existing routines that involve chemistry, and adding the impingement calculation routines. In addition to the sulfate impingement calculation described in section C.1, the SOA impingement calculation routine, impingeald2.f, was

added. The functionalities of this routine include: 1) calculate the degree of neutralization ($2[SO_4^{2-}] + [NO_3^-] - [NH_4^+]$), 2) estimate acidic PM mass concentrations assuming that 1 mol $[H^+]$ is associated with 160 grams of PM mass, and 3) perform the impingement calculations between aldehyde and acidic PM. Inputs for this routine include concentrations of gas and aerosols, temperature, pressure and chemistry time step. The impingement routine will update gas and aerosol concentrations.

**Table C.5.** Modifications and additions to the CAMx411x source code for the SOA modeling with additional absorbing mass.

| Subroutine | Function | Modifications/Description |
|---|---|---|
| Impingeald2.f (New.Called by fullaero.f) | Calculates SOA formation via impingement | Estimates acidic PM mass and Calculates SOA formation via impingement using ALD2 and acidic PM concentrations for every chemistry time step |

```
subroutine impingeald2(mxspec_c,tempk,pres_pa,con,dt_sec,Dsoa5)
c   Input arguments:
c      mxspec_c
c      con             species concentrations (ppm,ug/m3)
c      dt_sec           time step(sec)i
c      tempk            cell temperature (K)
c      pres_pa          cell pressure (Pa)
c
c   Output arguments:
c      con             species concentrations (ppm,ug/m3)
c      Doc             heterogeneous OC formation
c                     in this time step (ug/m3)
c   Called by fullaero.f
c
      include 'section.inc'
      include 'section_aq.inc'
      include 'camx_aero.inc'
      include 'camx_aero.com'
      include 'camx.prm'
      include 'filunit.com'
      include 'chmstry.com'
c
      real*4 con(mxspec_c+1)
      real*4 pres_pa,tempk,conv    !ug/m3,Pa,K
      real*4 ald20                 !ppm
      real*4 Dsoa5_Dt,Dsoa5,Dald2        !ug/m3.s,ug/m3,ppm
      real*4 dt_sec
```

```
      integer nsec
      real react_coef, gasconst, velocity, MWald2, MWsoa5
      real density, Dpvrm
      parameter (react_coef = 0.001)
      parameter ( gasconst = 8.314472)
      parameter ( velocity = 444.0)       ! m/s
      parameter (MWald2 = 32.0)           ! g/mol
      parameter (MWsoa5 = 32.0)           ! g/mol
      parameter (density = 1.5)          ! g/cm3
      parameter (Dpvrm = 0.25)            ! average mean volume Dp (um)
c
c Assume acidity parameter : 1 mol [H+] corresponds to 0.5 mol of H2SO4
c    Lower limit approximation of so4 in acidic PM
c    1 mol [H+] is form 0.5 mol [so4]= 48 g
c    PM is typically composed of 30% sulfate
c    48/0.3 = 160 ug acidic PM/umol [H+]
c------Calculate some conversion units
c       PV=nRT  ; n/V = P/RT
c       conv    ; ppm * conv = mol/m3
       conv = pres_pa*1.e-6/(gasconst*tempk)
c------Store ald2 concentration
        ald20 = con(kald2)
c------Clear soa5 formation (Reset mass)
        Dsoa5_Dt = 0.0
        Dald2 = 0.0
c------Calculate total CRST mass
        totpso4 = 0.0
        do knsec=1,nsec
          totpso4 = totpso4 + con(kpso4_c+(knsec-1))
        enddo
        totpno3 = 0.0
        do knsec=1,nsec
          totpno3 = totpno3 + con(kpno3_c+(knsec-1))
        enddo
        totpnh4 = 0.0
        do knsec=1,nsec
          totpnh4 = totpnh4 + con(kpnh4_c+(knsec-1))
       enddo
       totacid = 0.0
       totacid = (totpso4*2.0/96.0+totpno3/62.0-totpnh4/17.0)*160.0
c check if acidity is enough
       if(totacid.lt.0.0) then
         Dald2 = 0.0
         Dsoa5 = 0.0
         con(kald2) = ald20
         goto 224
       endif
c------Perform impingement calculation
       Dsoa5_Dt =0.25*con(kald2)*conv*totacid*(6.0/(density*Dpvrm))*
     &           velocity*MWsoa5*react_coef
       Dsoa5 = Dsoa5_Dt*dt_sec
```

```
c-----Update ALD2 concentrations
c     Dald2 (ppm)
       Dald2 = Dsoa5*1e-6/(MWsoa5*conv)

c----Check for Nan value (this happens when we start up
c    Dso2 got NaN value). In this case, ald2 concentration will
c    be restored.

       if(NANCHK(Dald2).OR.Dald2.lt.0.0) then
         Dald2 = 0.0
         Dsoa5 = 0.0
         con(kald2) = ald20
         goto 225
       endif
       con(kald2) = con(kald2)-Dald2
 225    continue

       if(con(kald2).lt.0.0) then
         Dald2 = 0.0
         Dsoa5 = 0.0
         con(kald2) = ald20
       endif
```

# References


Allen D.T. (2002). "Particulate matter concentrations, compositions, and sources in Southeast Texas." Texas Enviromental Research Consortium.

Andreae, M. O. and P. J. Crutzen (1997). "Atmospheric aerosols: Biogeochemical sources and role in atmospheric chemistry." Science 276(5315): 1052-1058.

Atmospheric and Environmental Research (AER) (2003), CRC project A-40-1, Performance evaluation of CMAQ and PM-CAMx for the July 1999 SOS episode.

Baldwin, A. C. (1982). "Heterogeneous Reactions of Sulfur-Dioxide with Carbonaceous Particles." International Journal of Chemical Kinetics 14(3): 269-277.

Blando, J. D., R. J. Porcja, T. H. Li, D. Bowman, P. J. Lioy and B. J. Turpin (1998). "Secondary formation and the Smoky Mountain organic aerosol: An examination of aerosol polarity and functional group composition during SEAVS." Environmental Science & Technology 32(5): 604-613.

Boonsongsup, L., K. Iisa and W. J. Frederick (1997). "Kinetics of the sulfation of NaCl at combustion conditions." Industrial & Engineering Chemistry Research 36(10): 4212-4216.

Bowman, F. M. and A. M. Karamalegos (2002). "Estimated effects of composition on secondary organic aerosol mass concentrations." Environmental Science & Technology 36(12): 2701-2707.

Bowman, F. M., J. R. Odum, J. H. Seinfeld and S. N. Pandis (1997). "Mathematical model for gas-particle partitioning of secondary organic aerosols." Atmospheric Environment 31(23): 3921-3931.

Britton, L. G. and A. G. Clarke (1980). "Heterogeneous Reactions of Sulfur-Dioxide and SO2-NO2 Mixtures with a Carbon Soot Aerosol." Atmospheric Environment 14(7): 829-839.

Brock, C. A., M. Trainer, T. B. Ryerson, J. A. Neuman, D. D. Parrish, J. S. Holloway, D. K. Nicks, G. J. Frost, G. Hubler, F. C. Fehsenfeld, J. C. Wilson, J. M. Reeves, B. G. Lafleur, H. Hilbert, E. L. Atlas, S. G. Donnelly, S. M. Schauffler, V. R. Stroud and C. Wiedinmyer (2003). "Particle growth in urban and industrial plumes in Texas." Journal of Geophysical Research-Atmospheres 108(D3).

Brodzinsky, R., S. G. Chang, S. S. Markowitz and T. Novakov (1980). "Kinetics and Mechanism for the Catalytic-Oxidation of Sulfur-Dioxide on Carbon in Aqueous Suspensions." Journal of Physical Chemistry 84(25): 3354-3358.

Brown, D., W. Dunn, M. Lazaro and A. Policastro (1999). "The FIREPLUME model: Tool for eventual application to prescribed burns and wildland fires." Proceedings from the Joint Fire Science Conference and Workshop, June 15-17, 1999.

Buzcu, B., Z. W. Yue, M. P. Fraser, U. Nopmongcol and D. T. Allen (2005). "Secondary Particle Formation and Evidence of Heterogeneous Chemistry During A Wood Smoke Episode in Texas." Journal of Geoohysical Research (in print).

Cachier H., L. C., Pertuisot MH., Gaudichet A., Echalar F., and Lacaux JP (1996). "African fire particulate emissions and atmospheric influence." Biomass Burning and Global Change 1(41): 428-440.

Calvert, J. G., F. Su, J. W. Bottenheim and O. P. Strausz (1978). "Mechanism of Homogeneous Oxidation of Sulfur-Dioxide in Troposphere." Atmospheric Environment 12(1-3): 197-226.

Canagaratna, M. R., P. J. Silva, J. L. Jimenez, A. Delia, Q. Zhang, K. M. Purvis, J. Jayne, C. E. Kolb, P. Davidovits and D. R. Worsnop (2005). "Time resolved aerosol size and chemical composition measured during the Texas Air Quality Study." (in preparation).

Chandramouli, B., M. S. Jang and R. M. Kamens (2003). "Gas-particle partitioning of semivolatile organic compounds (SOCs) on mixtures of aerosols in a smog chamber." Environmental Science & Technology 37(18): 4113-4121.

Christensen, K. A., M. Stenholm and H. Livbjerg (1998). "The formation of submicron aerosol particles, HCl and SO2 in straw-fired boilers." Journal of Aerosol Science 29(4): 421-444.

Claeys, M., W. Wang, A. C. Ion, I. Kourtchev, A. Gelencser and W. Maenhaut (2004). "Formation of secondary organic aerosols from isoprene and its gas-phase oxidation products through reaction with hydrogen peroxide." Atmospheric Environment 38(25): 4093-4098.

Cocker, D. R., B. T. Mader, M. Kalberer, R. C. Flagan and J. H. Seinfeld (2001b). "The effect of water on gas-particle partitioning of secondary organic aerosol: II. m-xylene and 1,3,5-trimethylbenzene photooxidation systems." Atmospheric Environment 35(35): 6073-6085.

Cocker, D. R., S. L. Clegg, R. C. Flagan and J. H. Seinfeld (2001a). "The effect of water on gas-particle partitioning of secondary organic aerosol. Part I: alpha-pinene/ozone system." Atmospheric Environment 35(35): 6049-6072.

Crutzen, P. J. and M. O. Andreae (1990). "Biomass Burning in the Tropics - Impact on Atmospheric Chemistry and Biogeochemical Cycles." Science 250(4988): 1669-1678.

Czoschke, N. M., M. Jang and R. M. Kamens (2003). "Effect of acidic seed on biogenic secondary organic aerosol growth." Atmospheric Environment 37(30): 4287-4299.

Dayton, D. C., R. J. French and T. A. Milne (1995). "Direct Observation of Alkali Vapor Release During Biomass Combustion and Gasification .1. Application of Molecular-Beam Mass-Spectrometry to Switchgrass Combustion." Energy & Fuels 9(5): 855-865.

Dentener, F. J. and P. J. Crutzen (1993). "Reaction of N2O5 on Tropospheric Aerosols - Impact on the Global Distributions of Nox, O3, and Oh." Journal of Geophysical Research-Atmospheres 98(D4): 7149-7163.

Desantis, F. and I. Allegrini (1992). "Heterogeneous Reactions of SO2 and NO2 on Carbonaceous Surfaces." Atmospheric Environment Part a-General Topics **26**(16): 3061-3064.

Edney, E. O., T. E. Kleindienst, M. Jaoui, M. Lewandowski, J. H. Offenberg, W. Wang and M. Claeys (2005). "Formation of 2-methyl tetrols and 2-methylglyceric acid in secondary organic aerosol from laboratory irradiated isoprene/NOx/SO2/air

mixtures and their detection in ambient PM2.5 samples collected in the eastern United States." Atmospheric Environment (in print).
ENVIRON International Corporation (2003), Final Report CRC project A-30, Development of an advanced photochemical model for particulate matter: PMCAMx.
ENVIRON International Corporation (2004). User's guide. Comprehensive Air Quality Model with Extensions (CAMx) version 4.10x. Navato.
ENVIRON International Corporation (2005), Comprehensive Air Quality Model with Extensions, available at www.camx.com.
Environmental Protection Agency (EPA) (1996). "Air Quality Criteria for Particulate Matter." Washington, DC: EPA EPA/600/P95/001cF, ORD.
Electric Power Research Institute (EPRI) (2002), "Community Multiscale Air Quality-Model of aerosol dynamics, reactions, ionization, and dissolution (CMAQ-MADRID)" Technical Documentation, Palo Alto, CA.
Evans, M. J. and D. J. Jacob (2005). "Impact of new laboratory studies of N2O5 hydrolysis on global model budgets of tropospheric nitrogen oxides, ozone, and OH." Geophysical Research Letters 32(9).
Fine, P. M., G. R. Cass and B. R. T. Simoneit (2002). "Chemical characterization of fine particle emissions from the fireplace combustion of woods grown in the southern United States." Environmental Science & Technology 36(7): 1442-1451.
Finlayson-Pitts, B. and J.N., Pitts Jr (1999). "Chemistry of the Upper and Lower Atmosphere:Theory, Experiments, and Applications." Academic Press, San Diego, CA.
Fraser, M. P. and K. Lakshmanan (2000). "Using levoglucosan as a molecular marker for the long-range transport of biomass combustion aerosols." Environmental Science & Technology **34**(21): 4560-4564.
Gao, S., M. Keywood, N. L. Ng, J. Surratt, V. Varutbangkul, R. Bahreini, R. C. Flagan and J. H. Seinfeld (2004a). "Low-molecular-weight and oligomeric components in secondary organic aerosol from the ozonolysis of cycloalkenes and alpha-pinene." Journal of Physical Chemistry A 108(46): 10147-10164.
Gao, S., N. L. Ng, M. Keywood, V. Varutbangkul, R. Bahreini, A. Nenes, J. W. He, K. Y. Yoo, J. L. Beauchamp, R. P. Hodyss, R. C. Flagan and J. H. Seinfeld (2004b). "Particle phase acidity and oligomer formation in secondary organic aerosol." Environmental Science & Technology 38(24): 6582-6589.
Gasparini, R., R. J. Li and D. R. Collins (2004). "Integration of size distributions and size-resolved hygroscopicity measured during the Houston Supersite for compositional categorization of the aerosol." Atmospheric Environment 38(20): 3285-3303.
Gaudichet, A., F. Echalar, B. Chatenet, J. P. Quisefit, G. Malingre, H. Cachier, P. Buatmenard, P. Artaxo and W. Maenhaut (1995). "Trace-Elements in Tropical African Savanna Biomass Burning Aerosols." Journal of Atmospheric Chemistry 22(1-2): 19-39.
Gleason, J. F., A. Sinha and C. J. Howard (1987). "Kinetics of the Gas-Phase Reaction Hoso2+O2- Ho2+So3." Journal of Physical Chemistry 91(3): 719-724.
Grantz, D. A., J. H. B. Garner and D. W. Johnson (2003). "Ecological effects of particulate matter." Environment International 29(2-3): 213-239.

Grassian, V. H. (2002). "Chemical reactions of nitrogen oxides on the surface of oxide, carbonate, soot, and mineral dust particles: Implications for the chemical balance of the troposphere." Journal of Physical Chemistry A 106(6): 860-877.
Grosjean, D. and J. H. Seinfeld (1989). "Parameterization of the Formation Potential of Secondary Organic Aerosols." Atmospheric Environment 23(8): 1733-1747.
Hallquist, M., D. J. Stewart, S. K. Stephenson and R. A. Cox (2003). "Hydrolysis of N2O5 on sub-micron sulfate aerosols." Physical Chemistry Chemical Physics 5(16): 3453-3463.
Hameri, K., M. Vakeva, P. P. Aalto, M. Kulmala, E. Swietlicki, J. Zhou, W. Seidl, E. Becker and C. D. O'Dowd (2001). "Hygroscopic and CCN properties of aerosol particles in boreal forests." Tellus Series B-Chemical and Physical Meteorology 53(4): 359-379.
Hammett, L. P. and A. J. Deyrup (1932). "A series of simple basic indicators. I. The acidity functions of mixtures of sulfuric and perchloric acids with water." Journal of the American Chemical Society 54: 2721-2739.
Hays, M. D., C. D. Geron, K. J. Linna, N. D. Smith and J. J. Schauer (2002). "Speciation of gas-phase and fine particle emissions from burning of foliar fuels." Environmental Science & Technology 36(11): 2281-2295.
Hildemann, L. M., G. R. Markowski and G. R. Cass (1991). "Chemical-Composition of Emissions from Urban Sources of Fine Organic Aerosol." Environmental Science & Technology 25(4): 744-759.
Iinuma, Y., O. Boge, T. Gnauk and H. Herrmann (2004). "Aerosol-chamber study of the alpha-pinene/O-3 reaction: influence of particle acidity on aerosol yields and products." Atmospheric Environment 38(5): 761-773.
Jang, M., R. M. Kamens, K. B. Leach and M. R. Strommen (1997). "A thermodynamic approach using group contribution methods to model the partitioning of semivolatile organic compounds on atmospheric particulate matter." Environmental Science & Technology 31(10): 2805-2811.
Jang, M. S. and R. M. Kamens (2001a). "Atmospheric secondary aerosol formation by heterogeneous reactions of aldehydes in the presence of a sulfuric acid aerosol catalyst." Environmental Science & Technology 35(24): 4758-4766.
Jang, M. S. and R. M. Kamens (2001b). "Characterization of secondary aerosol from the photooxidation of toluene in the presence of NOx and 1-propene." Environmental Science & Technology 35(18): 3626-3639.
Jang, M. S., N. M. Czoschke, S. Lee and R. M. Kamens (2002). "Heterogeneous atmospheric aerosol production by acid-catalyzed particle-phase reactions." Science 298(5594): 814-817.
Jang, M., S. Lee and R. M. Kamens (2003a). "Organic aerosol growth by acid-catalyzed heterogeneous reactions of octanal in a flow reactor." Atmospheric Environment 37(15): 2125-2138.
Jang, M. S., B. Carroll, B. Chandramouli and R. M. Kamens (2003b). "Particle growth by acid-catalyzed heterogeneous reactions of organic carbonyls on preexisting aerosols." Environmental Science & Technology 37(17): 3828-3837.
Jensen, J. R., L. B. Nielsen, C. Schultz-Moller, S. Wedel and H. Livbjerg (2000). "The nucleation of aerosols in flue gases with a high content of alkali - A laboratory study." Aerosol Science and Technology 33(6): 490-509.

Judeikis, H. S., T. B. Stewart and A. G. Wren (1978). "Laboratory Studies of Heterogeneous Reactions of SO2." Atmospheric Environment 12(8): 1633-1641.
Junquera, V., M.M. Russell, W. Vizuete, Y. Kimura and D.T. Allen (2005), Wildfires in eastern Texas in August and September 2000: Emissions, aircraft measurements and impact on photochemistry, Atmospheric Environment 39: 4983-4996.
Kalberer, M., D. Paulsen, M. Sax, M. Steinbacher, J. Dommen, A. S. H. Prevot, R. Fisseha, E. Weingartner, V. Frankevich, R. Zenobi and U. Baltensperger (2004). "Identification of polymers as major components of atmospheric organic aerosols." Science **303**(5664): 1659-1662.
Kamens, R., M. Jang, C. J. Chien and K. Leach (1999). "Aerosol formation from the reaction of alpha-pinene and ozone using a gas-phase kinetics aerosol partitioning model." Environmental Science & Technology 33(9): 1430-1438.
Kamens, R. M. and M. Jaoui (2001). "Modeling aerosol formation from alpha-pinene plus NOx in the presence of natural sunlight using gas-phase kinetics and gas-particle partitioning theory." Environmental Science & Technology 35(7): 1394-1405.
Kane, S. M., F. Caloz and M. T. Leu (2001). "Heterogeneous uptake of gaseous N2O5 by (NH4)(2)SO4, NH4HSO4, and H2SO4 aerosols." Journal of Physical Chemistry A 105(26): 6465-6470.
Kerminen, V. M. (1997). "The effects of particle chemical character and atmospheric processes on particle hygroscopic properties." Journal of Aerosol Science 28(1): 121-132.
Knudsen, J. N., P. A. Jensen and K. Dam-Johansen (2004). "Transformation and release to the gas phase of Cl, K, and S during combustion of annual biomass." Energy & Fuels 18(5): 1385-1399.
Kuhns, H., E. M. Knipping and J. M. Vukovich (2005). "Development of a United States-Mexico emissions inventory for the Big Bend Regional Aerosol and Visibility Observational (BRAVO) Study." Journal of the Air & Waste Management Association 55(5): 677-692.
Laden, F., L. M. Neas, D. W. Dockery and J. Schwartz (2000). "Association of fine particulate matter from different sources with daily mortality in six US cities." Environmental Health Perspectives 108(10): 941-947.
Lee, S. D., M. S. Jang and R. M. Kamens (2004). "SOA formation from the photooxidation of alpha-pinene in the presence of freshly emitted diesel soot exhaust." Atmospheric Environment 38(16): 2597-2605.
Li, J., M. Posfai, P. V. Hobbs and P. R. Buseck (2003). "Individual aerosol particles from biomass burning in southern Africa: 2, Compositions and aging of inorganic particles." Journal of Geophysical Research-Atmospheres 108(D13).
Liberti, A., D. Brocco and M. Possanzini (1978). "Adsorption and Oxidation of Sulfur-Dioxide on Particles." Atmospheric Environment 12(1-3): 255-261.
Limbeck, A., M. Kulmala and H. Puxbaum (2003). "Secondary organic aerosol formation in the atmosphere via heterogeneous reaction of gaseous isoprene on acidic particles." Geophysical Research Letters 30(19).
Longfellow, C. A., A. R. Ravishankara and D. R. Hanson (2000). "Reactive and nonreactive uptake on hydrocarbon soot: HNO3, O3, and N2O5." Journal of Geophysical Research-Atmospheres 105(D19): 24345-24350.

Mamane, Y. and J. Gottlieb (1989). "The Study of Heterogeneous Reactions of Carbonaceous Particles with Sulfur and Nitrogen-Oxides Using a Single-Particle Approach." Journal of Aerosol Science 20(5): 575-584.

Martin, L. R. and D. E. Damschen (1981). "Aqueous Oxidation of Sulfur-Dioxide by Hydrogen-Peroxide at Low pH" Atmospheric Environment 15(9): 1615-1621.

Martin, L. (1984). "Kinetic studies of sulfite oxidation in aqueous solution in SO2, NO and NO2 Oxidation Mechanisms: Atmospheric Considerations." Butterworth, Stoneham, MA: 63-100.

Martinez M., H. Harder, P. DiCarlo, W.H. Brune, E.J. Williams, S.R. Hall, R.E. Shetter, Kuster W. and Jobson T. (2001). "OH and HO2 concentrations, production and loss rates at LaPorte site during TexAQS2000." presented at the TexAQS Data Workshop, University of Texas, August.

Mozurkewich, M. and J. G. Calvert (1988). "Reaction Probability of N2O5 on Aqueous Aerosols." Journal of Geophysical Research-Atmospheres **93**(D12): 15889-15896.

Muhlbaier, J. L. (1981). "Report no. GMR-3730; General Motors Reserach Laboratories, Warren, MI."

National Oceanic and Atmospheric Administration (NOAA)(2002). "1-minute gas concentrations at La Porte during the Texas Air Quality Study" ftp.al.noaa.gov (accessed on 7/3/2003)

Nopmongcol, U. and D. Allen (2005). "Modeling of surface reactions on carbonaceous atmospheric particles during a wood smoke episode in Houston, Texas." Atmospheric Environment (submitted).

Novakov T., S.G. Chang and A.B. Harker (1974). "Sulfates as Pollution Particulates: Catalytic formation on carbon(soot) particles." Science, New Series 186(4160): 259-261.

Odum, J. R., T. Hoffmann, F. Bowman, D. Collins, R. C. Flagan and J. H. Seinfeld (1996). "Gas/particle partitioning and secondary organic aerosol yields." Environmental Science & Technology 30(8): 2580-2585.

Odum, J. R., T. P. W. Jungkamp, R. J. Griffin, H. J. L. Forstner, R. C. Flagan and J. H. Seinfeld (1997). "Aromatics, reformulated gasoline, and atmospheric organic aerosol formation." Environmental Science & Technology 31(7): 1890-1897.

Oros, D. R. and B. R. T. Simoneit (2001a). "Identification and emission factors of molecular tracers in organic aerosols from biomass burning Part 1. Temperate climate conifers." Applied Geochemistry 16(13): 1513-1544.

Oros, D. R. and B. R. T. Simoneit (2001b). "Identification and emission factors of molecular tracers in organic aerosols from biomass burning Part 2. Deciduous trees." Applied Geochemistry 16(13): 1545-1565.

Pankow, J. F. and T. F. Bidleman (1991). "Effects of Temperature, Tsp and Per Cent Nonexchangeable Material in Determining the Gas Particle Partitioning of Organic-Compounds." Atmospheric Environment Part a-General Topics 25(10): 2241-2249.

Pankow, J. F. (1994). "An Absorption-Model of Gas-Particle Partitioning of Organic-Compounds in the Atmosphere." Atmospheric Environment 28(2): 185-188.

Pilinis, C., S. N. Pandis and J. H. Seinfeld (1995). "Sensitivity of Direct Climate Forcing by Atmospheric Aerosols to Aerosol-Size and Composition." Journal of Geophysical Research-Atmospheres 100(D9): 18739-18754.

Platt, U. F., A. M. Winer, H. W. Biermann, R. Atkinson and J. N. Pitts (1984). "Measurement of Nitrate Radical Concentrations in Continental Air." Environmental Science & Technology 18(5): 365-369.

Pope, C. A., R. T. Burnett, M. J. Thun, E. E. Calle, D. Krewski, K. Ito and G. D. Thurston (2002). "Lung cancer, cardiopulmonary mortality, and long-term exposure to fine particulate air pollution." Journal of the American Medical Association 287(9): 1132-1141.

Reddy, M. S. and C. Venkataraman (2002a). "Inventory of aerosol and sulphur dioxide emissions from India: I - Fossil fuel combustion." Atmospheric Environment 36(4): 677-697.

Reddy, M. S. and C. Venkataraman (2002b). "Inventory of aerosol and sulphur dioxide emissions from India: Part II - biomass combustion." Atmospheric Environment 36(4), 699-712.

Reid, J., R. Koppmann, T. Eck and D. Eleuterio (2004). "A review of biomass burning emissions,part II: intensive physical properties of biomass burning particles." Atmospheric Chemistry and Physics Discussions 4: 5135-5200.

Riemer, N., H. Vogel, B. Vogel, B. Schell, I. Ackermann, C. Kessler and H. Hass (2003). "Impact of the heterogeneous hydrolysis of N2O5 on chemistry and nitrate aerosol formation in the lower troposphere under photosmog conditions." Journal of Geophysical Research-Atmospheres **108**(D4).

Rinehart, L. R. and B. Zielinska (2004). Spatial Characterization of PM2.5 Associated Organic Compounds. CRPAQS Annual Average Data Presentation

Robinson, M. S., J. Chavez, S. Velazquez and R. K. M. Jayanty (2004). "Chemical speciation of PM2.5 fires of the coconino national collected during prescribed forest near Flagstaff, Arizona." Journal of the Air & Waste Management Association 54(9): 1112-1123.

Russell, M. and D. T. Allen (2004a). "Seasonal and spatial trends in primary and secondary organic carbon concentrations in southeast Texas." Atmospheric Environment 38(20): 3225-3239.

Russell, M., D. T. Allen, D. R. Collins and M. P. Fraser (2004b). "Daily, seasonal, and spatial trends in PM2.5 mass and composition in Southeast Texas." Aerosol Science and Technology 38: 14-26.

Russell, M. and D. T. Allen (2005). "Predicting secondary organic aerosol formation rates in southeast Texas." Journal of Geophysical Research-Atmospheres **110**(D7).

Saathoff, H., K. H. Naumann, N. Riemer, S. Kamm, O. Mohler, U. Schurath, H. Vogel and B. Vogel (2001). "The loss of NO2, HNO3, NO3/N2O5, and HO2/HOONO2 on soot aerosol: A chamber and modeling study." Geophysical Research Letters 28(10): 1957-1960.

Sander B., Henriksen N., Skriver A., Ramsgaard-Nielsen C., Jensen JN, Livbjerg H., Thellefsen M., Dam-Johansen K. and Hansen J. (2000). "Emissions, corrosion and alkali chemistry in straw-fired combined heat and power plants." 1st World Conference on Biomass for Energy and Industry, 5-9 June 2000, Sevilla.

Saxena, P., L. M. Hildemann, P. H. McMurry and J. H. Seinfeld (1995). "Organics Alter Hygroscopic Behavior of Atmospheric Particles." Journal of Geophysical Research-Atmospheres 100(D9): 18755-18770.

Schauer, J. J., M. J. Kleeman, G. R. Cass and B. R. T. Simoneit (1999). "Measurement of emissions from air pollution sources. 1. C-1 through C-29 organic compounds from meat charbroiling." Environmental Science & Technology 33(10): 1566-1577.

Schauer, J. J., M. J. Kleeman, G. R. Cass and B. R. T. Simoneit (2001). "Measurement of emissions from air pollution sources. 3. C1-C29 organic coumpounds from fireplace combustion of wood." Environmental Science & Technology 35: 1716-1728.

Schultz, M. G., D. J. Jacob, J. D. Bradshaw, S. T. Sandholm, J. E. Dibb, R. W. Talbot and H. B. Singh (2000). "Chemical NOx budget in the upper troposphere over the tropical South Pacific." Journal of Geophysical Research-Atmospheres 105(D5): 6669-6679.

Schwartz, S. E. and J. E. Freiberg (1981). "Mass-Transport Limitation to the Rate of Reaction of Gases in Liquid Droplets - Application to Oxidation of SO2 in Aqueous-Solutions." Atmospheric Environment **15**(7): 1129-1144.

Schwartz, S. E. (1988). "Mass-Transport Limitation to the Rate of in-Cloud Oxidation of SO2 - Re-Examination in the Light of New Data." Atmospheric Environment 22(11): 2491-2499.

Seaman, N. L. and D. R. Stauffer (2003). "Final Report to Electric Power Research Institute Contract EP-p3883/C1886 for MM5 Modeling in support of the Big Bend Regional Aersol and visibility Observations Study (BRAVO)." EPRI, Palo Alto, CA.

Seinfeld, J. H. and S. N. Pandis (1998). Atmospheric Chemistry and Physics, From Air Pollution to Climate Change John Wiley & Sons, New York.

Seinfeld, J. H., G. B. Erdakos, W. E. Asher and J. F. Pankow (2001). "Modeling the formation of secondary organic aerosol (SOA). 2. The predicted effects of relative humidity on aerosol formation in the alpha-pinene-, beta-pinene-, sabinene-, Delta(3)-carene-, and cyclohexene-ozone systems (vol 35, pg 1806, 2001)." Environmental Science & Technology 35(15): 3272-3272.

Seinfeld, J. H. and J. F. Pankow (2003). "Organic atmospheric particulate material." Annual Review of Physical Chemistry **54**: 121-140.

Sheffield, A. E., G. E. Gordon, L. A. Currie and G. E. Riederer (1994). "Organic, Elemental, and Isotopic Tracers of Air-Pollution Sources in Albuquerque, NM." Atmospheric Environment 28(8): 1371-1384.

Simoneit, B. R. T., W. F. Rogge, M. A. Mazurek, L. J. Standley, L. M. Hildemann and G. R. Cass (1993). "Lignin Pyrolysis Products, Lignans, and Resin Acids as Specific Tracers of Plant Classes in Emissions from Biomass Combustion." Environmental Science & Technology 27(12): 2533-2541.

Simoneit, B. R. T., J. J. Schauer, C. G. Nolte, D. R. Oros, V. O. Elias, M. P. Fraser, W. F. Rogge and G. R. Cass (1999). "Levoglucosan, a tracer for cellulose in biomass burning and atmospheric particles." Atmospheric Environment 33(2): 173-182.

Smith, D. M. and A. R. Chughtai (1995). "The Surface-Structure and Reactivity of Black Carbon." Colloids and Surfaces A-Physicochemical and Engineering Aspects 105(1): 47-77.

Song, J., W. Vizuete, S. Chang, D. T. Allen, Y. Kimura, S. Kemball-Cook, G. Yarwood and E. C. McDonald-Buller. (2005). "Comparisons of modeled and observed isoprene concentrations in southeast Texas." Journal of Air and Waste Management (in print).

Stockwell, W. R. and J. G. Calvert (1983). "The Mechanism of the HO-SO2 Reaction." Atmospheric Environment 17(11): 2231-2235.

Swietlicki, E., J. C. Zhou, O. H. Berg, B. G. Martinsson, G. Frank, S. I. Cederfelt, U. Dusek, A. Berner, W. Birmili, A. Wiedensohler, B. Yuskiewicz and K. N. Bower (1999). "A closure study of sub-micrometer aerosol particle hygroscopic behaviour." Atmospheric Research 50(3-4): 205-240.

Tartarelli, R., P. Davini, F. Morelli and P. Corsi (1978). "Interactions between SO2 and Carbonaceous Particulates." Atmospheric Environment 12(1-3): 289-293.

Texas Commission on Environmental Quality (TCEQ) (2004a), Proposed revisions to the State Implementation Plan (SIP) for the control of ozone air pollution: Houston/Galveston/Brazoria ozone non-attainment area, http://www.tnrcc.state.tx.us/oprd/sips/june2004hgb_EDrec.html.

Texas Commission on Environmental Quality (TCEQ) (2004b), Houston/Galveston air quality science evaluation. http://www.tnrcc.state.tx.us/air/aqp/airquality_photomod.html#ei4c

Texas Commission on Environmental Quality (TCEQ) (2004c), Houston/Galveston Mid-Course Review MM5 Modeling Files for Aug. 18 - Sep. 6, 2000 http://bridge.atmet.org/texaqs.shtml

Texas Commission on Environmental Quality (TCEQ) (2004d), Ozone modeling performance statistics, ftp://ftp.tceq.state.tx.us/pub/OEPAA/TAD/Modeling/HGMCR/CAMx/output/camx403.base5b.psito2n2/

Thornton, J. A., C. F. Braban and J. P. D. Abbatt (2003). "N2O5 hydrolysis on sub-micron organic aerosols: the effect of relative humidity, particle phase, and particle size." Physical Chemistry Chemical Physics 5(20): 4593-4603.

Tie, X., G. Brasseur, L. Emmons, L. Horowitz and D. Kinnison (2001). "Effects of aerosols on tropospheric oxidants: A global model study." Journal of Geophysical Research-Atmospheres 106(D19): 22931-22964.

Tie, X. X., L. Emmons, L. Horowitz, G. Brasseur, B. Ridley, E. Atlas, C. Stround, P. Hess, A. Klonecki, S. Madronich, R. Talbot and J. Dibb (2003). "Effect of sulfate aerosol on tropospheric NOx and ozone budgets: Model simulations and TOPSE evidence." Journal of Geophysical Research-Atmospheres 108(D4).

Tobias, H. J., D. E. Beving, P. J. Ziemann, H. Sakurai, M. Zuk, P. H. McMurry, D. Zarling, R. Waytulonis and D. B. Kittelson (2001). "Chemical analysis of diesel engine nanoparticles using a nano-DMA/thermal desorption particle beam mass spectrometer." Environmental Science & Technology 35(11): 2233-2243.

Tolocka, M. P., M. Jang, J. M. Ginter, F. J. Cox, R. M. Kamens and M. V. Johnston (2004). "Formation of oligomers in secondary organic aerosol." Environmental Science & Technology 38(5): 1428-1434.

Trebs, I., S. Metzger, F. X. Meixner, G. N. Helas, A. Hoffer, Y. Rudich, A. H. Falkovich, M. A. L. Moura, R. S. da Silva, P. Artaxo, J. Slanina and M. O. Andreae (2005). "The NH4+-NO3--Cl--SO42--H2O aerosol system and its gas phase precursors at a pasture site in the Amazon Basin: How relevant are mineral cations and soluble organic acids?" Journal of Geophysical Research-Atmospheres 110(D7).

Tropp, R. J., S. D. Kohl, J. C. Chow and C. A. Frazier (1998). "Final report for the Texas PM2.5 sampling and analysis study, Prepared for Bureau of Air Quality Control, City of Houston, TX. Document No. 6570-685-7770.1.F. Prepared by Desert Research Institute."

Ullerstam, M., R. Vogt, S. Langer and E. Ljungstrom (2002). "The kinetics and mechanism of SO2 oxidation by O3 on mineral dust." Physical Chemistry Chemical Physics 4(19): 4694-4699.

Ullerstam, M., M. S. Johnson, R. Vogt and E. Ljungstrom (2003). "DRIFTS and Knudsen cell study of the heterogeneous reactivity of SO2 and NO2 on mineral dust." Atmospheric Chemistry and Physics 3: 2043-2051.

Walcek, C. J. and G. R. Taylor (1986). "A Theoretical Method for Computing Vertical Distributions of Acidity and Sulfate Production within Cumulus Clouds." Journal of the Atmospheric Sciences 43(4): 339-355.

Wang, Y. H., D. J. Jacob and J. A. Logan (1998). "Global simulation of tropospheric O3-NOx-hydrocarbon chemistry 1. Model formulation." Journal of Geophysical Research-Atmospheres 103(D9): 10713-10725.

Wiedinmyer, C., A. Guenther, M. Estes, I. W. Strange, G. Yarwood and D. T. Allen (2001). "A land use database and examples of biogenic isoprene emission estimates for the state of Texas, USA." Atmospheric Environment 35(36): 6465-6477.

Yamasaki, H., K. Kuwata and H. Miyamoto (1982). "Effects of Ambient-Temperature on Aspects of Airborne Polycyclic Aromatic-Hydrocarbons." Environmental Science & Technology 16(4): 189-194.

Yue, Z. W. and M. P. Fraser (2004). "Polar organic compounds measured in fine particulate matter during TexAQS 2000." Atmospheric Environment 38(20): 3253-3261.

Zhou, J. (2001). "Hygroscopic properties of atmospheric aerosol particles in various environment." Ph.D Thesis, Dept of Nuclear Physics, Lund University (April 2001)(ISBN 91-7874-120-3).

# Vita

Uarporn Nopmongcol was born in Bangkok, Thailand on 25 March, 1980, the daughter of Dr. Pradit Nopmongcol and Tipsuda Nopmongcol. She was raised in Bangkok and graduated from Triam Udom Suksa High School in 1997. She received a bachelor degree in Chemical Engineering with the first class honor from Chulalongkorn University, Thailand, in May 2001. She entered the Graduate School at the University of Texas at Austin, Department of Chemical Engineering in 2001.

Permanent Address: 312/4 Sri-Ayutthaya Rd., Rachatewee, Bangkok, Thailand 10400

This thesis was typed by the author.